Aus dem Institute of Lung Health and Immunity
(LHI, Helmholtz Zentrum München)
Direktor: Prof. Dr. Ali Önder Yildirim

Engineering a 3D human lung model system to study the disease crosstalk within the alveolar epithelium

Dissertation
zum Erwerb des Doktorgrades der Naturwissenschaft
an der Medizinischen Fakultät der
Ludwig-Maximilians-Universität München

vorgelegt von
Miriam Theresa Kastlmeier

aus
München

Jahr
2024

Erster Gutachter:	Prof. Dr. rer. nat. Magdalena Götz
Zweiter Gutachter:	Prof. Dr. rer. nat. Alexander Dietrich
Dekan:	Prof. Dr. med. Thomas Gudermann
Tag der mündlichen Prüfung:	17. Juli 2024

Affidavit

LUDWIG-MAXIMILIANS-UNIVERSITÄT MÜNCHEN	Promotionsbüro Medizinische Fakultät	MMRS	

Eidesstattliche Versicherung
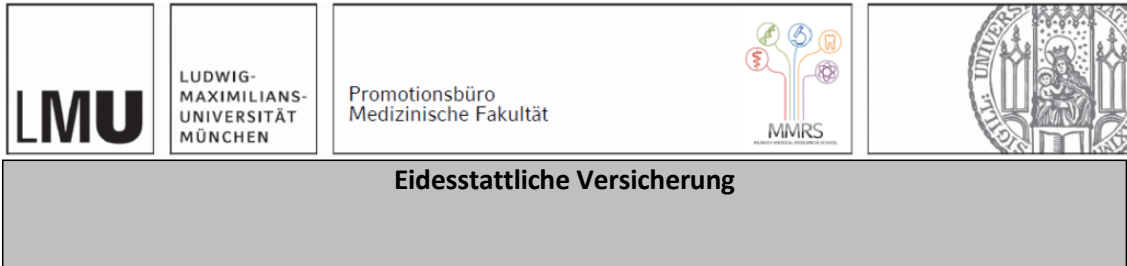
Kastlmeier Miriam Theresa
_____
Name, Vorname

Ich erkläre hiermit an Eides statt, dass ich die vorliegende Dissertation mit dem Titel:

Engineering a 3D human lung model system to study the disease crosstalk within the alveolar epithelium

selbständig verfasst, mich außer der angegebenen keiner weiteren Hilfsmittel bedient und alle Erkenntnisse, die aus dem Schrifttum ganz oder annähernd übernommen sind, als solche kenntlich gemacht und nach ihrer Herkunft unter Bezeichnung der Fundstelle einzeln nachgewiesen habe.

Ich erkläre des Weiteren, dass die hier vorgelegte Dissertation nicht in gleicher oder in ähnlicher Form bei einer anderen Stelle zur Erlangung eines akademischen Grades eingereicht wurde.

 München, 15. September 2024   Ort, Datum

 Miriam T. Kastlmeier   Unterschrift Doktorandin bzw. Doktorand

Table of Content

List of Abbreviation

ABCA3   ATB-binding cassette (ABC) subfamily A member 3
ABEs   Adenine base editors
AD   Autosomal dominant
AR   Autosomal recessive
ARDS   Acute respiratory distress syndrome
AT1 cell   Alveolar epithelial type 1 cell
AT2 cell   Alveolar epithelial type 2 cell
BMP   Bone morphogenic protein
CLD   Chronic lung disease
CLDN4   Claudin 4
DOCK8   Dedicator of cytokinesis-8
ECM   Extracellular matrix
EGF   Epidermal growth factor
EMT   Epithelial-to-mesenchymal transition
ESC   Embryonic stem cells
FACS   Fluorescence activated cell sorting
FGF   Fibroblast growth factor
HIES   Hyper-Immunoglobulin E syndrome
hiPSC   Human induced pluripotent stem cell
HSCT   Hematopoietic stem cell transplant
IgE   Immunoglobulin E
IL6   Interleukin 6
IL11   Interleukin 11
ILD   Interstitial lung disease
IPF   Idiopathic pulmonary fibrosis
Klf4   Krüppel-like factor 4
KRT8   Keratin 8
NKX2.1   NK2 homeobox 1 (TTF-1)
PDGFα   Platelet-derived growth factor α
SFTPC   Surfactant protein C
SP   Surfactant protein
STAT3   Signal transducer and activator of transcript 3
STEMCCA   Single lentiviral stem cell cassette
SFN   Stratifin
Sox2   SRY (sex determining region Y)-box transcription factor 2
Sox9   SRY (sex determining region Y)-box transcription factor 9
TGF-ß   Transforming growth factor-ß
Oct4   Octamer-binding transcription factor 4

List of Presentations and Publications

Poster presentations

Conference	Title	Year
1st DZL Academy Symposium	A 3D epithelial-mesenchymal IPF co-culture to model the disease-crosstalk under a clinically relevant hyperoxia intervention	2021
Epithelial Stem Cell-Niche Interactions in Lung Development, Homeostasis, Regeneration and Disease Virtual Conference, Fusion	Translating the disease-crosstalk of hyperoxia-treated human IPF fibroblasts into a 3D epithelial-mesenchymal model via secretom analysis	2021
19th ERS Lung Science Conference	Translating the disease-crosstalk of hyperoxia-treated human IPF fibroblasts into a 3D epithelial-mesenchymal model via secretom analysis	2021
Interact – 11th Conference by Young Researcher for Young Researcher	Modelling epithelial-fibroblastic crosstalk in vitro: using hiPSC-derived lung cells targeting fibrotic regeneration	2020
DZL Annual Meeting	hiPSCs in vitro lung model for therapeutic strategies in fibrotic regeneration	2020
Niche-epithelial Stem Cell Interactions in Lung Health and Disease Conference, Fusion	hiPSCs *in vitro* lung model for therapeutic strategies in fibrotic regeneration	2019

Talk

Conference	Topic	Year
Online CPC Research School Seminar Series	What are facts, what is fake: How to fight the dangerous infodemic about SARS-CoV-2/Covid-19	2021

Publications

Journal	Title	Year
Frontiers in Immunology, Section Cytokines and Soluble Mediator in Immunity. Volume 14 http://doi.org/10.3389/fimmu.2023/1128239 Miriam T. Kastlmeier, Erika Gonzalez Rodriguez, Phoebe Cabanis, Eva M. Guenther, Ann-Christine Koenig, Lianyong Han,	Cytokine signaling converging on IL11 in ILD fibroblasts provokes aberrant epithelial differentiation signatures	2023

Stefanie M. Hauck, Fenja See, Sara Asgharpour, Christina Bukas, Gerald Burgstaller, Marie Piraud, Mareike Lehmann, Rudolf A. Hatz, Juergen Behr, Tobias Stoeger, Anne Hilgendorff and Carola Voss		
International Journal of Molecular Sciences https://doi.org/10.3390/ijms232415666 Kastlmeier, M. T., Guenther, E. M., Stoeger. T., Voss, C	Lung Organoids for Hazard Assessment of Nanomaterials	2022
The CRISPR journal, Volume 4, Number 2, 178–190. https://doi.org/10.1089/crispr.2020.0111 Eberherr, A. C., Maaske, A., Wolf, C., Giesert, F., Berutti, R., Rusha, E., Pertek, A., Kastlmeier, M. T., Voss, C., Plummer, M., Sayed, A., Graf, E., Effner, R., Volz, T., Drukker, M., Strom, T. M., Meitinger, T., Stoeger, T., Buyx, A. M., Hagl, B., Renner, E. D.	Rescue of STAT3 Function in Hyper-IgE Syndrome Using Adenine Base Editing	2021

1.   Overview and contribution to publications

1.1   Contribution to publication 1

Eberherr et al. (2021). *Rescue of STAT3 Function in Hyper-IgE Syndrome Using Adenine Base Editing.*

The manuscript was published April 2021 in the journal *"The CRISPR Journal"* that is committed to science and the applications of gene editing. The *CRISPR Journal* serves as a central hub for determining information and in-dept analysis of revolutionary technology. Its primary goal is to strength and expand the community of forward-thinking researchers, policymakers and advocates who contribute to the field of gene editing.

Directed lung differentiation of healthy, CRISPR-Cas9-mediated corrected as well as signal transducer and activator of transcript 3 (STAT3) hyper-immunoglobulin E syndrome (HIES) mutated human induced pluripotent stem cells (hiPSCs) into mature alveolar type 2 cells (AT2s) were required for publication after the first revision to verify the potential therapeutic strategies of STAT3-HIES *in vitro*. The publication was used by Miriam T. Kastlmeier as co-author publication in this dissertation. Andreas C. Eberherr, supervised by Dr. Beate Hagl, both part of the research group of Dr. Ellen D. Renner, used this publication as first author publication in his cumulative dissertation as the topic represents the major part of Andreas C. Eberherr's research question.

Author contribution: The publication is focused on the STAT3-HIES and the potential of gene editing to correct the heterozygous STAT3 mutations causing the immunodeficient disease. The study aimed to demonstrate the correction efficiency of adenine base editors (ABEs)-based gene editing and the resulting potential for the treatment of STAT3-HIES. Miriam T. Kastlmeier was responsible for the complete section on stem cell differentiation in this publication. She performed the differentiation of patient (mutated) and edited (corrected) hiPSCs into lung progenitor cells and alveolar organoids. By validation through fluorescence staining and fluorescence activated cell sorting (FACS) analysis (Supplementary Figure S9), done by Miriam T. Kastlmeier, conserved plasticity of edited hiPSCs could be verified, needed as prerequisite for the therapeutic approach in the context of the paper.

Miriam T. Kastlmeier contributed to the interpretation of the results regarding human organoids derived from human patient and corrected iPSCs as well as drafting the manuscript. The final discussion of the paper in relation to treatment efficacy in a human organoid model was led by Miriam T. Kastlmeier, supported by Dr. Carola Voss and Dr. Tobias Stöger.

1.2 Contribution to publication II

Kastlmeier et al. (2023). Cytokine signaling converging on IL11 in ILD fibroblasts provokes aberrant epithelial differentiation signatures.

The manuscript was published May 2023 in the journal "*Frontiers in Immunology*", a well-regarded journal in the scientific community in the field of basic, translational and clinical immunology. *Frontiers in Immunology* is an open science journal that aims at scientist collaborating easier and innovating faster to generate knowledge enabling healthy lives.

Miriam T. Kastlmeier wrote the original version of the publication and adapted it during the revision and publication process based on the comments of reviewers with the help of Dr. Carola Voss. The paper represents the main part of the dissertation and was only used by Miriam T. Kastlmeier as first author paper. Throughout this publication Miriam T. Kastlmeier contributed significantly in the discussion about mediators of the mesenchymal-to-epithelial crosstalk and the effects related to interstitial lung diseases (ILDs). The paper demonstrates the potential of lung organoid co-culture systems as an *in vitro* model for chronic lung diseases (CLDs) by displaying the consequence of a perpetuating disease crosstalk and the resulting consequences through epithelial damage and aberrant differentiation.

Author contribution: The study design and experimental plan was created by Miriam T. Kastlmeier, supported by Dr. Carola Voss, Dr. Tobias Stöger and PD Dr. Anne Hilgendorff, as it constitutes the major topic of the doctoral thesis of Miriam T. Kastlmeier. The hypothesis of this paper was formulated by Miriam T. Kastlmeier together with Dr. Carola Voss.

A comprehensive literature review as well as the planning and execution of the experiments (co-culture of mature induced AT2s together with human fibroblasts, to study the mesenchymal-to-epithelial crosstalk, analysis via qPCR and WST, live-cell imaging of 3D co-cultures) was performed by Miriam T. Kastlmeier, representing the main part of the paper. High content imaging was performed in collaboration with Dr. Kenji Schorpp of the Research Unit Signaling and Transduction. Quantification of microscopic images was performed by Miriam T. Kastlmeier, with assistance from her student fellows, Eva M. Günther and Phoebe Cabanis. In collaboration with Helmholtz AI (Christina Bukas, Marie Piraud) and Dr. Mareike Lehmann and Dr. Gerald Burgstaller and their associated lab members Fenja See, Sara Asgharpour a machine learning approach was used to characterize size and number of lung organoids. Interpretation of the results was mainly done by Miriam T. Kastlmeier with support from Dr. Carola Voss. Human fibroblasts were supplied by the BioArchive of the Comprehensive Pneumology Center (CPC) led by PD Dr. Anne Hilgendorff (Ethic Vote #333-10, Study doctor: Prof. Dr. med. Jürgen Behr). Cultivation of human fibroblasts was performed by Erika Gonzalez Rodrigues. Interpretation of mass spectroscopy results, performed by Dr. Stephanie Hauck and Dr. Ann-Christine König,

and comparison with previously published data was mainly done by Miriam T. Kastlmeier with assistance from Dr. Carola Voss, Dr. Tobias Stöger, and PD Dr. Anne Hilgendorff. The statistical evaluation was done by Lianyong Han together with Miriam T. Kastlmeier. The figures were created by Miriam T. Kastlmeier.

The discussion was conducted by Miriam T. Kastlmeier with assistance from Dr. Carola Voss, Dr. Tobias Stöger, and PD Dr. Anne Hilgendorff.

1.3   Contribution to publication III (Appendix)

Kastlmeier et al. (2022) *Lung Organoids for Hazard Assessment of Nanomaterials.*

The perspective was published December 2022 in the journal *"International Journal of Molecular Science",* that provides among others a forum for molecular and cell biology, molecular biophysics and medicine as well as every aspect of molecular research in the field of chemistry. Through this paper Miriam T. Kastlmeier contributed to the debate of using human *in vitro* models as risk assessment of nanomaterial testing and human lung organoid cultures as a suitable method for examination. This publication was only used in the dissertation of Miriam T. Kastlmeier.

Author contribution: Miriam T. Kastlmeier and Eva M. Günter conducted an overall literature research on the field of lung organoids in the context of nanoparticle exposure. Miriam T. Kastlmeier prepared the original draft with focus of culture methods with hiPSCs and the generation of 3D human lung organoids as it reflects a major part of the dissertation. The paper contains original fluorescence images of human alveolospheres derived from hiPSCs prepared by Miriam T. Kastlmeier and from alveolar organoids derived from murine lung organoids prepared by Eva M. Günther.

The perspective is supported by self-performed culture methods and experiments using hiPSCs-derived alveolar epithelial cells and experiences of 3D *in vitro* organoid culture studies. These personal insights in connection with broad research and indicated interest in novel and innovative experimental setups were the base for the publication by Miriam T. Kastlmeier and Eva M. Günter that was supported by Dr. Carola Voss and Dr. Tobias Stöger.

2. Introduction

2.1 Structure and function of the human lung

2.1.1 Morphology and role of the pulmonary system

The lung is the essential organ of the respiratory system that most vital function is to facilitate the gas exchange from the surroundings into the bloodstream. 80 % of the total volume of the human lung is air, another 10 % is blood and the remaining 10 % corresponds to tissue. These 10 % of tissue, that do not exceed a few 100 grams, consists of more than 61 different cell types ("A cellular reference atlas of the human lung," 2023; Knudsen & Ochs, 2018).

During embryonic lung development, gastrulation is the first morphogenic key incident during organ development, were cells from the inner cell mass exit pluripotency and allocate to one of the three germs layers – i) the ectoderm, ii) mesoderm and the iii) definitive endoderm lineage (Figure 1.). The development of the human lung involves highly specified programs of growth and morphogenesis to generate the lung airway and vascular system with its complex architecture optimized for the one reason – to facility to gas exchange and therefore the ability to breath (Knudsen & Ochs, 2018; Land et al., 2014; Morrisey & Hogan, 2010).
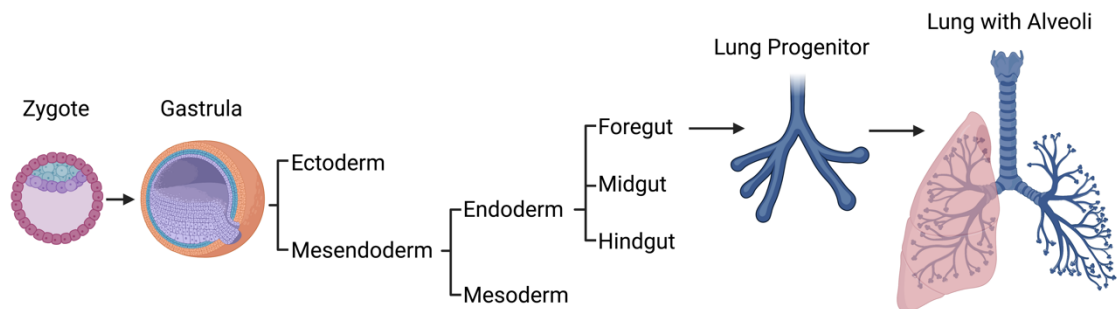

Figure 1. Overview of the developmental stages of human lung differentiation (Dayem et al., 2016; Kadzik & Morrisey, 2012).

The lungs, consisting of conducting airways, blood vessels and primarily the alveolar region, embed the heart from both sides - through three right and two left lobes - and itself are surrounded by the pleura. Together, the surface of the lungs is approximately 75 m², the same areas as a tennis court, and comprise around 2400 km of airways (Knudsen & Ochs, 2018; Morrisey & Hogan, 2010; Pavelka & Roth, 2010). The proximally located trachea divides the left and right main stem of the bronchial system. Further the main bronchus splits into secondary bronchi and following into evermore narrowing airways, until the smallest bronchioles end in the alveoli. The different sections are encased, whereby e.g., the bronchi are bolstered with a hyaline cartilage layer to maintain airway consistency. The bronchioles instead are encased by smooth muscles and finally the alveoli are secreting surfactant, creating a thin layer of lining fluid. Through the airways the air is transported to the alveolar septum, the primary location for the gas exchange (Akella & Deshpande, 2013; Nikolić et al., 2018).

2.1.2 Structure and function of the alveolar epithelium

The alveolar septum or air-blood-barrier separates the alveolar airspace from the capillary lumen. To fulfill efficient diffusion of oxygen and carbon dioxide between the air and blood, the alveolar septum requires a large surface area, and however a thin diffusion barrier, about 0.6 μm. Not only structural but even functional requirements must be met for proper gas exchange, including stability to prevent collapse of the alveoli, and flexibility to follow movement of the breathing cycle, at the same time. Therefore, a major function of the over 300 million alveoli is to maintain the alveolar fluid balance and so provide the optimal gas exchange (Haddad & Sharma, 2023; Knudsen & Ochs, 2018; Nikolić et al., 2018; Vadász & Sznajder, 2017).

The maintenance of air-filled alveoli requires the secretion of surfactant, necessary for a stable hydrostatic pressure. The alveolar lining layer, also named alveolar surfactant, is consisting of a heterogenous mixture of lipids and proteins that is necessary to lower the surface tension at the air-liquid interface to maintain airway patency and therefore is essential to breath (Barkauskas et al., 2017; Barkauskas et al., 2013).
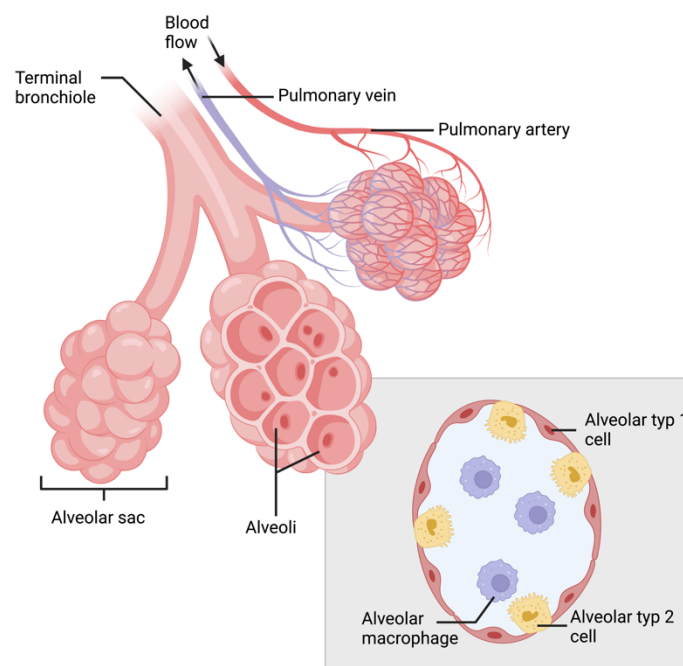

Figure 2. Schematic illustration of the gas exchange area. Terminal bronchioles lead to the alveolar sac, containing alveoli. Alveolus consisting of flat, squamous alveolar type 1 cells, small, cuboidal alveolar type 2 cells, and alveolar macrophages (Andreeva et al., 2007; Dockrell et al., 2022)

The surface tension within the alveoli essentially diminishes to near-zero levels, especially during the deflation phase when phospholipid particles draw closer together. When the alveoli reach full inflation, surfactant phospholipid molecules become more spaced out, leading to reduced lung compliance during deflation, a phenomenon known as hysteresis. Greater lung compliance

is an outcome of reduced surface tension. This reduced surface tension, in turn, leads to a decrease in the pressure gradient between capillaries and alveoli, ultimately reducing the ultrafiltration of fluids (Pérez-Gil, 2008; Prange, 2003).

The alveolar epithelium monolayer is composed of alveolar type 1 (AT1) and type 2 (AT2) cells, representing the critical components of lung homeostasis. Although the number of AT1 and AT2 cells in the lung is almost similar, AT1 cells occupy about 90 % of the surface and AT2 cells only about 10 % (Confalonieri et al., 2022; Guillot et al., 2013). This indicates that the shape of the alveolar cells is decisive (Figure 2.).

AT2s are small, cuboidal cells needed to synthesize and secrete pulmonary surfactant and additionally regulate the innate immunity in the lung via secretion of glycoproteins and anti-inflammatory, antimicrobial mediators such as lysozymes (Akella & Deshpande, 2013; Hite et al., 2012; Sanches Santos Rizzo Zuttion et al., 2022). Repair as well as renewal are provided by AT2s that constitute the progenitor cell population of the alveolar epithelial and in addition, AT2s have the ability to differentiate into AT1 cells during alveolar homeostasis and post injury (Confalonieri et al., 2022; Haddad & Sharma, 2023; Knudsen & Ochs, 2018; Strunz et al., 2020; Wang et al., 2018).

AT1s are membranous, large squamous cells especially forming the epithelial component of the thin air-blood barrier, due to their characteristically shape, AT1s maximize the surface area of the alveolar wall while minimizing the gas-blood barrier (Satora et al., 2022; Wang et al., 2018).

2.2 Response to environmental stress

2.2.1 Defense mechanisms and inflammatory response of the respiratory barrier

Alveolar epithelial cells cover the inner surface of the alveoli and serve as line of defense and contact barrier against exogenous stress factors and changing oxygen levels, as they are directly exposed to the external environment (Berggren-Nylund et al., 2023). Moreover, through the integrity of the apical lung surface, the alveolar epithelium is able to defend itself against inhaled pathogens and nanoparticles (Confalonieri et al., 2022; Sanches Santos Rizzo Zuttion et al., 2022). One major defense mechanism is the secretion and production of surfactant lipids and proteins by AT2 cells.

Numerous studies have employed various techniques, such as metabolic labeling strategies and lipidomic profiling of primary AT2 isolates in culture, to comprehensively explore the biosynthetic pathways, enzymes, and additional factors necessary for generating substantial intracellular compounds of surfactant, ready for release into the alveolar space (Andreeva et al., 2007; Beers & Moodley, 2017; Khudadah et al., 2023). In addition to that, AT2s are actively contributing to lung defense as they secrete cytokines as well as chemokines and participate in the activation and differentiation of immune cells. Together with macrophages, AT2s participate in the active

defense of the respiratory system. Especially alveolar macrophages display phagocytic ability and play an important role in the initiation and purpose of inflammatory response (Berggren-Nylund et al., 2023; Chuquimia et al., 2013).

Going beyond the physiological functions of AT2s, the regulation of injury and the process of regeneration are influenced by transcriptional regulators and growth factors released by niche cells. Thus, transcription factors as signal transducer and activator of transcript 3 (STAT3) and fibroblast growth factor (FGF) are critical for epithelial cell function and activated or increased in injury response and repair. Fibroblasts are known to release niche signals such as platelet-derived growth factor α (PDGFα) or Wnts to promote proliferation and differentiation in AT2s. The pathway of STAT3 is known to be involved in inflammatory response, as STAT3 is activated through injury and functionally critical for the repair of AT2 cells (Paris et al., 2020). It promotes the modulation of the surrounding fibroblast through alternating paracrine molecules and contributes to the differentiation from fibroblast to myofibroblasts (Chan & Liu, 2022; Pedroza et al., 2016).

2.2.2   Alveolar epithelia repair after injury

To ensure efficient gas exchange, also in severe cases of injury, which can lead to substantial epithelial loss of AT2s, AT1s and probably even bronchial cells. Both AT1 and AT2 cells can be regenerated by stem cell populations originating from the airways. However, the precise molecular mechanisms, as well as the temporal and spatial organization of the crucial signals, gene expression patterns, and pathways involved in the restoration of the AT1 cell layer, remain on research focus by delineating the essential factors (Beers & Moodley, 2017; Satora et al., 2022). However, it is speculated that pulmonary fibrosis and chronic lung diseases (CLDs) in general, might have their origins in malfunctioning molecular checkpoints for cell differentiation, resulting in the abnormal and prolonged presence of intermediate regenerative cell states (Strunz et al., 2020). Therefore, the impaired termination of stem cell differentiation process into AT1 represent a critical factor in the pathogenesis of progressive fibrosis observed in pulmonary fibrosis (Katzen & Beers, 2020; Strunz et al., 2020).

Subsequently after lung injury, several signaling pathways play a role regarding the stepwise AT2-mediated lung repair program displayed by injury, proliferation, partial de-differentiation, AT2 to AT1 transition and differentiation into AT1 cells. These include FGF and epidermal growth factors (EGF) that stimulate AT2 proliferation and uphold self-renewal capability. Consecutively, bone morphogenic protein (BMP) 4 signaling inhibits AT2 self-renewal capacity but promotes AT2 to AT1 transition, characterized by AT2 - AT1 intermediate cells expressing markers including Keratin 8 (KRT8), Claudin 4 (CLDN4) and Stratifin (SFN) (Chan & Liu, 2022; Strunz et al., 2020; Wu & Tang, 2021).

Wnt pathways are triggered after injury and assist in alveolar repair, as Wnt signaling plays a key role in the stem cell capacity of AT2 cells. Since one of the major functions of AT2s is to produce surfactant, dysregulation of the surfactant production may lead to defective lung repair and trigger pro-inflammatory processes. Therefore, the upregulation of Wnt activity is required for the initiation of repair processes as it stimulates the differentiation into surfactant producing AT2s and enhance epithelial repair (Chan & Liu, 2022; Olajuyin et al., 2019).

2.3   3D organoid system generated from hiPSCs

2.3.1   Directed lung differentiation into mature alveolar epithelial cells

Human induced pluripotent stem cells (hiPSCs) share the same characteristics of self-renewal and pluripotency as embryonic stem cells (ESC). Contrary to ESC, hiPSCs can be generated out of nearly any accessible cell origin, whereby providing a major source of different patient as well as disease specific PSCs (Jake Le Suer, 2021). hiPSCs were firstly generated by Takahashi et al. (Takahashi et al., 2007) via retroviral integration and overexpression of four transcription factors named "Yamanaka factors"– octamer-binding transcription factor 4 (Oct4), Krüppel-like factor 4 (Klf4), SRY (sex determining region Y)-box transcription factor 2 (Sox2) and c-MYC – into human adult dermal fibroblast (Shi et al., 2017).

The reprogramming of post-natal cells by defined transcription factors has allowed the generation of hiPSCs with similar functional and molecular phenotypic characteristics to embryonic stem cells, but lack the ethical concerns (Somers et al., 2010; Sommer et al., 2012). There are different methods to generate hiPSCs, including the above-mentioned retrovirus or lentivirus-mediated gene transduction or chemical induction. The retroviral vector required integration into host chromosomes to express reprogramming genes (Ghaedi & Niklason, 2019). By combining all 4 reprogramming factors Oct4, Sox2, Klf4, and x-Myc in a single lentiviral stem cell cassette (STEMCCA), STEMCCA accomplished reprogramming of human adult dermal fibroblasts with high efficiency and allowed the derivation of hiPSC containing a single viral integration (Lowry et al., 2008; Sommer et al., 2012).

The formation from hiPSCs into definitive endoderm is induced throw high levels of Nodal signaling, stimulated by Activin A, a signaling protein that activates the downstream signaling cascade as Nodal to induce a definitive endoderm phenotype (Ghaedi & Niklason, 2019; Ghaedi et al., 2015; Kadzik & Morrisey, 2012). Subsequent inhibition of BMP and transforming growth factor-ß (TGF-ß) signaling promotes the differentiation into anterior foregut with expression of anterior foregut markers Sox2 and FoxA2. Inducing Wnt and BMP signaling in the anterior foregut formation of ventral anterior foregut cells is promoted, followed by FGF10 treatment that induced the specification of lung progenitors, expressing NK2 homeobox 1 (NKX2.1), Sox2 and Sox9. Maturation of lung progenitors have been induced by treatment with a complex media of

growth factors and inhibitors and resulted in mature alveolar epithelial cells (A. Jacob et al., 2017; Jacob et al., 2019).

2.3.2   Application of 3D hiPSC-derived organoid model systems

Most results from studies, affecting the structure and function of the lung and reflecting dependent diseases, were generated via animal models. Though, animal models cannot fully recapitulate the human lung development and disease origination. *In vitro* models generated with hiPSC-derived iAT2s have the ability to replace animal models as they serve to better understand lung hemostasis and to reflect underlying cellular processes leading to alterations and disease (Miller et al., 2019; Miller & Spence, 2017). hiPSC-derived organoids simulate the fundamental developmental mechanisms that gives rise to an organ as well harbor the corresponding cell types of this tissue (Sharma et al., 2020). Lung organoids can recapitulate the 3D organizational structure of the lung *in vitro* including the composition through different cell types. In this way, mechanism that are underlying epithelial repair can be reflected and lung organoids can be used to study regulatory processes managing lung injury and drug development (Kong et al., 2021; Leibel et al., 2021). 3D culture systems utilizing human stem cells are amenable to study patient-specific diseases states, reflecting cell proliferation, morphology, and cellular functionality. These model systems enable disease modeling and support the understanding of ongoing vice-versa cellular communication mechanisms (Cidem et al., 2020).

Using innovative technologies of hiPSCs together with 3D cell culturing, the emerge of organoids created a new potential of human disease research. Organoids generated from hiPSCs are a self-organizing, unique 3D system, which is highly similar to human organs and complements the existing model system as well as extend basic biological research. They have the ability of representing effects of supplemented growth factors, oxygen availability as well as environmental factors (Miller & Spence, 2017). The experimental potential of organoids increases steadily, among others for therapeutic drug testing, molecular medicine, clinical studies and medical research (Kim et al., 2020).

3.   Overarching research question

The inflammatory perturbation of alveolar epithelial cells *in vitro* in response to intrinsic factors (genetic mutation e.g., STAT3-HIES), cell-cell contact and paracrine signaling (cellular crosstalk in fibrosis) as well as extrinsic stimuli (airborne and inhaled particles) remain to date elusive. To decipher such inflammatory perturbations of the epithelium, a responsive, human *in vitro* model of the respiratory epithelium is necessary. Therefore, the overarching research question focuses on the generation of a 3D *in vitro* alveolar organoid model from hiPSCs enabling the study of the cellular crosstalk in fibrosis and display the pro-inflammatory response, including cytokine release. By using this cell culture method, it is possible to identify relevant mediators for disease crosstalk and to find potential targets for therapeutic strategies.

3.1   Motivation behind the usage of hiPSCs-derived iAT2s

Relevant human material for *in vitro* studies offers a valid alternative to cell lines, as immortalized human lung cell lines have major drawbacks compared to primary tissue. By using immortalized cells lines the *in vivo* situation is not fully represented as these cell lines e.g., often lack polarity or key morphological features and therefore differenced from iAT2s in these contexts. Especially the heavy loss of physiological and transcriptionally relevant biomarkers during culturing considerably complicates conclusions. Foremost, AT2 cells from cell lines, as the central figure in lung injury and regeneration, show the absent production of a liquid lining fluid including surfactant proteins (SP), a key feature of the alveolar cell layer (Abo et al., 2020). Whereas iAT2 display markers for SP-B and SP-C, promoting their self-renewing capacity as needed for constant repetition of an experimental set-up. Another problem with either cancer-derived or virally immortalized cell lines is the continuous growth due to mutation or manipulation. They evade cellular senescence and undergo perpetually proliferation leading to e.g., functional alterations and genetic drifts, making it difficult to obtain comparable results (Anjali Jacob et al., 2017a; Kastlmeier et al., 2022). In contrast, hiPSC-derived iAT2s, encounter primary-like cell characteristics without the drawback of relying on patient material. iAT2s closely match primary human AT2s in cellular function, transcriptional makeup, and morphology in contrast to any of the existing cell lines (Anjali Jacob et al., 2017b; Jacob et al., 2019).

The projects used 3D *in vitro* lung organoid systems generated from hiPSCs-derived iAT2s to model pulmonary diseases by showing cellular responses, reflecting adverse outcomes (e.g., inflammation and cytokine release) as wells as dysregulating proliferation and differentiation.

3.2   Scientific background

3.2.1 STAT3 pathway as regulator of epithelial consistency and controller of inflammation in AT2s

Hyper-Immunoglobulin E syndrome (HIES) is a primary immunodeficiencies characterized by high levels of serum Immunoglobulin E (IgE) (Chandesris et al., 2012; Freeman & Holland, 2008;

Minegishi et al., 2007). HIES is a disease of multi-organ dysfunctions with symptoms including eczema, recurrent bacterial and fungal infections of the skin and lung, eosinophilia as well as delayed dental deciduation, osteopenia, scoliosis and hyperextensibility. Recurrent pneumonia is typically caused by *Staphylococcus aureus*, *Streptococcus pneumonia* and *Haemophilus influenzae* destroys the pulmonary tissue and leads to emphysemas or pneumatoceles and chronic suppurative lung diseases with progressive bronchiectasis (Holland et al., 2007; Kröner et al., 2019). Most cases are sporadic, but autosomal recessive (AR) as well as dominate (AD) variants were diagnosed (Al-Shaikhly & Ochs, 2019). AD-HIES is triggered by heterozygous dominate-negative mutations in the STAT3 gene, affecting the DNA-binding domain (Chandesris et al., 2012; Kröner et al., 2019), whereas biallelic mutation in the dedicator of cytokinesis-8 (DOCK8) gene were identified as the common cause for the recessive variant (Al-Shaikhly & Ochs, 2019). At this stage, the treatment of HIES is limited and refers mainly to reducing symptoms and preventing infections through antibiotic prophylaxis and Immunoglobulin substitution therapy (Freeman & Holland, 2008). Benefits of therapeutic approaches, like hematopoietic stem cell transplant (HSCT) are uncertain. Especially in term of STAT3-HIES, pulmonary complication such as pneumatoceles and bronchiectasis were observed after HSCT (Freeman & Holland, 2008; Kröner et al., 2019).

STAT3 dependent deficient repair mechanism leads to affected lung tissue destructions of the bronchiolar and alveolar epithelium. STAT3, as main controller of inflammation, regulates the expression of SFTPB, which is solely synthesized in AT2s, and controls maintenance of the surfactant homeostasis during lung injury, which is regulated through the Interleukin 6 (IL6) expression of the ATP-binding Cassette A3 (ABCA3) protein, a member of ATP-dependent transport proteins (Kröner et al., 2019). ABCA3 is highly expressed in AT2 cells and predominantly detected in the lamellar bodies. Together with surfactant protein C (SFTPC), ABCA3 is required for organization of lamellar bodies and therefore required for normal pulmonary function. Whereas mutations in the proteins are associated with reduced pulmonary surfactant function in AT2s, possibly resulting in respiratory distress (D'Amico et al., 2018; Kröner et al., 2019; Matsuzaki et al., 2008).

3.2.2   Inflammatory processes through misguided mesenchymal-to-epithelial crosstalk

Interstitial lung diseases (ILDs) comprise a heterogenous group of pulmonary dysfunctions, including idiopathic pulmonary fibrosis (IPF) and acute respiratory distress syndrome (ARDS) by sharing similar clinical, physiologic, radiological, or pathologic manifestations. Characteristics include interstitial wall thickening and/or fibrosis, beside variable alterations of the airway and alveolar architecture. Typical outcomes are named as a decreased lung volume and compliance or even inadequate oxygenation, due to impaired ventilation as well as impaired gas exchange (Bagnato & Harari, 2015; Confalonieri et al., 2022; Noble, 2008).

Pathological biogenesis is a dynamic process involving complex interactions between epithelial cells, fibroblasts, immune cells (like e.g., macrophages and T-cells), as well as endothelial cells. A major impact at the genesis of pulmonary fibrosis is sustained by the dysfunction of epithelial cells and fibrotic remodeling, thus conclude an aberrant regenerative response as main trigger (Choi et al., 2020; Confalonieri et al., 2022; Parimon et al., 2020).

A central role is ascribed to AT2s due to their critical function in lung homeostasis, through the production of pulmonary surfactant and stem cell potential including self-renewal and transdifferentiation into AT1s (Katzen & Beers, 2020). ILD is linked to defects in the pulmonary surfactant production, concluding AT2s as key drivers of the disease crosstalk (Confalonieri et al., 2022; Yang et al., 2020). AT2s develop an altered state in ILDs as they acquire a profibrotic phenotype that promotes expansion to the mesenchymal compartment ensued by myofibroblast activation and matrix deposition. The loss of their self-repair ability during alveolar injury can lead to scar formation. Thence, the activation of TGF-ß through AT2s seems to be self-perpetuating, as through injured AT2s the surface tension rises, which is a crucial factor in pulmonary fibrosis. Furthermore, AT2s have a reduced capacity for transdifferentiation into AT1s in an injured lung (Figure 3.) (Parimon et al., 2020).

Lung fibrotic disorders are characterized by accumulating fibroblasts, originating myofibroblasts and extracellular matrix (ECM), leading to respiratory failure (Bagnato & Harari, 2015). The disease development appears to be driven through the interplay of alveolar epithelial cells and fibroblasts. Due to the loss of the characteristic epithelial phenotype towards a mesenchymal phenotype and the activation of fibroblasts leading to myofibroblasts transition, a profibrogenic microenvironment arises (Confalonieri et al., 2022; Rout-Pitt et al., 2018).

The transformation of epithelial cells into mesenchymal cells is defined as epithelia-to-mesenchymal transition (EMT) and permit a direct vice-versa crosstalk between cells (Noble, 2008). EMT occurs through activation of AT2s as well as ECM deposition and is a complex process in response to extracellular stimuli that involves interactome including protein to protein and genetic interactions. The EMT crosstalk is disrupted in ILDs whereby AT2s acquire a profibrotic phenotype to aberrant secrete profibrotic mediators that stimulate and activate fibroblasts migration and recruit inflammatory cells, after recurrent injury of the alveolar niche (Figure 3.) (Kong et al., 2021; Parimon et al., 2020).

Regarding epithelial repair, Interleukin 11 (IL11) impair the epithelial-mesenchymal communication as it affects the progenitor function of AT2s by suppressing the activation and formation into mature iAT2s (Kortekaas et al., 2022; Kortekaas et al., 2021).
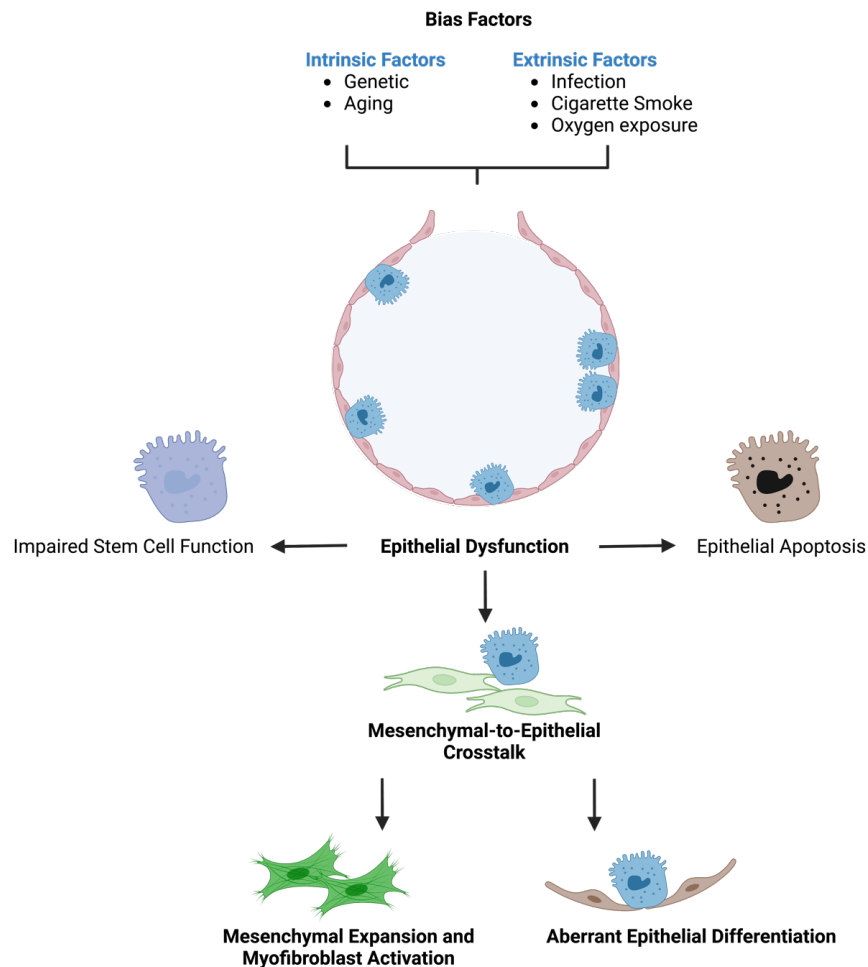
Figure 3. Schematic illustration of ILD pathogenesis driven by intrinsic and extrinsic factors. Bias Factors generate through multiple pathways vulnerable AT2s representing dysfunctional epithelial manners. Targeted AT2s show a disturbance in their characteristic behavior e.g., by an increased external stress response, the loss of their stem cell function or incipient apoptosis. In context of ILD the dysfunctional alveolar niche represents subsequent mechanisms as increased proliferation of AT2s, impaired transdifferentiation to AT1s or transition to a senescent stage. The vice versa mesenchymal-to-epithelial crosstalk with activated myofibroblasts can lead to matrix deposition and a disrupted injury response. The resultant consequence is the loss of the typical lung architecture, fibrotic remodeling and aberrant modifications in the structure of the gas exchange area, characteristic for the ILD phenotype (Chan & Liu, 2022; Katzen & Beers, 2020).

Genetic factors (intrinsic) like aging, as well as environmental (extrinsic) determinants like infection and air pollution are besides repetitive alveolar epithelial injury the main causes for ILD (Confalonieri et al., 2022; Katzen & Beers, 2020). With regard to histological hallmarks, interstitial pneumonia pattern arises, identified by disposed myofibroblasts into fibroblastic foci, in the context of temporally and spatially heterogenous chronic interstitial fibrosis. While fibroblasts accumulation represents the central aspect, honeycombing of the distal lung regions affects regions originating bronchiolization tagged by hyperplastic AT2s and proximal airway cells including basal, ciliated and goblet cell lineages. A further considerable feature is marked by hyperplasia of AT2s and in contrast a loss of AT1s, display two characteristic pathological attributes of ILD – aberrant epithelial cells and mesenchymal expansion (Figure 3.) (Basil et al., 2020; Confalonieri

et al., 2022; Katzen & Beers, 2020; Parimon et al., 2020). The pathological process behind outlines a crosstalk between activated fibroblasts and damaged epithelial cells.

3.3 Publications in relation to research question

As discussed above, alveolar organoids are a versatile tool to study the cellular crosstalk in fibrosis and display the pro-inflammatory response in a lung epithelial cell-based culture model. The generation of a complex 3D organoid model of iAT2s opened the research aim whether a human lung model can be generated, responding realistic to the perturbating vice-versa disease crosstalk or engendered mutation. The potential of utilizing mutant hiPSCs is notably exemplified in their ability to authentically replicate the disease manifestations from the inception. This capability gives invaluable insights into the intricate progression of diseases. In a dynamic 3D culture model, generated by iAT2s from mutant hiPSCs, every stage of organoid development can be meticulously examined. These diseases iAT2s realistically display the behavior of the human lung and provides an opportunity to gain comprehensive insights into the progress of diseases. Moreover, the utilization of human mutant material obviates the need for mechanical cell modifications, which often come at the cost of cell viability and integrity. This non-invasive approach enables to directly emulate the realistic disease patterns observed in clinical settings. It opens new avenues for therapeutic exploration, with a focus not only on the final disease phenotype but also on the intricate cellular processes that underpin the entire disease development.

However, since these cells must go through a complex pathway of directed lung differentiation to become mature alveolar cells, it was not clear whether it is feasible to pass diseased cells through this process in order to differentiate. Through the collaboration with AG Renner, TU Munich, the opportunity was given to differentiate alveolar organoids out of hiPSCs from patients with STAT3 mutation as well as a CRISPR-Cas9-corrected cell line and generate an organotypic human disease model *in vitro*. During the directed differentiation it was possible to compare typical transcription markers of lung progenitor stages and to get an understanding of the complex interplay between growth factors and proteins. The use of various analytical methods revealed both intracellular and phenotypical differences between the hiPSCs lines. The publication "*Rescue of STAT3 Function in Hyper-IgE Syndrome Using Adenine Base Editing*" displays that iAT2s generated from hiPSCs obtained by patients in a 3D culture system represent characteristic HIES disease markers and can be used for further research questions regarding the inflammatory response after stimulation of the STAT3-signaling pathway.

Furthermore, iAT2s showed their potential to study cellular crosstalk perpetuating in ILD, that is inflammatory driven. Hereby, the vice-versa crosstalk between the different cell types should be investigated and potential trigger factors leading to a disturbed inflammatory lung pattern

should be identified. This could be either the direct interplay of cells in a co-culture model or by adding specific cytokines to cultured iAT2 to analyze their response and demonstrate their cellular as well as phenotypic changes.

The CPC-M bioArchive provided tissue from ILD patients to rebuild a co-culture model of human fibroblast together with iAT2s. Primary human lung fibroblast from ILD patients and non-chronic lung disease controls were cultivated to create a 3D co-culture model together with iAT2s, resulting in the formation of alveolar organoids and displaying a realistic *in vivo* set-up of the human alveoli. The model provided deeper insights into the mesenchymal-to-epithelial cross-talk as observed by changes in the organoid phenotype. The morphologic changes of the alveo-lospheres as shown in "*Cytokine signaling converging on IL11 in ILD fibroblasts provokes aberrant epithelial differentiation signatures*" displayed the ability of an organoid co-culture model to show critical consequence of the vice-versa disease crosstalk. Screening results of the supernatant from mono-cultured human fibroblasts from ILD patients demonstrated cytokines from the C-X-C motif family, indicating their increased occurrence in ILD and their leading role in the path-ogenesis of fibrosis and inflammation. Moreover, specific proteins were detected that directly inhibit Wnt signaling and thus regulate cell growth and differentiation from AT2 to AT1 cells. This shift in the Wnt signaling pathway could be accountable for the change in the number of organoids and their size, displayed in their gene expression levels and concluded in the presence of EMT in ILD. In addition, the secretome of fibroblasts showed expression of IL11, which is characteristically expressed by pro-inflammatory fibroblasts in pulmonary fibrosis. IL11 can on the one hand activate fibroblasts to differentiate into myofibroblasts or, on the other hand stim-ulate epithelial cells that results in either cellular dysfunction and impaired regeneration, as well as cellular senescence or EMT. In relation to that, mono-cultures of iAT2s treated with IL11, showed similar effects as stem cell dysfunction, ECM production and EMT.

The paper demonstrates the potential of a 3D organoid co-culture lung model of iAT2s and human fibroblasts, displaying the leading role of the perpetuating crosstalk of activated fibroblast and injured epithelial cells in the progression of pulmonary inflammation. It displays the conse-quences of epithelial damage and aberrant differentiation in CLDs and confirmed IL11 as key player in the pathogenesis of ILD.

Taken together, the publications punctuate the remarkable potential inherent in a 3D co-culture model derived from hiPSCs. These complex *in vitro* lung models effectively display the intricate interplay between mesenchymal and epithelial cells, presenting phenomena such as dedifferenti-ation and morphological transformation. Moreover, it demonstrates its suitability for investigat-ing disease scenarios in a highly realistic in vitro setting, thereby offering valuable insights into the dynamics of diseases under a realistic clinical picture, and prerequisites for new therapeuti-cally approaches.

4. Zusammenfassung

Durch direkte Differenzierung ist es möglich, induzierte Alevolarzellen des Typ 2 (iAT2s) aus humanen induzierten pluripotenten Stammzellen (hiPSCs) zu erzeugen. Das 3D alveolar-Organoid-Modell stellt eine vielversprechende Methode dar, um die zelluläre Interaktion während Lungenfibrose *in vitro* zu untersuchen, pro-fibrotische Mediatoren aufzuzeigen und potenzielle Ziele für therapeutische Ansätze zur Behandlung von Lungenkrankheiten zu identifizieren.

In **Kapitel 6.1** "*Rescue of STAT3 Function in Hyper-IgE Syndrome Using Adenine Base Editing*" lag der Schwerpunkt auf der Korrektur der häufigsten STAT3-HIES verursachenden heterozygoten STAT3-Mutationen durch CRISPR-Cas9-vermittelte Adenin-Basen-Editoren (ABEs). Die aus Patienten gewonnenen hiPSCs zeigten eine erhaltene Plastizität durch ihre Fähigkeit, sich erfolgreich in Lungenvorläuferzellen und anschließend in alveolaren Sphäroiden zu differenzieren. Im Hinblick auf therapeutisch relevante Zwecke ist es eine wesentliche Annahme, dass mit ABE behandelte hiPSCs ihre Plastizität beibehalten. Durch den Nachweis, dass reparierte iPSCs, die aus Fibroblasten von Patienten stammen, alveoläre Sphäroide generieren können, kann dies als Grundsatzbeweis dafür angesehen werden, dass es unter therapeutischen Gesichtspunkten möglich ist, genetische Verfahren für die Behandlung von STAT3-HIES einzusetzen.

Pneumozyten vom Typ 2 (AT2) haben eine sekretorische und regenerative Rolle in der Lungenhomöostase und dienen als zelluläre Vorläufer der Alveolen. Durch die Sekretion von Surfaktanzien ist es die Aufgabe der AT2-Zellen die Oberflächenspannung zu senken und den Kollaps der Alveolen zu verhindern. Eine gestörte funktionelle Entwicklung sowie der Verlust der Fähigkeit zur Sekretion von Surfaktanzien, fördern einen pro-fibrotischen Phänotyp und tragen zum Fortschreiten interstitieller Lungenerkrankungen (ILD) bei.

Kapitel 6.2 "*Cytokine signaling converging on IL11 in ILD fibroblast provokes aberrant epithelial differentiation signatures*" zielte darauf ab, relevante Mediatoren der vice-versa Kommunikation von mesenchymalen zu epithelialen Zellen zu identifizieren. Mittels Massenspektrometrie charakterisierten wir das Sekretom von Lungenfibroblasten mit ILD und Fibroblasten von Patienten mit nicht-chronischer Lungenerkrankung und entdeckten 47 häufig vorkommende Proteine im Vergleich der beiden Gruppen. Das Sekretom der Fibroblasten mit ILD bestand überwiegend aus Chemokinen, signalgebenden Wachstumsfaktoren wie Interleukin 11 (IL11) und Proteinen, die für den Umbau der extrazellulären Matrix und bei dem Übergang vom Epithel zum Mesenchym benötigt werden. Indem wir 3D-Monokulturen von iAT2s mit IL11 behandelten, rekapitulierten wir die Ergebnisse der Co-Kultur mit primären ILD-Fibroblasten, einschließlich der Veränderungen der Stoffwechselaktivität sowie der Fähigkeit Sphäroide zu genieren. Durch unsere Analyse konnten wir mesenchymale Mediatoren identifizieren, welche bei der krankheitserhaltenden Kommunikation vom Mesenchym zum Epithel bei ILD auftauchen. Durch den Einsatz hochentwickelter alveolärer Co-Kulturen konnten wir die Bedeutung der durch Zytokine ausgelösten divergenten Epithelialdifferenzierung nachweisen und IL11 als Schlüsselakteur bei ILD bestätigen.

5.   Abstract

By direct differentiation it is possible to generate induced alveolar type II cells (iAT2s) from human induced pluripotent stem cells (hiPSCs). The 3D alveolar organoid model represents a promising method to study vice-versa cellular crosstalk during lung fibrosis *in vitro,* display pro-fibrotic mediators and identify potential targets for therapeutic approaches of treating lung diseases.

Capture 6.1 *"Rescue of STAT3 Function in Hyper-IgE Syndrome Using Adenine Base Editing"* put the focus on correcting the most common STAT3-HIES causing heterozygous STAT3 mutations via CRISPR-Cas9-mediated adenine base editors (ABEs). The generated patient-derived hiPSCs showed preserved plasticity by their capability to successfully differentiate into lung progenitors and consecutively alveolar organoids. It is an essential assumption with regard to therapeutic relevant purposes that hiPSCs treated with ABE retain their plasticity. Respectively, by demonstrating that repaired hiPSCs derived from patient fibroblasts can generated alveolar organoids, it can be seen as proof-of-principle that it is feasible in a therapeutically aspect to use gene editing in the treatment of STAT3-HIES.

Alveolar epithelial type 2 cells (AT2s) have secretory and regenerative roles in lung homeostasis and serve as cellular progenitors of the lung alveoli. Through the secretion of surfactant, it is the task of the AT2s to lower the surface tensions and prevent the alveoli to collapse. Impaired functional development and loss of the capacity to secret surfactant promote a pro-fibrotic phenotype and contributes to the progression of interstitial lung diseases (ILDs).

Capture 6.2 *"Cytokine signaling converging on IL11 in ILD fibroblast provokes aberrant epithelial differentiation signatures"* aimed to identify pertinent mediators of the vice-versa mesenchymal-to-epithelial crosstalk. Through mass spectrometry we characterized the secretom of ILD lung fibroblast and non-chronic lung disease fibroblasts from patients and detected 47 abundant proteins by comparing the two set-ups. The ILD secretome consisted prevalent of chemokines, signaling growth factors like Interleukin 11 (IL11) and proteins needed for extracellular matrix (ECM) remodeling and epithelial-to-mesenchymal transition. However, treating 3D monocultures of iAT2s with IL11 we recapitulated the co-culture results obtained with primary ILD fibroblasts including changes in metabolic activity as well as organoid formation capacity and size. Our analysis identified mesenchyme-derived mediators contributing to the disease-perpetuating mesenchymal-to-epithelial crosstalk in ILD. By using sophisticated alveolar organoid co-cultures, we indicated the importance of cytokine-driven divergent epithelial differentiation and confirmed IL11 as a key player in ILD.

6.   Publications

6.1   Rescue of STAT3 function in H-IgE syndrome using adenine base editing

Andreas C. Eberherr,[1,2, #] Andre Maaske,[1,2, #] Christine Wolf, [1,2, #] Florian Giesert,[3, 4] Riccardo Berutti,[5-7] Ejona Rusha,[8] Anna Pertek,[8] Miriam T. Kastlmeier,[9] Carola Voss,[9] Michelle Plummer,[1, 2] Amina Sayed,[1, 2, 9] Elisabeth Graf,[6] Renate Effner,[1, 2] Thomas Volz,[10] Micha Drukker,[8] Tim M. Strom,[5, 6] Thomas Meitinger,[5, 6] Tobias Stoeger,[9] Alena M. Buyx,[11] Beate Hagl, [1,2, **, *] and Ellen D. Renner [1,2, **]

[1] Translational Immunology in Environmental Medicine, Klinikum Rechts der Isar, Technical University of Munich, Munich, Germany

[2] Translational Immunology, Institute of Environmental Medicine, Helmholtz Zentrum Munich, Neuherberg, Germany

[3] Institute of Developmental Genetics, Helmholtz Zentrum Munich, Neuherberg, Germany

[4] Chair of Developmental Genetics, Technical University of Munich, Munich, Germany

[5] Institute of Human Genetics, Technical University of Munich, Munich, Germany

[6] Institute of Human Genetics, Helmholtz Zentrum Munich, Neuherberg, Germany

[7] Institute of Neurogenomics, Helmholtz Zentrum Munich, Neuherberg, Germany

[8] iPSC Core Facility, Institute of Stem Cell Research, Helmholtz Zentrum Munich, Neuherberg, Germany

[9] Institute of Lung Biology and Disease, Helmholtz Zentrum Munich, Neuherberg, Germany

[10] Department of Dermatology and Allergology, Klinikum Rechts der Isar, Technical University of Munich, Munich, Germany

[11] Institute for History and Ethics of Medicine, Technical University of Munich, Munich, Germany

[#] These authors contributed equally to this work.
** These authors contributed equally to this work.
* Address correspondence to: Beate Hagl, Translational Immunology in Environmental Medicine, Technical University of Munich and Helmholtz Zentrum München, Ingolstädter Landstrasse 1, 85764 Neuherberg, Germany, E-mail: beate.hagl@helmholtz-muenchen.de

The
CRISPR
Journal

RESEARCH ARTICLE

Rescue of STAT3 Function in Hyper-IgE Syndrome Using Adenine Base Editing

Andreas C. Eberherr,[1,2,‡] Andre Maaske,[1,2,†] Christine Wolf,[1,2,†] Florian Giesert,[3,4] Riccardo Berutti,[5–7] Ejona Rusha,[8] Anna Pertek,[8] Miriam T. Kastlmeier,[9] Carola Voss,[9] Michelle Plummer,[1,2] Amina Sayed,[1,2,9] Elisabeth Graf,[6] Renate Effner,[1,2] Thomas Volz,[10] Micha Drukker,[8] Tim M. Strom,[5,6] Thomas Meitinger,[5,6] Tobias Stoeger,[9] Alena M. Buyx,[11] Beate Hagl,[1,2,**,*] and Ellen D. Renner[1,2,**]

Abstract

STAT3-hyper IgE syndrome (STAT3-HIES) is a primary immunodeficiency presenting with destructive lung disease along with other symptoms. CRISPR-Cas9-mediated adenine base editors (ABEs) have the potential to correct one of the most common STAT3-HIES causing heterozygous *STAT3* mutations (c.1144C>T/p.R382W). As a proof-of-concept, we successfully applied ABEs to correct *STAT3* p.R382W in patient fibroblasts and induced pluripotent stem cells (iPSCs). Treated primary STAT3-HIES patient fibroblasts showed a correction efficiency of 29%±7% without detectable off-target effects evaluated through whole-genome and high-throughput sequencing. Compared with untreated patient fibroblasts, corrected single-cell clones showed functional rescue of STAT3 signaling with significantly increased STAT3 DNA-binding activity and target gene expression of *CCL2* and *SOCS3*. Patient-derived iPSCs were corrected with an efficiency of 30%±6% and differentiated to alveolar organoids showing preserved plasticity in treated cells. In conclusion, our results are supportive for ABE-based gene correction as a potential causative treatment of STAT3-HIES.

Introduction

STAT3-hyper IgE syndrome (STAT3-HIES) is a primary immunodeficiency presenting as a multiorgan disease including but not limited to high serum IgE, eczema, recurrent skin and lung infections, and skeletal manifestations.[1–5] STAT3-HIES is caused by heterozygous *STAT3* mutations, resulting in a dominant-negative effect on STAT3 signaling. In particular, the destructive lung disease caused by recurrent lung infections impacts patients' quality of life.[6,7] The treatment of this devastating immunodeficiency is mainly limited to reducing symptoms and preventing infections through antibiotic prophylaxis and immunoglobulin substitution therapy.[4,5,7,8] Thus far, the overall benefit of hematopoietic stem cell transplantation remains uncertain, especially regarding chronic lung disease in STAT3-HIES.[8–10] Consequently, additional therapeutic approaches, in particular a causative treatment of the lung disease, need to be developed for STAT3-HIES. Due to the dominant-negative effect of mutated STAT3, gene substitution therapy is not suitable to cure STAT3-HIES. The defective protein must instead be eliminated or repaired to rescue STAT3 function.

Adenine base editors (ABEs) mediate correction of single-nucleotide changes from G·C to A·T, which account for half of all known disease-associated mutations,[11] including the two most prevalent STAT3-HIES causing *STAT3* mutations c.1144C>T/p.R382W and c.1145G>A/p.R382Q.[2,3] We chose the heterozygous

[1]Translational Immunology in Environmental Medicine, Klinikum Rechts der Isar, Technical University of Munich, Munich, Germany; [2]Translational Immunology, Institute of Environmental Medicine, Helmholtz Zentrum Munich, Neuherberg, Germany; [3]Institute of Developmental Genetics, Helmholtz Zentrum Munich, Neuherberg, Germany; [4]Chair of Developmental Genetics, Technical University of Munich, Munich, Germany; [5]Institute of Human Genetics, Technical University of Munich, Munich, Germany; [6]Institute of Human Genetics, Helmholtz Zentrum Munich, Neuherberg, Germany; [7]Institute of Neurogenomics, Helmholtz Zentrum Munich, Neuherberg, Germany; [8]iPSC Core Facility, Institute of Stem Cell Research, Helmholtz Zentrum Munich, Neuherberg, Germany; [9]Institute of Lung Biology and Disease, Helmholtz Zentrum Munich, Neuherberg, Germany; [10]Department of Dermatology and Allergology, Klinikum Rechts der Isar, Technical University of Munich, Munich, Germany; and [11]Institute for History and Ethics of Medicine, Technical University of Munich, Munich, Germany.

[†]These authors contributed equally to this work.
[**]These authors contributed equally to this work.
[‡]ORCID ID (https://orcid.org/0000-0002-9330-9650).

*Address correspondence to: Beate Hagl, Translational Immunology in Environmental Medicine, Technical University of Munich and Helmholtz Zentrum München, Ingolstädter Landstrasse 1, 85764 Neuherberg, Germany, E-mail: beate.hagl@helmholtz-muenchen.de

STAT3 mutation c.1144C>T/p.R382W to test the therapeutic applicability of ABEs to correct STAT3-HIES causing point mutations. The p.R382W mutation is located in the DNA-binding domain of STAT3 and results in a dominant-negative effect on STAT3 function caused by defective STAT3 proteins.[1,3] STAT3 signaling is activated upon phosphorylation, and dimerization is mediated by cytokines such as interleukin-6 (IL-6). STAT3 dimers translocate to the nucleus, bind to DNA, and function as transcription factors. Heterozygous *STAT3* p.R382W mutations result in heterodimer formation of wild-type and mutated STAT3 proteins with reduced nuclear localization and STAT3 DNA-binding capacity, while initial STAT3 phosphorylation by cytokine activation remains unaffected.[1,3,12]

Materials and Methods

Institutional review board approval

Skin samples were taken after institutional review board-approved informed consent of the patient and healthy controls.

Primary cell culture

Fibroblasts were isolated from a skin sample of an STAT3-HIES patient heterozygous for the p.R382W mutation (STAT3$^{+/R382W}$ fibroblasts) and two healthy individuals (control). Normal human adult primary dermal fibroblasts (ATCC PCS-201-012, STAT3$^{+/+}$) were purchased from ATCC. Fibroblasts were cultured in Dulbecco's modified Eagle's medium (PAN Biotech) with 10% fetal bovine serum (FBS) superior (Biochrom) and 1% antibiotic/antimycotic (Thermo Fisher Scientific) at 37°C and 5% CO_2. Single-cell clones were isolated via seeding of a 5-cell/μL cell suspension in a 96-well format with a 1:1 dilution of normal fibroblast medium and medium conditioned by culturing STAT3$^{+/R382W}$ fibroblasts for 48 h. Twenty-four hours after seeding, wells containing only one fibroblast were selected for further cultivation.

Patient-derived induced pluripotent stem cell generation

Fibroblasts were harvested as a single-cell solution using trypsin-EDTA (Thermo Fisher Scientific). The transfections were prepared using $1.5 \times 10E6$ cells resuspended in the MEF 1 Nucleofector Kit (Lonza) solution plus 12 μg of plasmid DNA (MIP 247 CoMiP 4in1 with shRNA p53: pCXLE-hMLN; Addgene). The cells were pulsed with the T-020 program using the Nucleofector 2b Device (Lonza). Two transfections were pooled together and plated in a Matrigel-coated (Corning) 100 mm tissue culture dish. The cells were incubated in FBS (GE Healthcare)-based fibroblast growth medium supplemented with 0.2 mM sodium butyrate (Sigma)

and 64 μg/mL ascorbic acid (Sigma) for 24 h. On day 2, a reprogramming medium consisting of essential 6 (Thermo Fisher) supplemented with 100 ng/mL basic fibroblast growth factor (Peprotech), 0.2 mM sodium butyrate, and 50 μg/mL ascorbic acid, and 100 nM hydrocortisone (Sigma) was added to the culture. On day 20, the first colonies were observed and the culture medium was switched to StemMACS iPS-Brew XF (Miltenyi Biotec). The colonies were picked on day 28. Subsequently, the cells were expanded and cultured in feeder-free conditions with Matrigel/iPS Brew XF.

Induced pluripotent stem cell pluripotency analyses

For pluripotency testing via immunostaining, cells were grown on Matrigel-coated (Corning) ibidi eight-well chamber slides (Ibidi) until they reached 80% confluency. The cells were fixed with 4% paraformaldehyde/96% phosphate buffered saline (PBS) solution [Pierce™ 16% Formaldehyde (w/v), methanol-free, Thermo Fisher and Dulbeccos' phosphate buffered saline, no calcium, no magnesium, Thermo Fisher] and permeabilized with 0.2% TritonX-100/PBS (Sigma Aldrich). The following primary and secondary antibodies were used and diluted according to the manufacturers' recommendations: anti-human/mouse Sox2, anti-human Nanog (D73G4), anti-human/mouse Oct-4A (C30A3), anti-human/mouse Lin28 (all Cell Signaling Technologies), and Alexa Fluor® 488 goat anti-rabbit IgG (H+L; Thermo Fisher). The slides were mounted using ProLong Glass Antifade Mountant with NucBlue Stain (Thermo Fisher). Imaging was performed using a Zeiss Axio Imager M.2 with Colibri 7.

Potency characterization for the patient-induced pluripotent stem cells (iPSCs) was performed following directed differentiation protocols for the ectoderm, mesoderm, and endoderm.[13-15] iPSCs from two consecutive passages were seeded in a 24-well format and the differentiation was initiated when the wells were 90% confluent. The cells were differentiated for 5 days. RNA extraction and reverse transcription were performed using the RNeasy Mini Kit (Qiagen) and SuperScript III Reverse Transcriptase (Thermo Fisher) following the manufacturer's instructions. Quantitative real-time polymerase chain reaction (PCR) was performed in Power SYBR™ Green PCR Master Mix (Thermo Fisher) using the default program from the Quant-Studio 12K Flex Real-Time PCR System (Thermo Fisher). Relative expression levels were calculated using the Delta-Delta Ct method normalized with glyceraldehyde 3-phophate dehydrogenase.[16]

Directed differentiation of human iPSCs

To investigate plasticity after gene editing, untreated STAT3$^{+/R382W}$ iPSCs, a corrected iPSC SCC and the

control iPSC line BU3NGST were differentiated into lung progenitor cells and alveolar type 2 epithelial cells (iAEC2) as described previously.[17,18] The control iPSC line BU3NGST was kindly provided by Prof. Darrell Kotton, Boston University, Center for Regenerative Medicine.[17] Shortly, iPSCs are consecutively induced for definitive endoderm and anterior foregut formation. At day 14 of differentiation, lung progenitor specification was evaluated by immunofluorescence staining of NKX2.1 and albumin (ALB). NKX2.1-positive lung progenitor cells were enriched by flow cytometry (BD FACSAria) by expression of cell surface markers CD47^{hi}/CD26^{lo} based on a previously described protocol.[19] Purified lung progenitors were seeded in 3D Matrigel (Corning) domes and passaged every second week at a cell density of 50 cells/μL according to published protocols.[17] At day 45 of differentiation, emerging iAEC2 were enriched using the surface marker CPM and subsequently cultured as 3D alveolospheres.

To ensure iAEC2 identity, immunofluorescence of PFA-fixed and paraffin-embedded alveolar spheres was performed. Three micrometer sections were deparaffinized followed by antigen retrieval using citrate buffer (pH 6.0). After permeabilization and blocking, slides were stained with primary antibodies overnight. Secondary antibodies were applied 1 h before counterstaining with DAPI for 30 min. The slides were mounted with DAKO fluorescence antifade agent and imaged using the Zeiss Axio Imager.

The following primary and secondary antibodies were used: anti-human/mouse/rat Nkx2.1 (clone 8G7G3/1; Invitrogen), anti-human albumin (clone 188835; R&D Systems), anti-CPM (014-27501; Wako), Alexa 647 goat anti-mouse, anti-proSPC (AB3786A; Millipore), Alexa 647 Plus goat anti-rabbit, Alexa 488 goat anti-mouse IgG1, Alexa 647 goat anti-mouse IgG2a (all Invitrogen), PE anti-human CD26 (clone BA5b), APC anti-human CD47 (clone CC2C6), PE mouse IgG1, κ isotype control (MOPC-21), and APC mouse IgG1, κ isotype control (MOPC-21; all BioLegend). Imaging was performed using a Zeiss LSM 880 with Airyscan. Images were edited using ZEN 2.5 lite software. Flow cytometric analysis was performed with a BD FACSCanto II Cell Analyzer with BD FACS Diva Software v. 6.1.3. For the evaluation of the dot plots, FlowJo Version 7.2.1 was used.

Electroporation of ribonucleoproteins and plasmids

Fibroblasts were electroporated with the 4D-Nucleofector X System (program DT-130) by using the P2 Primary Cell Kit L, and iPSCs (program CA-137) by using the P4 Primary Cell Kit S, according to the manufacturer's instructions (both Lonza). Ribonucleoproteins (RNPs) were assembled with Alt-R® S.p. Cas9 nuclease (Integrated DNA Technologies) and single-guide RNAs (sgRNAs) *in vitro* synthesized with the EnGen sgRNA Synthesis Kit, *Streptococcus pyogenes* (New England Biolabs), according to the manufacturer's instructions.

The plasmid encoding the ABE pCMV-ABE7.10 was ordered from Addgene as was the plasmid, pBS-U6-chimaericRNA, encoding a non-target control guide RNA under U6 promoter control. The non-target control sgRNA contained an 18 bp protospacer sequence (5′-GGGTCTTCGAGAAGACCT-3′) without targets with less than three mismatches according to CCTop[20] and nucleotide BLAST[21] in the human DNA and no adenines in the editing window of ABE7.10. The target-specific sgRNA gW382R-ABE (gWRA) sequence containing the protospacer 5′-ATTTCCAGGATCTGAATCAC-3′ was cloned into the pBS-U6-chimaeric RNA vector by excision of the non-target control guide RNA sequence.

Sanger sequencing

Sanger sequencing was performed with PCR fragments of the target regions and exonic gWRA off-targets with four mismatches predicted by CRISPOR[22] and CCTop[20]; primer sequences are listed in Supplementary Table S1. Editing efficiencies were determined via *in silico* analysis using EditR[23] and were calculated from the percentage of A signal in the chromatogram in untreated cells versus treated cells. Chromatograms were received from Eurofins Genomics GmbH.

Deep whole-genome sequencing

The genomic library was prepared from 1000 ng of genomic DNA with the TruSeq DNA PCR-Free Kit (Illumina). DNA was fragmented to an average length of 350 bp by sonication. Libraries were validated according to standard procedures and sequenced via 150 bp paired-end on a NovaSeq 6000 platform. Reads were aligned using the mem algorithm of the Burrows-Wheeler Aligner version 0.7.5a and aligned to the hg19 reference with decoy sequences and masked pseudo autosomal regions. Base quality scores are recalibrated using GATK[24] (version 4) BaseRecalibrator with enlarged context size for single-nucleotide variants (SNVs) and insertions and deletions (indels) of, respectively, 4 and 8 bp (instead of the default values 2 and 3). Variants were called and inspected both with GATK and custom scripts. Data are annotated with custom in house scripts using refSeq genes.

Whole-genome sequencing (WGS) data of ABE7.10/gWRA-treated and -untreated STAT3[+/R382W] fibroblasts were analyzed and compared to search for treatment-induced SNVs and indel variants. A deliberately low threshold of 3 supporting reads to call a variant was set, requiring a minimum of 20 reads on the position to retain

it. To avoid confounding errors, we restricted only to the high confidence regions calculated by the Genome in a Bottle consortium,[25] we rejected repeats as marked in UCSC RepeatMasker[26,27] and low complexity regions. We required a minimum mapping quality of 30 in the Phred quality score and a minimum base quality of 20 for the genomic distribution analysis, and a minimum mapping quality of 50 in the Phred quality score and a minimum base quality of 25 for all other analyses. The genome was divided into 1279 similarly sized chunks and searched for variants uniquely detected in the ABE7.10/gWRA-treated sample and not in the untreated sample and vice versa.

Structural variants were called using a set of different structural variant callers: BreakDancer,[28,29] Delly,[30] CNVnator,[31] Lumpy-SV,[32] Manta,[33] and Pindel[34,35] focusing on insertions, deletions, inversions, duplications, and translocations. The variants of each caller were combined together when overlap was detected for two separate calls of the same variant class.

Potential integration of plasmid DNA was assessed by checking the presence of the plasmid sequences in the WGS data. To test for integration of the detected plasmid sequences, we analyzed read pairs in which one read mapped on the plasmid sequence and the other read on the human nuclear genome. We inspected the reads manually using the Integrative Genomics Viewer.[36] Of each pair, we scanned both the read on the plasmid and the read on the nuclear genome for signs of integration, for example, the sequence being disrupted from a certain point to the 3′- or 5′-end. Second, we inspected the nearby region to the matched read on the nuclear genome to detect signs of an insertion, for example, reads whose alignment is disrupted from a certain position on. To avoid confounding effects, we compared simultaneously the reads from our WGS sample from both the alignments with and without plasmid sequence and we added a different genomic sample to avoid reference genome effects.

Off-target sites predicted using CRISPOR[22] and CCTop[20] were analyzed using the WGS data. Further sites were tested by independently aligning the protospacer sequence of gWRA to the hg19 reference genome and evaluating variants in nearby sites (±45 bp). Variants uniquely detected in the ABE7.10/gWRA-treated and not the untreated sample were analyzed by Levenshtein distance analysis for potential binding of the sgRNA gWRA in a sliding window starting 45 bp upstream and ending 45 bp downstream of each variant position as previously reported.[37]

High-throughput sequencing

Primers for the *STAT3* target region and exonic gWRA off-targets with four mismatches predicted by CRISPOR[22] and CCTop[20] were designed to amplify 450- to 500-bp-long amplicons (Supplementary Table S1) centered on the off-target regions. The adapter sequence 5′-ACACTCTTTCCCTACACGACGCTCTTCCGATCT-3′ was attached to forward primers and 5′-GACTGGAGTT CAGACGTGTGCTCTTCCGATCT-3′ to reverse primers at the 5′-end. PCR amplicons were sent for high-throughput sequencing (HTS) and subsequent commercial bioinformatic analysis (Eurofins Genomics). Sequencing was performed on an Illumina MiSeq with an average of 80,000 to 90,000 read pairs per amplicon.

STAT3 DNA-binding enzyme-linked immunosorbent assay (TransAM)

Nuclear extracts of unstimulated and IL-6 (20 ng/mL for 20 min) (Biochrom)-stimulated STAT3$^{+/R382W}$ fibroblasts were prepared with the Nuclear Extract Kit (Active Motif) according to the manufacturer's instructions. Nuclear extract protein concentrations were measured via the Bradford assay (Bio-Rad), and STAT3 DNA-binding activity was analyzed via STAT3 TransAM (Active Motif) according to the manufacturer's instructions.

Quantitative real-time PCR

RNA isolations from unstimulated and IL-6 (20 ng/mL for 60 min) (Biochrom)-stimulated STAT3$^{+/R382W}$ fibroblasts were performed with the innuPREP RNA Mini Kit 2.0 (Analytik Jena) with DNase digestion according to the manual. cDNA was generated by the High-Capacity cDNA Reverse Transcription Kit (Applied Biosystems) according to the manufacturer's instructions. Gene expression was analyzed by quantitative real-time PCR in SsoAdvanced Universal SYBR Green Supermix and a CFX Connect Real-Time PCR Detection System (Bio-Rad); primer sequences are listed in Supplementary Table S1. Relative target gene expression of *CCL2* and *SOCS3* relative to expression of *TATA-box-binding-protein* (*TBP*) was performed as described previously.[16]

Western blot

Western blot analysis was performed using 10–15 μg of nuclear extracts. Following sodium dodecyl sulfate–polyacrylamide gel electrophoresis (SDS-PAGE) with NuPAGE 4–12% Bis-Tris protein gels (Invitrogen), blots were probed with phospho-stat3 (Tyr705) (3E2) mouse mAb (1:1000) and TBP (D5C9H) XP rabbit mAb (1:1000; all Cell Signaling Technology) and developed with secondary antibodies stabilized goat anti-rabbit/anti-mouse IgG, peroxidase conjugated (Thermo Scientific) and Super Signal West Femto Maximum Sensitivity Substrate Kit (Thermo Scientific) and an Intas ChemoCam imaging device (Intas Science Imaging Instruments GmbH). Page Ruler Prestained Protein

Ladder (Thermo Scientific) was used as a size standard. Quantification was performed using LabImage 1D (Intas Science Imaging GmbH).

Statistical analysis

Data were analyzed by two-way ANOVA to check for overall differences and with a Bonferroni's post-test comparing each sample with the untreated cell population using GraphPad Prism software (version 5.03), unless noted otherwise. For all graphs, the mean and individual measurements from the indicated number of independent experiments are shown.

Results and Discussion

To correct *STAT3* c.1144C>T/p.R382W, we designed the sgRNA gW382R-ABE (gWRA) with the protospacer sequence 5′-ATTTCCAGGATCTGAATCAC-3′ (Fig. 1). gWRA was constructed to specifically target the mutation site to enable editing of the pathogenic A·T base pair resulting from the p.R382W mutation. When using gWRA, no additional adenines except the pathogenic A·T base pair causing the p.R382W mutation lie in the editing window of ABE7.10, reducing the likelihood of unwanted editing effects at the target site.

To check the specificity of gWRA, we performed *in silico* off-target analyses using CCTop[20] and CRISPOR[22] and found predicted off-target sites distributed over the whole genome (Supplementary Fig. S1). All predicted exonic off-targets had at least four mismatches between the target sequence and the human genome, while no off-target sequences with fewer than three mismatches comprising intronic and intergenic regions were predicted.

To test the functionality of the sgRNA gWRA, we successfully induced double strand breaks (DSBs) in a PCR fragment containing the target sequence using preassembled RNP complexes of gWRA and recombinant Cas9 protein (Supplementary Fig. S2A).

Since fibroblasts have been shown to play a fundamental role in impaired wound healing and angiogenesis in STAT3-HIES,[38] they provide a valuable *ex vivo* model to investigate ABE-mediated gene repair. Thus, we isolated skin fibroblasts of an STAT3-HIES patient with a heterozygous *STAT3* p.R382W mutation (STAT3$^{+/R382W}$ fibroblasts) and found a pronounced defect in STAT3 function (Supplementary Fig. S3). To confirm functionality of gWRA in primary cells, we transfected the STAT3$^{+/R382W}$ fibroblasts with Cas9/gWRA RNPs. DNA isolated 48 h after RNP transfection showed aberrant sequences starting from the expected cutting site, indicating indels and thus a successful induction of DSBs at the mutation site (Supplementary Fig. S2B).

To correct the STAT3 p.R382W mutation, we used a plasmid encoding ABE7.10 under CMV promoter control in combination with a plasmid encoding the sgRNA gWRA under U6 promoter control and transfected both plasmids into STAT3$^{+/R382W}$ fibroblasts. Sanger sequencing of the targeted mutation site revealed a decrease of the monoallelic adenine signal in the chromatogram of a heterogeneous bulk population of ABE7.10/gWRA-treated cells compared with green fluorescent protein-treated cells. An analysis of the Sanger sequences via EditR[23] revealed a robust editing efficiency of $29\% \pm 7\%$ 48 h after electroporation in a set of three experiments (Supplementary Fig. S4).
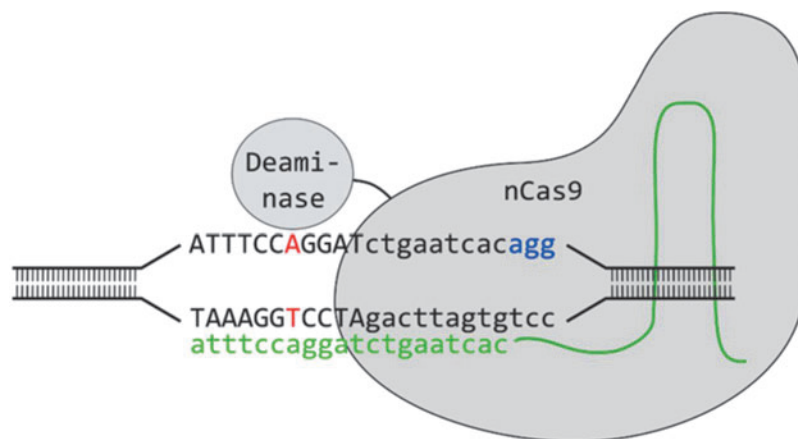

FIG. 1. *STAT3* R382W-specific adenine base editing complex. Schematic base editing complex consisting of the ABE (deaminase) linked to Cas9 D10A nickase (nCas9). The target-specific sequence of the sgRNA gWRA is shown in *green*; *upper case*: exonic sequence; *lower case*: intronic sequence; *red letter*: mutation site; *blue letters*: PAM sequence. ABE, adenine base editor; PAM, protospacer adjacent motif; sgRNA, single-guide RNA.

To validate the editing efficiency at the target site and to investigate potential gRNA-dependent and -independent off-target effects, we assessed a bulk population of ABE7.10/gWRA-treated and -untreated STAT3$^{+/R382W}$ fibroblasts using deep WGS with an increased coverage of >70× and HTS. WGS and HTS data revealed a high editing efficiency of ABE7.10/gWRA-treated STAT3$^{+/R382W}$ fibroblasts of 39% and 46%, respectively, at the target site compared with untreated cells (Supplementary Fig. S5).

Searching for off-targets in ABE7.10/gWRA-treated STAT3$^{+/R382W}$ fibroblasts, we analyzed every detectable SNV or short indel supported by a minimum base quality of 25 in at least 3 reads with minimum mapping quality of 50, both in the Phred scale, on the *Genome in a Bottle consortium* callable regions.[39] SNVs present in ABE7.10/gWRA-treated and -untreated STAT3$^{+/R382W}$ fibroblasts were excluded as cell intrinsic.

Analyzing the genomic distribution, no genomic hotspot with a considerable increase in unique SNVs was found in ABE7.10/gWRA-treated compared with untreated cells (Fig. 2A). To reduce potential sequencing errors, a subsequent filtration allowing two supporting reads on the untreated sample was applied before analysis of variant distribution. No increase in the A·T to G·C fraction in ABE7.10/gWRA-treated cells compared with untreated cells and an internal control was detected (Fig. 2B). Thus, our results indicated no distinct global effect of the ABE7.10/gWRA treatment.

To examine for possible dependency of variants unique to ABE7.10/gWRA-treated STAT3$^{+/R382W}$ fibroblasts on the specific gRNA sequence, we analyzed potential gWRA binding sites in proximity to the variant sites using Levenshtein distance analysis (Fig. 2C and Supplementary Table S2). The minimum Levenshtein distance indicates differences in the sequence in proximity to a detected SNV compared with the gWRA protospacer sequence. Since for all SNVs the minimum Levenshtein distance was four and for A·T to G·C conversions six, any detected variants were likely independent of gRNA binding. Thus, the detected variants are caused by naturally occurring mutations during cell culturing rather than by the ABE7.10/gWRA treatment.

The detected variation between samples might also be a result of false-positive variants due to the low threshold chosen for variant calling of three supporting reads. Plotting the distribution of variants uniquely detected in the different samples per 1 Mbp genomic chunk to compare ABE7.10/gWRA-treated and untreated STAT3$^{+/R382W}$ fibroblasts, and the two internal controls, revealed scarcely any differences between the corresponding samples (Supplementary Fig. S6). The narrower curve of the internal controls is explained by the lower target coverage (40× instead of >70×) resulting in fewer detected variants per 1Mbp genomic chunk.

When examining potential off-target sites predicted by CCTop and CRISPOR,[20,22] we analyzed every alteration detected in at least two reads to obtain the highest sensitivity possible using WGS data. We did not detect any alterations in predicted exonic, intronic, or intergenic off-target sites (Supplementary Table S3). We did detect one G>T alteration at chr15:85121513 within a sliding window of 45 bp up- and downstream of the predicted off-target region at chr15:85121446-85121468. As C>A and thus G>T conversions have only been reported as rare and "unanticipated mutations" within the gRNA-specific ABE target site,[40,41] the SNV is probably a result of genetic drift during cell culturing or a false-positive variant due to the low threshold of two supporting reads rather than a real off-target event. A

FIG. 2. WGS data analysis. **(A)** Substantially symmetric patterns in genomic distribution of the absolute number of SNVs per megabase uniquely detected in untreated (pointing *downward*, *light colors*) and ABE7.10/gWRA-treated (pointing *upward*, *dark colors*) STAT3$^{+/R382W}$ fibroblasts suggest a dependency on the sequencing content and complexity rather than on real variant patterns. Different *colors* indicate different chromosomes. **(B)** Relative distribution of SNVs of total genetic variants detected in WGS data of untreated (*white dots*) and ABE7.10/gWRA-treated STAT3$^{+/R382W}$ fibroblasts (*gray dots*) compared with two control genomes from two different tissues of one person analyzed on the same platform with equally prepared libraries (*black lines*) showed no increase in A·T to G·C conversions in treated cells. **(C)** Levenshtein analysis of edits (SNVs, deletions, insertions) necessary to align the protospacer sequence of sgRNA gWRA to the genomic region 45 bp up- and downstream of each variant unique to the ABE7.10/gWRA-treated STAT3$^{+/R382W}$ fibroblasts. The minimum Levenshtein distance of all detected SNVs (*white bars*) in ABE7.10/gWRA-treated STAT3$^{+/R382W}$ fibroblasts was four, whereas the minimum Levenshtein distance of all A/T>G/C SNVs (*gray bars*) was six. **(D)** Substantially symmetric patterns in genomic distribution of the absolute number of indel variants per megabase uniquely detected in untreated (pointing *downward*, *light colors*) and ABE7.10/gWRA-treated (pointing *upward*, *dark colors*) STAT3$^{+/R382W}$ fibroblasts suggest a dependency on the sequencing content and complexity rather than on real variant patterns. Different *colors* indicate different chromosomes. SNVs, single-nucleotide variants; WGS, whole-genome sequencing.
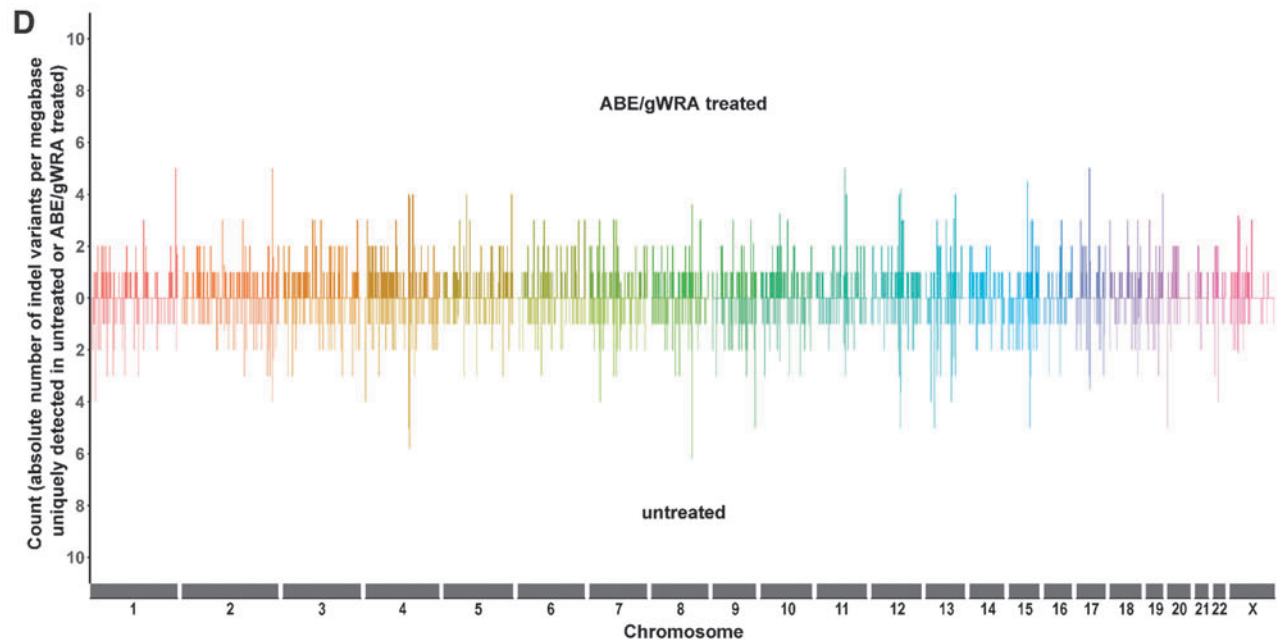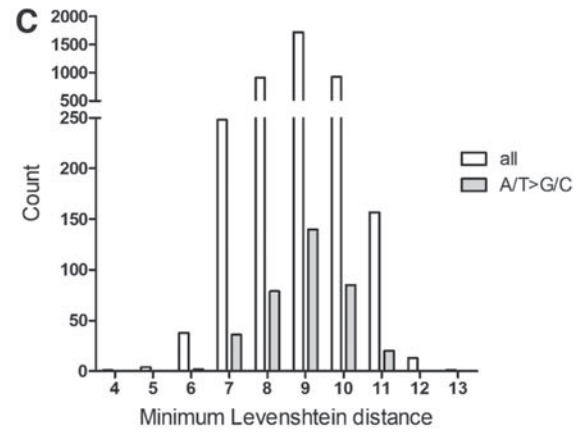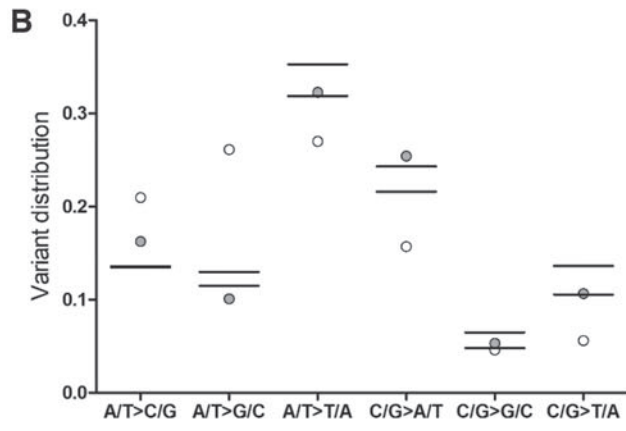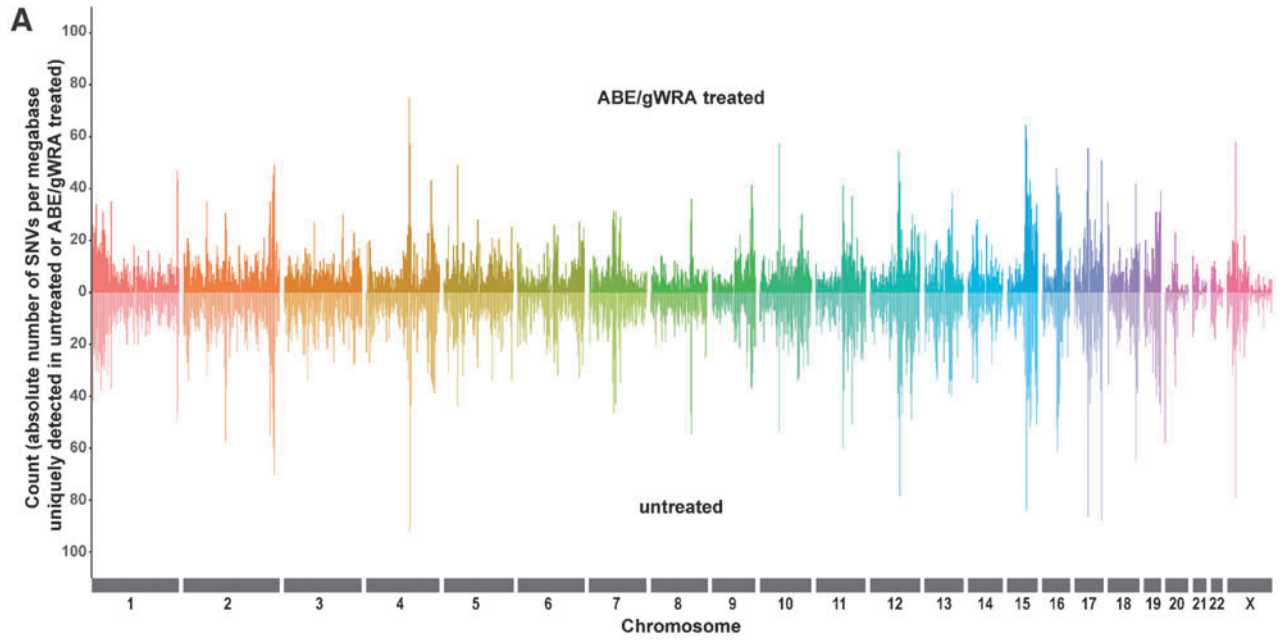
more detailed analysis using HTS neither observed off-target effects and all detected variants were present in comparable frequencies in ABE7.10/gWRA-treated and -untreated STAT3$^{+/R382W}$ fibroblasts (Supplementary Table S4). HTS of the *STAT3* target site, however, showed A·T to G·C variants with a low, yet higher frequency in ABE7.10/gWRA-treated than in untreated STAT3$^{+/R382W}$ fibroblasts (Supplementary Table S5). The most commonly detected A·T to G·C variant (*STAT3* c.1141T>C, p.S381P) had a frequency of about 1.1% in the HTS data and was also identified in the WGS data (Supplementary Fig. S5A and Supplementary Table S5). Despite the fact that all detected A·T to G·C variants were also identified in untreated STAT3$^{+/R382W}$ fibroblasts, the higher frequency indicates a potential adverse effect mediated by ABE7.10/gWRA editing at the target site, which may need a more detailed investigation if not resolved by using further developed ABE systems.

No significant induction of DSBs by the ABE7.10 treatment was observed. Indels uniquely detected in ABE7.10/gWRA-treated and -untreated STAT3$^{+/R382W}$ fibroblasts were similarly distributed across the genome in both samples (Fig. 2D). All major structural variants detected were found in treated and untreated samples. Consequently, no plasmid integration into the genome was observed in contrast to findings in DSB-mediated Cas9 approaches.[42] Reads from both plasmids used were detected with a low coverage (pBS-U6-gWRA: 2.29×, pCMV-ABE7.10: 3.87×) representing a plasmid fraction remaining in the treated fibroblasts during cultivation for seven passages after electroporation.

Thus, we can confirm the low frequency of off-target effects of ABE7.10[11,40,43] and speculate that the observed putative adverse effects at the target site can be resolved by using the ABE system in the form of RNPs instead of plasmids or advanced ABE systems.

To assess whether ABE7.10/gWRA treatments improve the disturbed STAT3 function upon IL-6 stimulation in STAT3$^{+/R382W}$ fibroblasts, we generated corrected single-cell clones (repaired SCCs) from ABE7.10/gWRA-treated STAT3$^{+/R382W}$ fibroblasts (bulk gWRA). The bulk gWRA population was corrected with an efficiency of 29% compared with a non-target control as estimated by Sanger sequencing and EditR analysis. Chromatograms of the Sanger sequencing showed a reduced mutation-specific adenine peak in bulk gWRA and the complete correction of the mutation in repaired SCCs compared with untreated and ABE7.10/non-target control-treated cells 48 h after transfection (Fig. 3A).

For functional analysis, untreated STAT3$^{+/R382W}$ fibroblasts, non-target control, and bulk gWRA STAT3$^{+/R382W}$ fibroblasts, as well as repaired SCCs, were stimulated with IL-6, and nuclear extracts were evaluated using Western blot and TransAM DNA-binding enzyme-linked immunosorbent assay (Fig. 3B, C). Quantification of Western blot band intensities (Fig. 3B and Supplementary Table S6) showed that the amount of nuclear phosphorylated—hence activated—STAT3 (pSTAT3) increased slightly in bulk gWRA (1.5±0.7-fold) and markedly in repaired SCCs (2.4±1.0-fold) compared with untreated patient cells. Since STAT3 phosphorylation is not affected by the STAT3 p.R382W mutation, the observed differences in the level of nuclear pSTAT3 are likely caused by DNA binding-mediated nuclear retention.[3,44] Improved functionality of STAT3 was further confirmed by a slightly increased DNA-binding activity in bulk gWRA (1.9±0.7-fold) and by a significant increase in repaired SCCs (3.5±1.4-fold) upon stimulation compared with untreated cells (Fig. 3C).

To investigate restored STAT3 downstream signaling, we measured mRNA levels of the STAT3 target genes *CCL2*

FIG. 3. Adenine base editing of STAT3$^{+/R382W}$ fibroblasts and functional analysis of untreated, non-target control treated, and edited STAT3$^{+/R382W}$ fibroblasts. **(A)** gDNA chromatograms of untreated, non-target control treated, and ABE7.10/gWRA-treated (bulk gWRA) STAT3$^{+/R382W}$ fibroblasts and a successfully edited single-cell clone (repaired SCC) sequenced in reverse show a shift from adenine (A) to guanine (G) in bulk gWRA, whereas the successfully repaired SCC completely lost the A signal. **(B)** Western blot analysis of nuclear extracts, **(C)** TransAM DNA-binding assay and **(D, E)** quantitative real-time PCR of unstimulated (−) or IL-6-stimulated (+) untreated, non-target control treated, ABE7.10/gWRA-treated (bulk gWRA) STAT3$^{+/R382W}$ fibroblasts, and successfully repaired single-cell clones (repaired SCCs) show **(B)** increased nuclear translocation of STAT3 phosphorylated at Tyr705 (pSTAT3) (nuclear loading control TBP), **(C)** significantly increased STAT3 DNA-binding activity, and **(D)** significantly increased expression of *CCL2* and **(E)** *SOCS3* in repaired SCCs compared with untreated STAT3$^{+/R382W}$ fibroblasts. Target gene expression was assessed relative to the housekeeping gene *TBP*. Bars indicate mean values, dots individual experiments, error bars represent SEM, significant differences *$p < 0.05$, ***$p < 0.001$ assessed by two-way ANOVA and Bonferroni post-test. IL-6, interleukin-6; PCR, polymerase chain reaction; SEM, standard error of the mean; TBP, TATA-box-binding-protein.
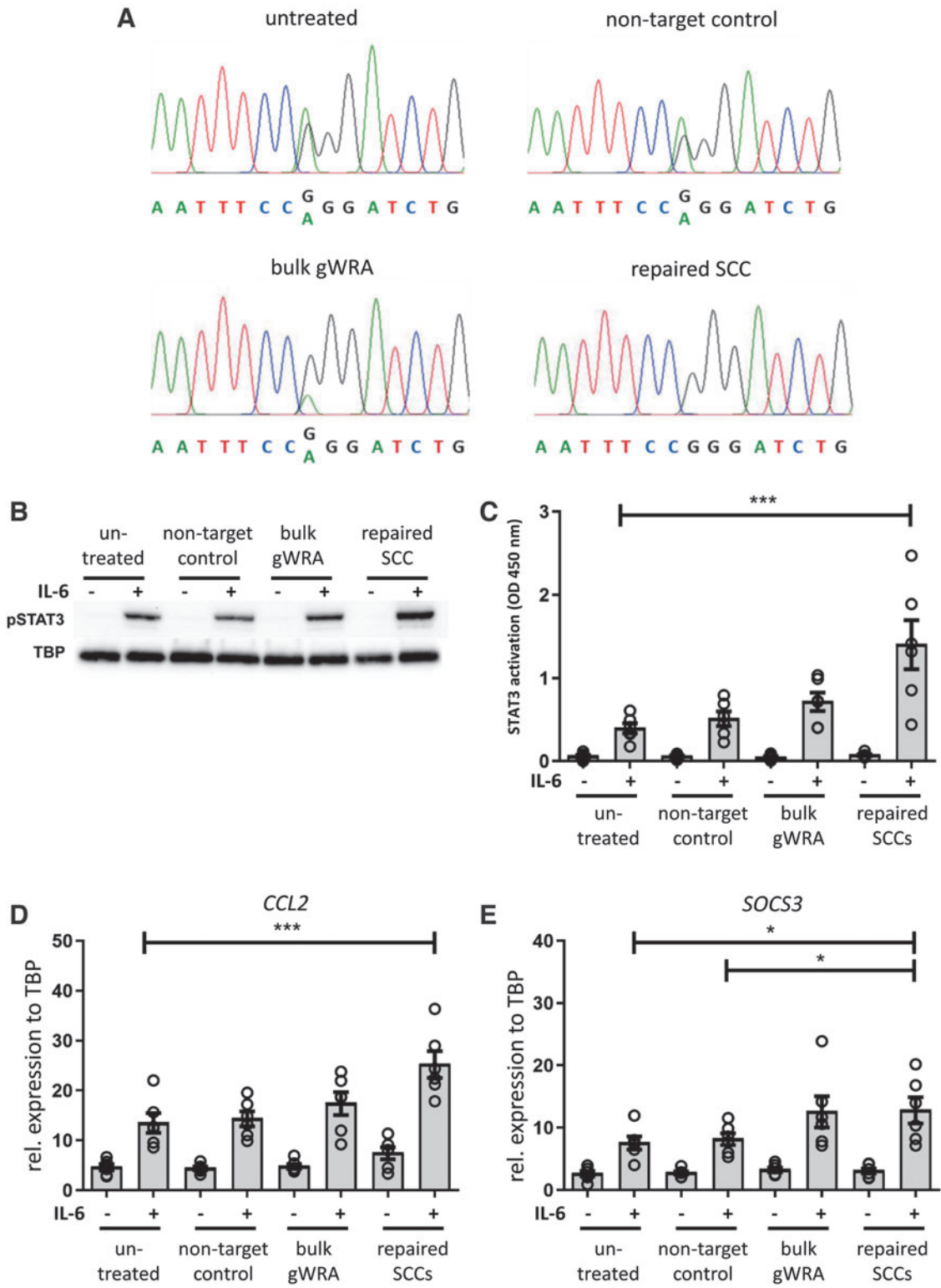
and *SOCS3* after IL-6 stimulation.[45] Comparing stimulated untreated, non-target control treated, and ABE7.10/gWRA-treated STAT3[+/R382W] fibroblasts *SOCS3* expression was increased in bulk gWRA (1.7 ± 0.8-fold) compared with untreated cells, while *SOCS3* and *CCL2* expression was significantly increased in repaired SCCs (*SOCS3*: 1.7 ± 0.4-fold; *CCL2*: 1.9 ± 0.2-fold) (Fig. 3D, E). Non-target control-treated STAT3[+/R382W] fibroblasts were comparable with untreated cells indicating no unspecific effect due to the treatment alone.

To estimate the functional impact of the STAT3 correction in comparison with the wild-type STAT3 function, we isolated fibroblasts of healthy individuals and repeated the above experiment analyzing STAT3 target gene expression in these healthy control fibroblasts compared with untreated and ABE7.10/gWRA-treated STAT3[+/R382W] fibroblasts (Fig. 4A, B). Expression levels after stimulation were comparable or slightly higher in repaired SCCs than in healthy control fibroblasts. Thus, ABE7.10/gWRA gene editing significantly improved STAT3 function and provides a first proof-of-concept warranting further exploration of base editing as a therapeutic approach in STAT3-HIES.

Several cell types have been reported as reduced in function or number in STAT3-HIES patients, including, but not limited to, fibroblasts and pulmonary and hematopoietic cells.[1–5,7,38] To evaluate ABE-mediated gene repair in a cell type of direct relevance for complementary cellular therapy, we reprogrammed STAT3[+/R382W] fibroblasts to iPSCs. After reprogramming, STAT3[+/R382W] iPSC colonies were successfully checked for iPSC identity by morphology and immunofluorescence staining with the pluripotency factors OCT4, SOX2, NANOG, and LIN28 (Supplementary Fig. S7A, B). Pluripotency was further validated by directed *in vitro* differentiation into the progenitor progeny of the three germ layers: ectoderm, mesoderm, and endoderm. Although some variation compared with control iPSCs was observed, STAT3[+/R382W] iPSCs showed expression of the respective germ layer markers after differentiation (Supplementary Fig. S7C).

While treating STAT3[+/R382W] iPSCs with the ABE7.10/gWRA system resulted in no detectable editing, we obtained an editing efficiency of $30\% \pm 6\%$ with ABEmax, a refined version of ABE7.10 (Supplementary Fig. S8).[46] Sanger sequencing of all CCTop[20] and CRISPOR[22] predicted off-target sites classified as exonic showed no off-target editing in two selected single-cell clones (Supplementary Table S7). Furthermore, ABE-treated STAT3[+/R382W] iPSCs showed preserved plasticity by their capability to successfully differentiate to lung progenitor cells and alveolar organoids (Supplementary Fig. S9). Preserved plasticity of iPSCs after ABE treatment is an essential prerequisite in regard to differentiation of corrected iPSCs to therapeutically relevant somatic cells.
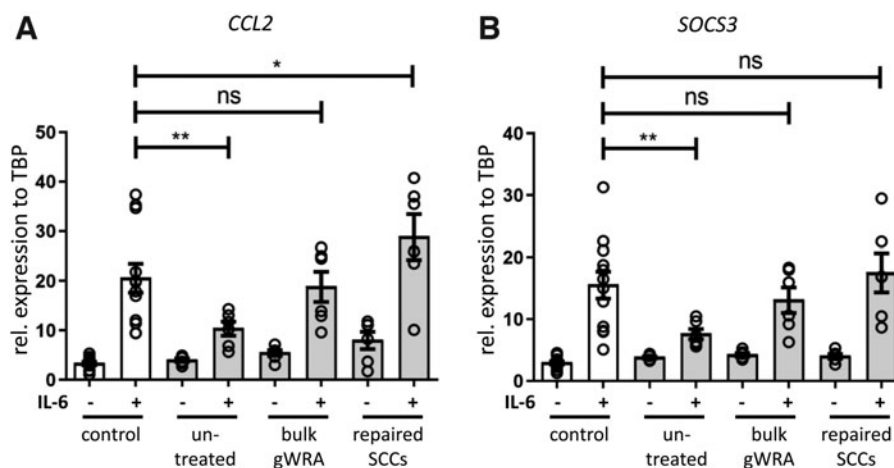

FIG. 4. Comparison of STAT3 target gene expression of healthy control and adenine base-edited STAT3[+/R382W] fibroblasts. **(A, B)** Quantitative real-time PCR of unstimulated (−) or IL-6-stimulated (+) healthy control, untreated, ABE7.10/gWRA-treated (bulk gWRA) STAT3[+/R382W] fibroblasts, and successfully edited single-cell clones (repaired SCCs) show significantly decreased expression of **(A)** *CCL2* and **(B)** *SOCS3* in IL-6-stimulated untreated STAT3[+/R382W] fibroblasts and comparable (ns) or increased expression in bulk gWRA STAT3[+/R382W] fibroblasts and repaired SCCs compared with control fibroblasts. Target gene expression was assessed relative to the housekeeping gene *TBP*. *Bars* indicate mean values, dots individual experiments, error bars represent SEM, significant differences *$p < 0.05$, **$p < 0.01$ assessed by two-way ANOVA and Bonferroni post-test. ns, not significant.

In addition to these results, the successful use of ABEs in cellular and animal models of other monogenic diseases, such as Xeroderma pigmentosum, tyrosinemia, Duchenne muscular dystrophy, and Hutchinson/Gilford progeria syndrome, confirms that ABEs are a promising tool for the treatment of monogenic diseases lacking a curative therapy option such as STAT3-HIES.[47–50] However, additional studies concerning the safety of ABEs are required. In this regard, developments such as the ABE variant ABEmaxAW or alternative forms of delivery, for example, ABE RNP instead of ABE encoding plasmid, might further improve the safety profile of the treatment modality.[51]

As potential therapeutic strategies in the multiorgan disease STAT3-HIES, ABE-mediated base editing may be considered for *ex vivo* and *in vivo* therapeutic approaches. These approaches could consist of using patient iPSC-derived therapeutically relevant cell types for cell replacement therapy or directly inhaling ABE/gRNA-loaded adeno-associated virus particles or RNA-based gene editing systems for functional repair of lung tissue, the latter comparable with concepts being tested for cystic fibrosis.[52–54]

To further test the applicability and safety of ABE-based gene therapy in STAT3-HIES, additional studies using appropriate models are needed. Thus far, no animal model harboring the STAT3 p.R382W mutation is available to test therapeutic applications. Human organoid systems derived from patient iPSCs might provide a valuable model to further address off-target effects and treatment efficacy in a human model.

Currently, there is no agreed-upon best method to monitor possible off-target effects and to distinguish these effects from spontaneous mutations and individual variation. Thus, best practice standards, required for safety considerations and ethical implications, need to be developed to ensure responsible translation into clinical practice.[55–57] To facilitate exchanges on best practice standards and to centralize information, all clinical trials with ABE should be registered with the newly launched WHO registry on human genome editing[58] and should fulfill any national regulatory frameworks as well as the governance standards yet to be developed by the WHO.[59,60]

Conclusion

The successful functional rescue of STAT3 signaling in STAT3-HIES patient fibroblasts and the effective repair of iPSCs derived from patient fibroblasts are an important proof-of-principle for the therapeutic applicability of gene editing in the treatment of STAT3-HIES and other primary immunodeficiencies. However, building upon this proof-of-principle, further studies are needed to demonstrate therapeutic applicability. Furthermore, to create responsible approaches toward translation into broader clinical use, best practice standards for appropriate analysis of the safety and ethical implications of gene editing are urgently needed.

Authors' Contributions

A.C.E., A.M., C.W., R.B., E.R., A.P., M.T.K., C.V., M.P., A.S., and E.G. designed and performed the research and analyzed data; F.G., R.E., M.D., T.M.S., T.M., T. S., B.H., and E.D.R. designed and supervised the research and analyzed data; T.V. consented individuals and provided human biomaterial; A.M.B. evaluated the ethical aspects. All authors reviewed the article and contributed to the writing.

Acknowledgments

Author Disclosure Statement

The authors declare no conflicts of interest except for A.M.B. who is a member of the WHO Expert Advisory Committee on Developing Global Standards for Governance and Oversight of Human Genome Editing.

Funding Information

Supplementary Material

Supplementary Figure S1
Supplementary Figure S2
Supplementary Figure S3
Supplementary Figure S4
Supplementary Figure S5
Supplementary Figure S6
Supplementary Figure S7
Supplementary Figure S8
Supplementary Figure S9
Supplementary Table S1
Supplementary Table S2
Supplementary Table S3
Supplementary Table S4
Supplementary Table S5
Supplementary Table S6
Supplementary Table S7

References

1. Minegishi Y, Saito M, Tsuchiya S, et al. Dominant-negative mutations in the DNA-binding domain of STAT3 cause hyper-IgE syndrome. *Nature.* 2007;448:1058–1062. DOI: 10.1038/nature06096.

2. Holland SM, DeLeo FR, Elloumi HZ, et al. STAT3 mutations in the hyper-IgE syndrome. *N Engl J Med.* 2007;357:1608–1619. DOI: 10.1056/NEJMoa073687.

3. Renner ED, Rylaarsdam S, Anover-Sombke S, et al. Novel signal transducer and activator of transcription 3 (STAT3) mutations, reduced T(H)17cell numbers, and variably defective STAT3 phosphorylation in hyper-IgE syndrome. *J Allergy Clin Immunol.* 2008;122:181–187. DOI: 10.1016/j.jaci.2008.04.037.

4. Chandesris MO, Melki I, Natividad A, et al. Autosomal dominant STAT3 deficiency and hyper-IgE syndrome: Molecular, cellular, and clinical features from a French national survey. *Medicine (Baltimore).* 2012;91:e1–e19. DOI: 10.1097/MD.0b013e31825f95b9.

5. Hagl B, Heinz V, Schlesinger A, et al. Key findings to expedite the diagnosis of hyper-IgE syndromes in infants and young children. *Pediatr Allergy Immunol.* 2016;27:177–184. DOI: 10.1111/pai.12512.

6. Freeman AF, Renner ED, Henderson C, et al. Lung parenchyma surgery in autosomal dominant hyper-IgE syndrome. *J Clin Immunol.* 2013;33:896–902. DOI: 10.1007/s10875-013-9890-5.

7. Kroner C, Neumann J, Ley-Zaporozhan J, et al. Lung disease in STAT3 hyper-IgE syndrome requires intense therapy. *Allergy.* 2019;74:1691–1702. DOI: 10.1111/all.13753.

8. Hsu AP, Davis J, Puck JM, et al. STAT3 hyper IgE syndrome. In: *GeneReviews*®. (Adam MP, Ardinger HH, Pagon RA, et al.; eds). Seattle, WA: University of Washington, Seattle. 1993.

9. Castagnoli R, Delmonte OM, Calzoni E, et al. Hematopoietic stem cell transplantation in primary immunodeficiency diseases: Current status and future perspectives. *Front Pediatr.* 2019;7:295. DOI: 10.3389/fped.2019.00295.

10. Yanagimachi M, Ohya T, Yokosuka T, et al. The potential and limits of hematopoietic stem cell transplantation for the treatment of autosomal dominant hyper-IgE syndrome. *J Clin Immunol.* 2016;36:511–516. DOI: 10.1007/s10875-016-0278-1.

11. Gaudelli NM, Komor AC, Rees HA, et al. Programmable base editing of A*T to G*C in genomic DNA without DNA cleavage. *Nature.* 2017;551:464–471. DOI: 10.1038/nature24644.

12. Pelham SJ, Lenthall HC, Deenick EK, et al. Elucidating the effects of disease-causing mutations on STAT3 function in autosomal-dominant hyper-IgE syndrome. *J Allergy Clin Immunol.* 2016;138:1210–1213.e1215. DOI: 10.1016/j.jaci.2016.04.020.

13. Borchin B, Chen J, Barberi T. Derivation and FACS-mediated purification of PAX3+/PAX7+ skeletal muscle precursors from human pluripotent stem cells. *Stem Cell Rep.* 2013;1:620–631. DOI: 10.1016/j.stemcr.2013.10.007.

14. D'Amour KA, Agulnick AD, Eliazer S, et al. Efficient differentiation of human embryonic stem cells to definitive endoderm. *Nat Biotechnol.* 2005;23:1534–1541. DOI: 10.1038/nbt1163.

15. Shi Y, Kirwan P, Livesey FJ. Directed differentiation of human pluripotent stem cells to cerebral cortex neurons and neural networks. *Nat Protoc.* 2012;7:1836–1846. DOI: 10.1038/nprot.2012.116.

16. Livak KJ, Schmittgen TD. Analysis of relative gene expression data using real-time quantitative PCR and the 2(-Delta Delta C(T)) method. *Methods.* 2001;25:402–408. DOI: 10.1006/meth.2001.1262.

17. Jacob A, Morley M, Hawkins F, et al. Differentiation of human pluripotent stem cells into functional lung alveolar epithelial cells. *Cell Stem Cell.* 2017;21:472–488.e410. DOI: 10.1016/j.stem.2017.08.014.

18. Jacob A, Vedaie M, Roberts DA, et al. Derivation of self-renewing lung alveolar epithelial type II cells from human pluripotent stem cells. *Nat Protoc.* 2019;14:3303–3332. DOI: 10.1038/s41596-019-0220-0.

19. Hawkins F, Kramer P, Jacob A, et al. Prospective isolation of NKX2-1-expressing human lung progenitors derived from pluripotent stem cells. *J Clin Invest.* 2017;127:2277–2294. DOI: 10.1172/JCI89950.

20. Stemmer M, Thumberger T, Del Sol Keyer M, et al. CCTop: An intuitive, flexible and reliable CRISPR/Cas9 target prediction tool. *PLoS One.* 2015;10:e0124633. DOI: 10.1371/journal.pone.0124633.

21. Ladunga I. Finding similar nucleotide sequences using network BLAST searches. *Curr Protoc Bioinformatics.* 2017;58:3 3 1–3 3 25. DOI: 10.1002/cpbi.29.

22. Concordet JP, Haeussler M. CRISPOR: Intuitive guide selection for CRISPR/Cas9 genome editing experiments and screens. *Nucleic Acids Res.* 2018;46:W242–W245. DOI: 10.1093/nar/gky354.

23. Kluesner MG, Nedveck DA, Lahr WS, et al. EditR: A method to quantify base editing from Sanger sequencing. *CRISPR J.* 2018;1:239–250. DOI: 10.1089/crispr.2018.0014.

24. McKenna A, Hanna M, Banks E, et al. The Genome Analysis Toolkit: A MapReduce framework for analyzing next-generation DNA sequencing data. *Genome Res.* 2010;20:1297–1303. DOI: 10.1101/gr.107524.110.

25. Krusche P, Trigg L, Boutros PC, et al. Best practices for benchmarking germline small-variant calls in human genomes. *Nat Biotechnol.* 2019;37:555–560. DOI: 10.1038/s41587-019-0054-x.

26. Chen N. Using RepeatMasker to identify repetitive elements in genomic sequences. *Curr Protoc Bioinformatics.* 2004;Chapter 4:Unit 4.10. DOI: 10.1002/0471250953.bi0410s05.

27. Tarailo-Graovac M, Chen N. Using RepeatMasker to identify repetitive elements in genomic sequences. *Curr Protoc Bioinformatics.* 2009;Chapter 4:Unit 4.10. DOI: 10.1002/0471250953.bi0410s25.

28. Chen K, Wallis JW, McLellan MD, et al. BreakDancer: An algorithm for high-resolution mapping of genomic structural variation. *Nat Methods.* 2009;6:677–681. DOI: 10.1038/nmeth.1363.

29. Fan X, Abbott TE, Larson D, et al. BreakDancer: Identification of genomic structural variation from paired-end read mapping. *Curr Protoc Bioinformatics.* 2014;45:15.6.1-11. DOI: 10.1002/0471250953.bi1506s45.

30. Rausch T, Zichner T, Schlattl A, et al. DELLY: Structural variant discovery by integrated paired-end and split-read analysis. *Bioinformatics.* 2012;28:i333–i339. DOI: 10.1093/bioinformatics/bts378.

31. Abyzov A, Urban AE, Snyder M, et al. CNVnator: An approach to discover, genotype, and characterize typical and atypical CNVs from family and population genome sequencing. *Genome Res.* 2011;21:974–984. DOI: 10.1101/gr.114876.110.

32. Layer RM, Chiang C, Quinlan AR, et al. LUMPY: A probabilistic framework for structural variant discovery. *Genome Biol.* 2014;15:R84. DOI: 10.1186/gb-2014-15-6-r84.

33. Chen X, Schulz-Trieglaff O, Shaw R, et al. Manta: Rapid detection of structural variants and indels for germline and cancer sequencing applications. *Bioinformatics.* 2016;32:1220–1222. DOI: 10.1093/bioinformatics/btv710.

34. Ye K, Schulz MH, Long Q, et al. Pindel: A pattern growth approach to detect break points of large deletions and medium sized insertions from paired-end short reads. *Bioinformatics.* 2009;25:2865–2871. DOI: 10.1093/bioinformatics/btp394.

35. Ye K, Guo L, Yang X, et al. Split-read indel and structural variant calling using PINDEL. *Methods Mol Biol.* 2018;1833:95–105. DOI: 10.1007/978-1-4939-8666-8_7.

36. Robinson JT, Thorvaldsdottir H, Wenger AM, et al. Variant review with the integrative genomics viewer. *Cancer Res.* 2017;77:e31–e34. DOI: 10.1158/0008–5472.CAN-17-0337.

37. Moretti A, Fonteyne L, Giesert F, et al. Somatic gene editing ameliorates skeletal and cardiac muscle failure in pig and human models of Duchenne muscular dystrophy. *Nat Med.* 2020;26:207–214. DOI: 10.1038/s41591-019-0738-2.

38. Dmitrieva NI, Walts AD, Nguyen DP, et al. Impaired angiogenesis and extracellular matrix metabolism in autosomal-dominant hyper-IgE syndrome. *J Clin Invest.* 2020;130:4167–4181. DOI: 10.1172/JCI135490.

39. Zook JM, McDaniel J, Olson ND, et al. An open resource for accurately benchmarking small variant and reference calls. *Nat Biotechnol.* 2019;37:561–566. DOI: 10.1038/s41587-019-0074-6.

40. Lee HK, Willi M, Miller SM, et al. Targeting fidelity of adenine and cytosine base editors in mouse embryos. *Nat Commun.* 2018;9:4804. DOI: 10.1038/s41467-018-07322-7.

41. Liu Z, Lu Z, Yang G, et al. Efficient generation of mouse models of human diseases via ABE- and BE-mediated base editing. *Nat Commun.* 2018;9:2338. DOI: 10.1038/s41467-018-04768-7.

42. Kim S, Kim D, Cho SW, et al. Highly efficient RNA-guided genome editing in human cells via delivery of purified Cas9 ribonucleoproteins. *Genome Res.* 2014;24:1012–1019. DOI: 10.1101/gr.171322.113.

43. Jin S, Zong Y, Gao Q, et al. Cytosine, but not adenine, base editors induce genome-wide off-target mutations in rice. *Science.* 2019;364:292–295. DOI: 10.1126/science.aaw7166.

44. Hinde E, Pandzic E, Yang Z, et al. Quantifying the dynamics of the oligomeric transcription factor STAT3 by pair correlation of molecular brightness. *Nat Commun.* 2016;7:11047. DOI: 10.1038/ncomms11047.

45. Griesinger AM, Josephson RJ, Donson AM, et al. Interleukin-6/STAT3 pathway signaling drives an inflammatory phenotype in group A ependymoma. *Cancer Immunol Res.* 2015;3:1165–1174. DOI: 10.1158/2326–6066.CIR-15-0061.

46. Koblan LW, Doman JL, Wilson C, et al. Improving cytidine and adenine base editors by expression optimization and ancestral reconstruction. *Nat Biotechnol.* 2018;36:843–846. DOI: 10.1038/nbt.4172.

47. Lee C, Hyun Jo D, Hwang GH, et al. CRISPR-Pass: Gene rescue of nonsense mutations using adenine base editors. *Mol Ther.* 2019;27:1364–1371. DOI: 10.1016/j.ymthe.2019.05.013.

48. Ryu SM, Koo T, Kim K, et al. Adenine base editing in mouse embryos and an adult mouse model of Duchenne muscular dystrophy. *Nat Biotechnol.* 2018;36:536–539. DOI: 10.1038/nbt.4148.

49. Song C-Q, Jiang T, Richter M, et al. Adenine base editing in an adult mouse model of tyrosinaemia. *Nat Biomed Eng.* 2020;4:125–130. DOI: 10.1038/s41551-019-0357-8.

50. Koblan LW, Erdos MR, Wilson C, et al. In vivo base editing rescues Hutchinson-Gilford progeria syndrome in mice. *Nature.* 2021;589:608–614. DOI: 10.1038/s41586-020-03086-7.

51. Rees HA, Wilson C, Doman JL, et al. Analysis and minimization of cellular RNA editing by DNA adenine base editors. *Sci Adv.* 2019;5:eaax5717. DOI: 10.1126/sciadv.aax5717.

52. Kormann MS, Hasenpusch G, Aneja MK, et al. Expression of therapeutic proteins after delivery of chemically modified mRNA in mice. *Nat Biotechnol.* 2011;29:154–157. DOI: 10.1038/nbt.1733.

53. Mahiny AJ, Dewerth A, Mays LE, et al. In vivo genome editing using nuclease-encoding mRNA corrects SP-B deficiency. *Nat Biotechnol.* 2015;33:584–586. DOI: 10.1038/nbt.3241.

54. Levy JM, Yeh WH, Pendse N, et al. Cytosine and adenine base editing of the brain, liver, retina, heart and skeletal muscle of mice via adeno-associated viruses. *Nat Biomed Eng.* 2020;4:97–110. DOI: 10.1038/s41551-019-0501-5.

55. NCOB. Genome editing—An ethical review. London, England: Nuffield Council on Bioethics. 2016.

56. National Academies of Sciences Engineering, and Medicine; National Academy of Medicine; National Academy of Sciences; Committee on Human Gene Editing. Human Genome Editing: Science, Ethics, and Governance. Human genome editing: Science, ethics, and governance. Washington, DC: National Academies Press. 2017.

57. NCOB. Patient access to experimental treatments. Bioethics Briefing Note of the Nuffield Council on Bioethics. 2018.

58. WHO launches global registry on human genome editing. https://www.who.int/news/item/29-08-2019-who-launches-global-registry-on-human-genome-editing (last accessed April 12, 2021).

59. Cornel MC, Howard HC, Lim D, et al. Moving towards a cure in genetics: What is needed to bring somatic gene therapy to the clinic? *Eur J Hum Genet.* 2019;27:484–487. DOI: 10.1038/s41431-018-0309-x.

60. Nicol D, Eckstein L, Morrison M, et al. Key challenges in bringing CRISPR-mediated somatic cell therapy into the clinic. *Genome Med.* 2017;9:85. DOI: 10.1186/s13073-017-0475-4.

6.2 Cytokine signaling converging on IL11 in ILD fibroblasts provokes aberrant epithelial differentiation signatures

Miriam T. Kastlmeier[1], Erika Gonzalez-Rodriguez[1], Phoebe Cabanis[1], Eva M. Guenther[1], Ann-Christine Koenig[2], Lianyong Han[1], Stefanie M. Hauck[2], Fenja See[1], Sara Asgharpour[1], Christina Bukas[3], Gerald Burgstaller[1], Marie Piraud[3], Mareike Lehmann[1,4], Rudolf A. Hatz[5], Juergen Behr[6], Tobias Stoeger[1], Anne Hilgendorff[1,7]* and Carola Voss[1]*

[1] Institute of Lung Health and Immunity, Helmholtz Center Munich, German Research Center for Environmental Health (GmbH), Comprehensive Pneumology Center Munich with the CPC-M bioArchive, Member of the German Center of Lung Research (DZL), Munich, Germany

[2] Metabolomics and Proteomics Core (MPC), Helmholtz Center Munich, German Research Center for Environmental Health (GmbH), Munich, Germany

[3] Helmholtz AI, Helmholtz Center Munich, German Research Center for Environmental Health (GmbH), Munich, Germany

[4] Institute for Lung Research, Philipps-University Marburg, Universities of Giessen and Marburg Lung Center, Member of the German Center for Lung Research (DZL), Marburg, Germany

[5] Klinik für Thoraxchirurgie, Asklepios Fachkliniken München-Gauting, Thoraxchirurgie, Munich, Germany

[6] Department of Medicine V, University Hospital, Ludwig-Maximilians University Munich, Comprehensive Pneumology Center, Member of the German Center for Lung Research (DZL), Munich, Germany

[7] Dr. von Haunersche Children's Hospital, Hospital of the Ludwig-Maximilians University, Member of the German Lung Research Center (DZL), Munich, Germany

* Correspondence:
Carola Voss carola.voss@helmholtz-muenchen.de
Anne Hilgendorff anne.hilgendorff@med.uni-muenchen.de

Cytokine signaling converging on *IL11* in ILD fibroblasts provokes aberrant epithelial differentiation signatures

Miriam T. Kastlmeier[1], Erika Gonzalez-Rodriguez[1],
Phoebe Cabanis[1], Eva M. Guenther[1], Ann-Christine König[2],
Lianyong Han[1], Stefanie M. Hauck[2], Fenja See[1],
Sara Asgharpour[1], Christina Bukas[3], Gerald Burgstaller[1],
Marie Piraud[3], Mareike Lehmann[1,4], Rudolf A. Hatz[5],
Jürgen Behr[6], Tobias Stoeger[1], Anne Hilgendorff[1,7*]
and Carola Voss[1*]

[1]Institute of Lung Health and Immunity, Helmholtz Center Munich, German Research Center for
Environmental Health (GmbH), Comprehensive Pneumology Center Munich with the CPC-M
bioArchive, Member of the German Center of Lung Research (DZL), Munich, Germany,
[2]Metabolomics and Proteomics Core (MPC), Helmholtz Center Munich, German Research Center for
Environmental Health (GmbH), Munich, Germany, [3]Helmholtz AI, Helmholtz Center Munich, German
Research Center for Environmental Health (GmbH), Munich, Germany, [4]Institute for Lung Research,
Philipps-University Marburg, Universities of Giessen and Marburg Lung Center, Member of the
German Center for Lung Research (DZL), Marburg, Germany, [5]Klinik für Thoraxchirurgie, Asklepios
Fachkliniken München-Gauting, Thoraxchirurgie, Munich, Germany, [6]Department of Medicine V,
University Hospital, Ludwig-Maximilians University Munich, Comprehensive Pneumology Center,
Member of the German Center for Lung Research (DZL), Munich, Germany, [7]Dr. von Haunersche
Children's Hospital, Hospital of the Ludwig-Maximilians University, Member of the German Lung
Research Center (DZL), Munich, Germany

Introduction: Interstitial lung disease (ILD) is a heterogenous group of lung disorders where destruction and incomplete regeneration of the lung parenchyma often results in persistent architectural distortion of the pulmonary scaffold. Continuous mesenchyme-centered, disease-relevant signaling likely initiates and perpetuates the fibrotic remodeling process, specifically targeting the epithelial cell compartment, thereby destroying the gas exchange area.

Methods: With the aim of identifying functional mediators of the lung mesenchymal-epithelial crosstalk with potential as new targets for therapeutic strategies, we developed a 3D organoid co-culture model based on human induced pluripotent stem cell-derived alveolar epithelial type 2 cells that form alveolar organoids in presence of lung fibroblasts from fibrotic-ILD patients, in our study referring to cases of pulmonary fibrosis, as well as control cell line (IMR-90).

Results: While organoid formation capacity and size was comparable in the presence of fibrotic-ILD or control lung fibroblasts, metabolic activity was significantly increased in fibrotic-ILD co-cultures. Alveolar organoids cultured with fibrotic-ILD fibroblasts further demonstrated reduced stem cell function as reflected by reduced Surfactant Protein C gene expression together with an aberrant basaloid-prone differentiation program indicated by elevated Cadherin

2, Bone Morphogenic Protein 4 and Vimentin transcription. To screen for key mediators of the misguided mesenchymal-to-epithelial crosstalk with a focus on disease-relevant inflammatory processes, we used mass spectrometry and characterized the secretome of end stage fibrotic-ILD lung fibroblasts in comparison to non-chronic lung disease (CLD) patient fibroblasts. Out of the over 2000 proteins detected by this experimental approach, 47 proteins were differentially abundant comparing fibrotic-ILD and non-CLD fibroblast secretome. The fibrotic-ILD secretome profile was dominated by chemokines, including CXCL1, CXCL3, and CXCL8, interfering with growth factor signaling orchestrated by Interleukin 11 (IL11), steering fibrogenic cell-cell communication, and proteins regulating extracellular matrix remodeling including epithelial-to-mesenchymal transition. When in turn treating alveolar organoids with IL11, we recapitulated the co-culture results obtained with primary fibrotic-ILD fibroblasts including changes in metabolic activity.

Conclusion: We identified mediators likely contributing to the disease-perpetuating mesenchymal-to-epithelial crosstalk in ILD. In our alveolar organoid co-cultures, we were able to highlight the importance of fibroblast-initiated aberrant epithelial differentiation and confirmed IL11 as a key player in fibrotic-ILD pathogenesis by unbiased fibroblast secretome analysis.

GRAPHICAL ABSTRACT
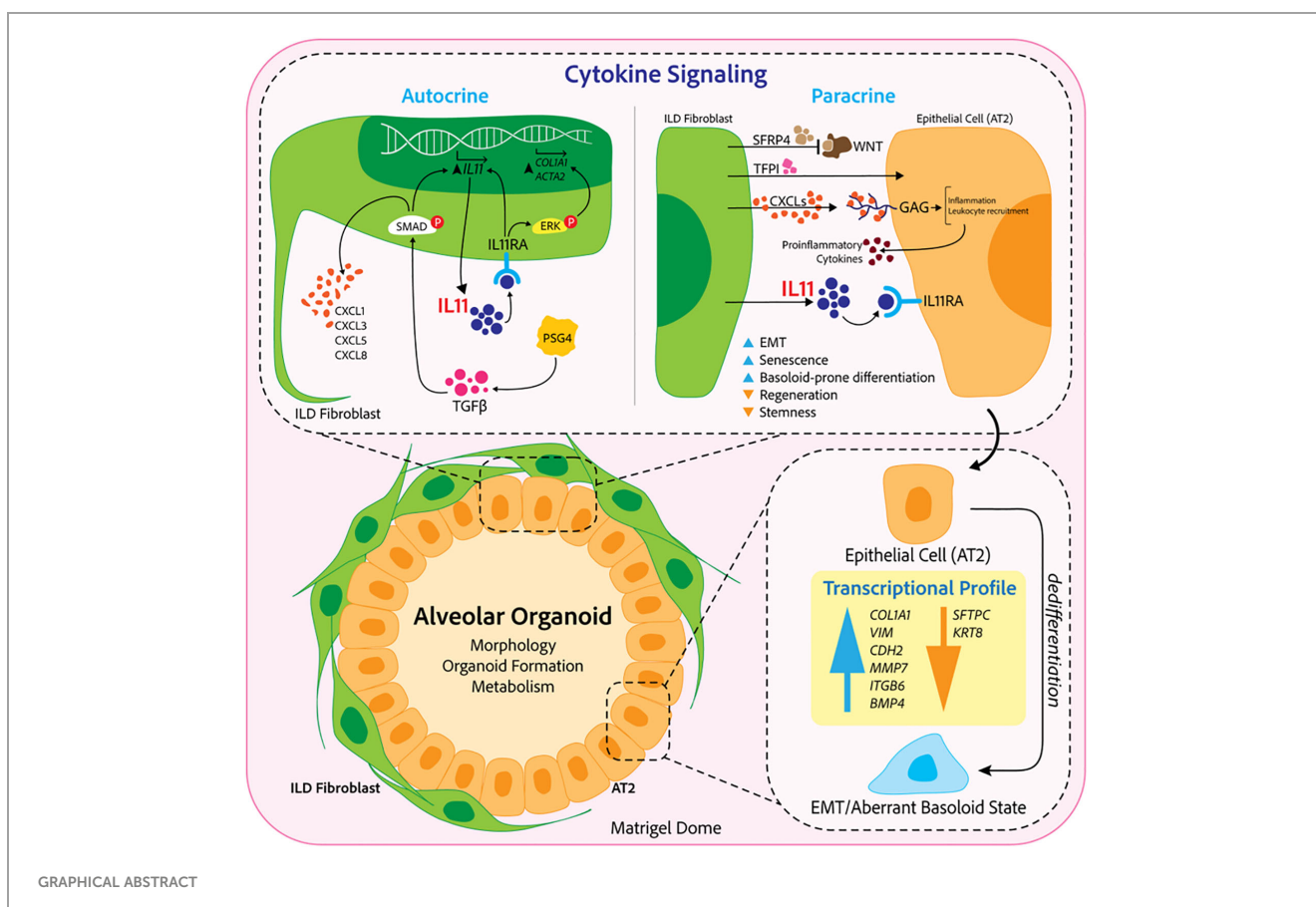
1 Introduction

Interstitial lung diseases (ILDs) comprise a variety of chronic pulmonary conditions that are characterized by structural remodeling of the gas exchange area (1). ILD pathophysiology is centered on sustained inflammation and progressive scarring, ultimately resulting in irreversible tissue destruction and organ failure. Despite the exact pathogenesis of ILD still being unclear, genetic predisposition, age, sex and environmental exposure are known drivers of the disease (2, 3).

In ILD pathogenesis, fibroblast activation occurs through the impact of exogenous stimuli side-by-side with their activation through innate immune cells, especially monocytes and neutrophils, communicating *via* growth factor signaling and cytokine secretion. Subsequently, lactic acid release from fibroblasts as well as epithelial cells, induced by matrix metalloproteinases (MMPs), fibroblast growth factors and metabolic changes in turn further enhances fibroblast activation and accumulation (4). As a result, fibroblasts become the main loci of extracellular matrix (ECM) production and deposition. Induced by repeated inflammatory epithelial injury that leads to further leucocyte attraction and infiltration of the airspace and further perpetuating the pro-fibrotic circle of events, activated fibroblasts are discussed to induce epithelial-to-mesenchymal transition (EMT) in alveolar epithelial cells *via* SMAD and MAPK signaling (5), (6).

Driving and upholding the outlined pathophysiologic processes in ILD that ultimately result in severe tissue destruction and loss of the alveolar epithelium in end-stage ILD, a tightly knit crosstalk between the activated fibroblast and the damaged epithelium has been proposed (7–9). Here, the role of pathologic growth factor signaling and secreted cytokines such as *transforming growth factor ß (TGF-β)* and *Interleukin 17 (IL17)* were highlighted.

Adding to their detrimental role, activated fibroblasts – next to their capacity for pro-fibrotic signaling and EMT induction – have been shown to alter repair and regeneration of the injured gas-exchange area by affecting alveolar epithelial type 2 stem cell potential (10).

To address apparent knowledge gaps in the cytokine-driven, disease-relevant mesenchymal-to-epithelial crosstalk, we used lung organoids derived from human induced pluripotent stem cells (hiPSCs) through chemical directed differentiation into a sophisticated co-culture model. hiPSC-derived alveolar type 2 cells (iAT2s) are recognized as a useful tool to study lung diseases and regeneration capacities, and are recently emerging as a novel tool in environmental and occupational hazard assessment (11, 12). iAT2-derived alveolar organoids recapitulate the characteristic three-dimensional (3D) structure of alveoli and are thereby ideal to mimic important functions of the gas exchange area *in vitro*. Their potential to study pulmonary disease *in vitro* (13, 14) is particularly versatile when targeting underlying molecular mechanisms (3).

By the integration of this sophisticated methodology in a novel co-culture model, we were able to investigate the impact of primary lung fibroblasts from ILD patients, in our study referring to cases of pulmonary fibrosis, on critical functions of hiPSC-derived alveolar organoids. The combination of this approach with unbiased secretome analysis allowed us to delineate functionally relevant signals of the pathologic crosstalk from the lung mesenchyme towards the alveolar epithelium with the aim to identify potential therapeutic targets.

2 Material and methods

2.1 Human induced pluripotent stem cells (hiPSCs) and directed differentiation into lung progenitors

The hiPSC line BU3NGST was kindly provided by Prof. Darrell Kotton, Boston University, Center for Regenerative Medicine. This cell line is a dual-reporter construct composed of fluorochrome-encoding cassettes targeted to the endogenous NKX2.1 and SFTPC loci (BU3 NKX2.1^{GFP}; SFTPC^{tdTomato}) (15). hiPSCs were maintained in mTeSR1 (StemCell Technologies), on Matrigel (Corning) coated cell culture plates at 37°C/5% CO_2 in a cell culture CO_2 incubator. Cells were subcultured by using ReLeSR (StemCell Technologies) or Gentle Cell Dissociation Reagent (StemCell Technologies) (16, 17).

BU3NGSTs were differentiated into NKX2.1$^+$ lung progenitor cells and iAT2s as described previously by Jacob et al. (16, 17). In short, hiPSCs were checked for their pluripotency *via* Alkaline Phosphatase staining (ES Cell Characterization Kit, CHEMICON International) or immunofluorescence staining of TRA 181 and SSEA 4 (ES cell characterization Kit, CHEMICON International). Induction of definitive endoderm was conducted *via* STEMdiff Definitive Endoderm Kit, (StemCell Technologies). On day 14 of differentiation, lung progenitor specification was evaluated by immunofluorescence staining of NKX2.1 (Invitrogen) and Albumin (ALB, R&D Systems). NKX2.1^{GFP+} lung progenitor cells were enriched by GFP signal for NKX2.1 based on a previously described protocol. The sorting was performed by FACS cell sorting at MACSQuant Tyto Cell Sorter (Miltenyi Biotec). For data evaluation FlowJo Version 7.2.1 and v10 was used. Purified lung progenitors were seeded in Matrigel (Corning) domes at a cell density of 50 cells/µL and passaged every second week. To increase SFTPC$^{tdTomato+}$ cells CHIR withdrawal and addback was performed. At day 45 of differentiation, iAT2s were enriched by flow cytometry (MACSQuant Tyto Cell Sorter, Miltenyi Biotec) using tdTomato signal for SFTPC expression and subsequently cultured as 3D alveolar organoids. Differentiated SFTPC$^{tdTomato+}$ iAT2s in 3D Matrigel were grown in CK+DCI medium, with media changes every 48 – 72 h. Alveolar organoids were passaged every 14 days.

2.2 Primary human fibroblast culture

Primary human lung fibroblasts from ILD patients, in our study referring to cases of pulmonary fibrosis,and non-CLD (P4) for co-culture experiments (ILD fibroblasts) and MS based secretome

analysis (ILD and non-CLD fibroblasts) were isolated according to a published protocol (18) and obtained through the CPC-M bioArchive at the Comprehensive Pneumology Center in Munich, Germany.

All patients underwent surgery at the LMU Hospital and the Asklepios Pulmonary Hospital Munich-Gauting. Tissue from ILD patients (n = 3, Table 1) was provided through lung transplantation. Control fibroblasts were derived from lung tissue resections of age-matched non-CLD patients (female n = 1, = 3, male n = 2).

The study was approved by the local ethics committee of the Ludwig-Maximilians University of Munich, Germany (Ethic vote #333-10) and written informed consent form was obtained for all study participants.

Human fetal lung fibroblasts (IMR-90, P8) for control co-cultures were obtained from ATCC (Catalog # CCL-186^{TM}) and grown in Dulbecco's Modified Eagle Medium: Nutrient F-12 (DMEM/F12; Gibco) with 20% fetal bovine serum (FBS SUPERIOR, Sigma) and 1% penicillin-streptomycin (Pen Strep, Gibco).

Cells were seeded in 6-well plates. at a density of $1x10^5$ cells in 2 mL media (DMEM/F12, 20% FBS, 1% penicillin/streptomycin) per well until reaching 80% confluency. Once confluent, each well was washed three times with a 15-minute incubation per wash with 1 mL of FBS-free culturing medium (DMEM/F12, 1% penicillin/ streptomycin) to eliminate remaining FBS. Fibroblasts were cultured for 48 h in FBS-free medium, supernatants were collected and stored at -80°C for further analysis.

2.3 Secretome analysis by mass spectrometry

2.3.1 Sample preparation for proteomics

Each 500 μL supernatant was subjected to tryptic digest applying a modified filter aided sample preparation procedure (19, 20). After protein reduction and alkylation using DTT and iodoacetamide, samples were denatured in UA buffer (8 M urea in 0.1 M Tris/HCl pH 8.5) and centrifuged on a 30 kDa cut-off filter device (PALL or Sartorius) and washed thrice with UA buffer and twice with 50 mM ammoniumbicarbonate (ABC). Proteins were proteolysed for 2 h at room temperature using 0.5 μg Lys-C (Wako) and subsequently for 16 h at 37°C using 1 μg trypsin (Promega). Peptides were collected by centrifugation and acidified with 0.5% trifluoroacetic acid.

2.3.2 Mass spectrometric measurements

LC-MSMS analysis was performed on a Q-Exactive HF mass spectrometer (Thermo Scientific) each online coupled to a nano-RSLC (Ultimate 3000 RSLC; Dionex). For subsequent analysis on the Q-Exactive HF, tryptic peptides were accumulated on a nano trap column (300 μm inner diameter × 5 mm, packed with Acclaim PepMap100 C18, 5 μm, 100 Å; LC Packings) and then separated by reversed phase chromatography (nanoEase MZ HSS T3 Column, 100 Å, 1.8 μm, 75 μm X 250 mm; Waters) in a 80 minutes non-linear gradient from 3 to 40% acetonitrile in 0.1% formic acid at a flow rate of 250 nL/min. Eluted peptides were analyzed by the Q-Exactive HF mass spectrometer equipped with a PepSep PSS1 source. Full scan MS spectra (from m/z 300 to 1500) and MSMS fragment spectra were acquired in the Orbitrap with a resolution of 60.000 or 15.000 respectively, with maximum injection times of 50 ms each. The up to ten most intense ions were selected for HCD fragmentation depending on signal intensity (TOP10 method). Target peptides already selected for MS/MS were dynamically excluded for 30 seconds. Data are available *via* ProteomeXchange with identifier PXD039554 (21, 22).

2.3.3 Protein identification and label-free quantification

Proteome Discoverer 2.5 software (Thermo Fisher Scientific; version 2.5.0.400) was used for peptide and protein identification *via* a database search (Sequest HT search engine, SequestHT score:1) against Swissprot human database (Release 2020_02, 20432 sequences), considering full tryptic specificity, allowing for up to two missed tryptic cleavage sites, precursor mass tolerance 10 ppm, fragment mass tolerance 0.02 Da. Carbamidomethylation of Cys was set as a static modification. Dynamic modifications included deamidation of Asn, Gln and Arg, oxidation of Pro and Met; and a combination of Met loss with acetylation on protein N-terminus. Percolator was used for validating peptide spectrum matches and peptides, accepting only the top-scoring hit for each spectrum, and satisfying the cutoff values for false discovery rate (FDR) < 5%, and posterior error probability < 0.01.

The quantification of proteins was based on abundance values for unique peptides. Abundance values were normalized on total peptide amount and protein abundances were calculated summing up the abundance values for admissible peptides. The final protein ratio was calculated using median abundance values. The statistical significance of the ratio change was ascertained employing the T-test approach

TABLE 1　Patient characteristics.

Patient	Diagnosis	Age at sample collection (years)	Sex	Surgery	Smoking history
1	Connective Tissue Disease related ILD	48	F	Lung transplantation (single)	no
2	Idiopathic pulmonary fibrosis	62	M	Lung transplantation (single)	no
3	Hypersensitivity Pneumonitis, Rheumatoid arthritis	57	F	Lung transplantation	no

described in 23 (23), which is based on the presumption that we look for expression changes for proteins that are just a few in comparison to the number of total proteins being quantified. The quantification variability of the non-changing "background" proteins can be used to infer which proteins change their expression in a statistically significant manner. Proteins with increased or decreased abundance were filtered with the following criteria: proteins were considered to be decreased in abundance below an abundance of ratio of 0.5 fold and increased abundance above 2 fold, proteins identified with a single peptide were excluded and just significant proteins were considered (P value < 0.05, P values were adjusted for multiple testing by Benjamini-Hochberg correction). Additionally, at least two MSMS identifications had to be identified to include the protein ratio.

2.3.4 Enrichment analysis

Pathway enrichment analyses were performed in Cytoscape (3.9.0) with the ClueGo plugin (v2.5.8) for significantly increased or decreased proteins. The following ontologies were used: KEGG (8093), GO_MolecularFunction-EBI-UniProt (18336), GO_BiologicalProcess-EBI-UniProt (18058). Accession IDs were used as identifiers and the analysis was performed with the standard software settings provided in the ClueGo app (24).

2.4 Mesenchymal-epithelial co-culture

Primary lung ILD fibroblasts and IMR-90 (control fibroblast cell line) were grown in cell culture flasks until 70% confluency. A single cell suspension was prepared using 0.25% EDTA-Trypsin (Gibco). iAT2s were grown into alveolar organoids for up to two weeks in Matrigel domes. Single cell suspension was obtained with Dispase (Corning) and 0.25% EDTA-Trypsin as described by Jacob et al. (17). Human ILD and IMR-90 fibroblasts as well as iAT2s were counted and directly seeded either in equal 1:1 (F_{low}) or 1:5 (F_{high}) iAT2s to fibroblasts seeding densities in undiluted Matrigel domes in 8-chamber wells (20 µL Drops, Falcon), 96-well plates (50 µL Drops, Greiner) or 12-well plates (50 µL Drops, Greiner). Co-cultures used CK+DCI media that was changed every 48 h to 72 h for up to 12 days of cultivation.

2.5 Immunofluorescence microscopy

3D alveolar organoids mono- and co-cultures as described in section 2.1 (mono-culture) and 2.4 (co-culture) were cultured in 8-chamber wells for immunofluorescence analysis (Nunc Lab-Tek Chamber Slide System, 8-well, Permanox slide, 0.8 cm^2/well). After alveolar organoids were formed, fixation was achieved with ice cold methanol and acetone (1:1v/v) for 5 minutes at -20°C. Cells were washed with PBS and stained with the respective primary antibody in buffer containing 0.1% BSA and 0.1% Triton X-100 overnight at 4°C. The next day, cells were washed 3 times with PBS and incubated in buffer with the respective fluorescent conjugated secondary antibody at a dilution of 1:500 and DAPI diluted 1:1.000 overnight at 4°C. The following day, cells were washed

gently, growth camber removed and remaining microscope slide mounted with fluorescent mounting media (Dako) and covered with a coverslip. Slides were stored at 4°C until imaging. Imaging was performed using a confocal laser scanning microscope (CLSM) Zeiss LSM 880 with Airyscan and edited afterwards using ZEN 2.5 software (Zeiss). Detailed information on the primary and secondary antibodies are given in Supplementary Table 1.

2.6 Operetta high content imaging and Napari organoid counter

Live imaging of all alveolar organoid mono- and co-cultures was performed using the Operetta CLS high-content analysis system (Operetta CLS, PerkinElmer) at time points 5, 8 and 12 days during the co-culture experimental set-up. Pictures were analyzed by the Harmony 3.5.2 high-content imaging and analysis software with PhenoLOGIC.

Multi-plane confocal 3D images were visualized in Napari image viewer (Python) as maximum intensity projections and the automatic measurements obtained from the "Napari organoid counter" (25) were visually checked and manually curated, resulting in output of size and numbers of formed alveolar organoids between iAT2s and human fibroblasts (ILD and control IMR-90). The Canny Edge Detection (26) algorithm is used for identifying the organoids, while pre- and post-processing steps have been included, to ensure the image matches the detector's expected input and the number of detected organoids along with their size is returned. More specifically, the organoids are approximated to ellipses and the algorithm fits orthogonal bounding boxes around each, with the height and width of each box corresponding to the two diameters of the organoid which are then in turn used to approximate the object's area.Quantitative real-time PCR

Co-cultures were lysed in RLT Plus Lysis Buffer (Qiagen) and RNA isolation was performed with the RNeasy Mini Kit (Qiagen) according to the manufacturer's instructions. Cell lysis from organoids and co-culture assays was performed with peqGOLD TriFast (VWR Life Science) as recommended by the manufactures followed by RNA isolation with the RNeasy Mini Kit (Qiagen). RNA was transcribed into cDNA by reverse transcriptase using the High-Capacity cDNA Reverse Transcription Kit (Thermo Fisher Scientific) according to the manufacturer's instructions. 5 ng of cDNA was added to a final concentration volume of 10 µL, Random Nonamers (Metabion) and master mix (Invitrogen, Thermo Fisher Scientific) was added to each RNA sample. cDNA was diluted with ultrapure H_2O. qPCR was performed in 96-well format using the quantitative real-time PCR System (Roche 480 LightCycler). 2 µL cDNA were added to a final reaction volume of 10 µL containing H_2O, 480 SYBR Green (LightCycler, Roche Diagnostics) and the primer mix (100 µM). Gene expression was normalized to *ß-Actin* control for genes *Vimentin* (*VIM*), *Integrin Subunit Beta 6* (*ITGB6*) and *Cadherin 2* (*CDH2*), and normalized to an average of *ß-Actin* and *HRPT* control for genes *Surfactant Protein C* (*SFTPC*), *Keratin 8* (*KRT8*), *Collagen 1A1* (*Col1A1*), *Matrix Metallopeptidase* (*MMP7*) and *Bone*

Morphogenic Protein 4 (*BMP4*), the fold change was calculated using the 2^ (-ddC) method. Sequence information of used primers are given in Supplementary Table 2. Data obtained from qPCR are presented relative to respective control co-cultures, to demonstrate influence of disease background.

2.7 Metabolic activity estimated by WST-1 assay

WST-1 assays were performed at day 2, 3, 5 and 7 of alveolar organoid co-cultures (human ILD or IMR-90 control fibroblasts). WST-1 reagent (Roche Diagnostics) was added to the culture medium in a 1:10 dilution. The culture medium was used as background control. After 2 h of incubation at 37°C and 5% CO_2, 100 µL of media from every sample was transferred to a microplate (Thermo Scientific; Fisher Scientific) and the absorbance of the sample against the background was measured with a TECAN reader (TECAN; infinite M200 PRO).

3 Results

3.1 Fibroblast induced changes in organoid formation and metabolic activity in co-cultured alveolar organoids

An overview of the experimental workflow is provided in Supplementary Figures 1A–C. iAT2s (Figure 1A) were successfully co-cultured with both ILD, in our study referring to cases of pulmonary fibrosis, or IMR-90 control fibroblasts, resulting in the formation of proliferative alveolar organoids (Figure 1B). Cell-cell contact of iAT2s and fibroblasts in (ILD) co-culture was demonstrated by partial encapsulation of alveolar organoids by α-SMA expressing fibroblasts (Figure 1C, white arrows).

Image analysis of the 3D co-cultures revealed a reduction in organoid formation capacity in the presence of human fibroblasts (Figure 1D). Although alveolar organoid size was not significantly affected by fibroblast co-culture (Figures 1B, E), quantitative assessment of organoid size (area, µm^2) and number of images obtained from alveolar organoids and co-cultures with either ILD or IMR-90 control fibroblasts in 1:1 ($F_{ILD/Control\ low}$) or 1:5 ($F_{ILD/Control\ high}$) seeding density (Figures 1B, D) demonstrated a negative correlation of fibroblast seeding density (ILD or IMR-90) with the alveolar organoid formation capacity.

In contrast, co-culture with ILD fibroblasts significantly increased metabolic activity of alveolar organoid in comparison to IMR-90 control co-cultures (Figure 1F).

3.2 Presence of ILD fibroblasts leads to aberrant epithelial gene expression changes

In order to relate the observed changes in organoid formation capacity and metabolic activity (Figure 1) to changes in gene expression, we measured critical markers of stem cell function and epithelial differentiation in co-cultured organoids.

Indicating changes in (stem) cell function and epithelial injury, we showed decreased expression of the alveolar stem cell marker *SFTPC* in the presence of ILD fibroblasts in both seeding ratios (F_{low} and F_{high}; Figure 2A). In line with this, *Keratin 8* (*KRT8*) expression levels were reduced under the impact of ILD primary fibroblasts (Figure 2A). Further, the distal epithelial marker *Integrin Subunit Beta 6* (*ITGB6*) as well as *Bone Morphogenetic Protein 4* (*BMP4*) showed increased transcription in ILD co-cultures when high seeding densities were applied (Figure 2A). Genes associated with regulation of extracellular matrix formation and remodeling including *Collagen 1A1* (*Col1A1*), *N-Cadherin 2* (*CDH2*) and *Vimentin* (*VIM*) showed increased expression in alveolar organoids co-cultured with ILD fibroblasts in high seeding ratios (Figure 2B). Likewise, expression levels of *Matrix Metallopeptidase 7* (*MMP7*) were increased in ILD co-cultures compared to control co-cultures. (Figure 2B).

3.3 ILD fibroblast secretome reveals proinflammatory signaling converging on *IL11* stimulating epithelial remodeling

To characterize fibroblast driven communication resulting in gene expression and phenotypical changes in the alveolar epithelium in ILD, supernatants of ILD and non-CLD fibroblasts were subjected to mass spectrometry (MSMS).

MS analysis detected an overall of 2625 expressed proteins, of which 47 were significantly more and 55 significantly less abundant when comparing ILD-derived fibroblast to non-CLD controls (Supplementary Table 3, 4, Figure 3A). The top 15 differentially expressed proteins (increased and decreased abundance) are listed in Supplementary Tables 1, 2.

Proteins with increased abundance predominantly belonged to the C-X-C motif chemokine family (*CXCL1, CXCL3*, and *CXCL8*), as well as to the interleukin family (*IL13RA, IL11*) and included gap junction proteins (*connexin 43, GJA1*). Further, *Pregnancy Specific Beta-1-Glycoprotein 4 (PSG4)* as well as WNT signaling modulator *SFRP4* were found amongst the top 15 proteins.

Accordingly, pathway enrichment analysis of proteins with increased abundance classified the responses as cytokine activity, chemokine-mediated signaling pathway and TNF-signaling pathway. Furthermore, cellular/response to chemokines, *IL17* signaling pathways and neutrophil chemotaxis were identified, indicative of a strong inflammatory response.

ClueGo, a Cytoscape plug-in for network analysis, highlighted proteins associated with rheumatoid arthritis, a disease often complicated by the development of lung fibrosis and characterized by the presence of inflammatory chemokines (Figure 3B).

Proteins with decreased abundance in the in ILD secretome were dominated by candidates involved in ECM production, ECM assembly or ECM reorganization as well as coordination of myofibroblast differentiation (*PDGFRL*) together with a downregulation of proteins involved in complement and coagulation cascade pathways (Figure 3C).
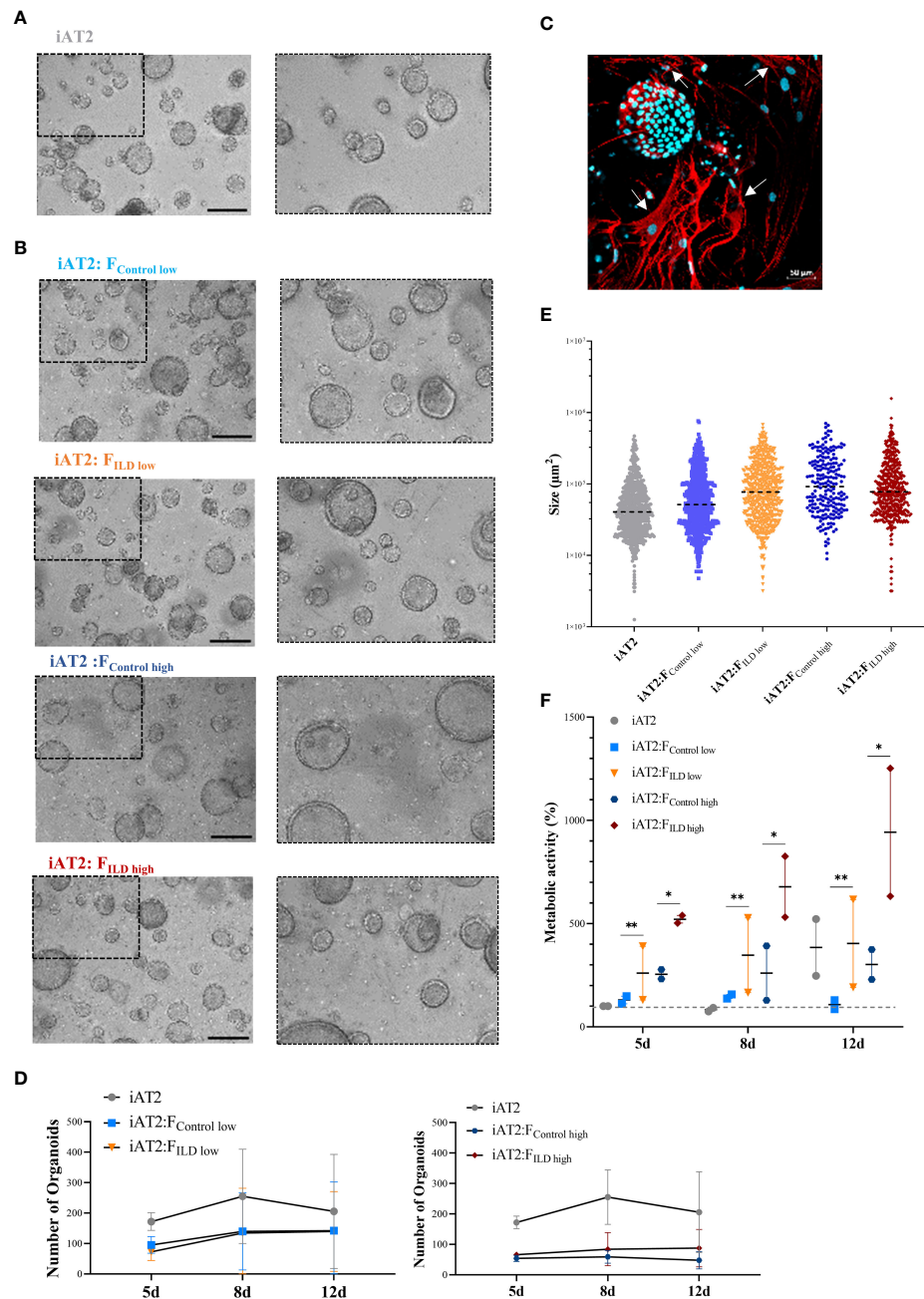
FIGURE 1
(A) Representative maximum intensity projections from high-content images of iAT2s growing as alveolar organoids at day 12. Scale bar 500µm.
(B) Immunofluorescence of 3D co-culture of iAT2s with ILD fibroblasts at day 12 (α-SMA: red, DAPI: cyan). Scale bar 50 µm. **(C)** Representative maximum intensity projections from high-content images of different co-culture conditions showing iAT2s growing with human fibroblasts for 12 days. Scale bar 500 µm. Zoom-ins show a 3x optical magnification. **(D)** Scatter plots (dashed black lines: median) indicate size (µm2) of organoids in co-cultures at day 12 across three independent biological replicates. **(E)** Number of formed organoids in co-cultures at day 12, N = 3. **(F)** Metabolic activity of co-cultured organoids at 5, 8 and 12 days of co-culture. Results show the increase in percentage across two biological replicates in comparison to d5 iAT2 organoids alone, representing the baseline of 100% metabolic activity (dashed grey line across dataset). Statistics: unpaired t-Test, *p<0.05, **p<0.01.

3.4 *IL11* acts as a driver for aberrant signatures in hiPSC-derived alveolospheres

Based on the MSMS secretome analysis, *IL11* emerged as a top player in the mesenchymal-to-epithelial disease crosstalk. In consequence, we exposed alveolar organoids (Figure 4A) to *IL11*

in order to investigate its functional relevance. Experiments (Dose$_{low}$ = 0.5 ng/mL, Dose$_{high}$ = 5 ng/mL) (Figures 4B–D) recapitulated the results observed in epithelial-fibroblasts co-cultures (section 3.1), *i.e.*, we demonstrated reduced organoid formation capacity (Figures 4Biii, C) and increased metabolic activity (WST-1) in *IL11* treated alveolar organoids (treatment
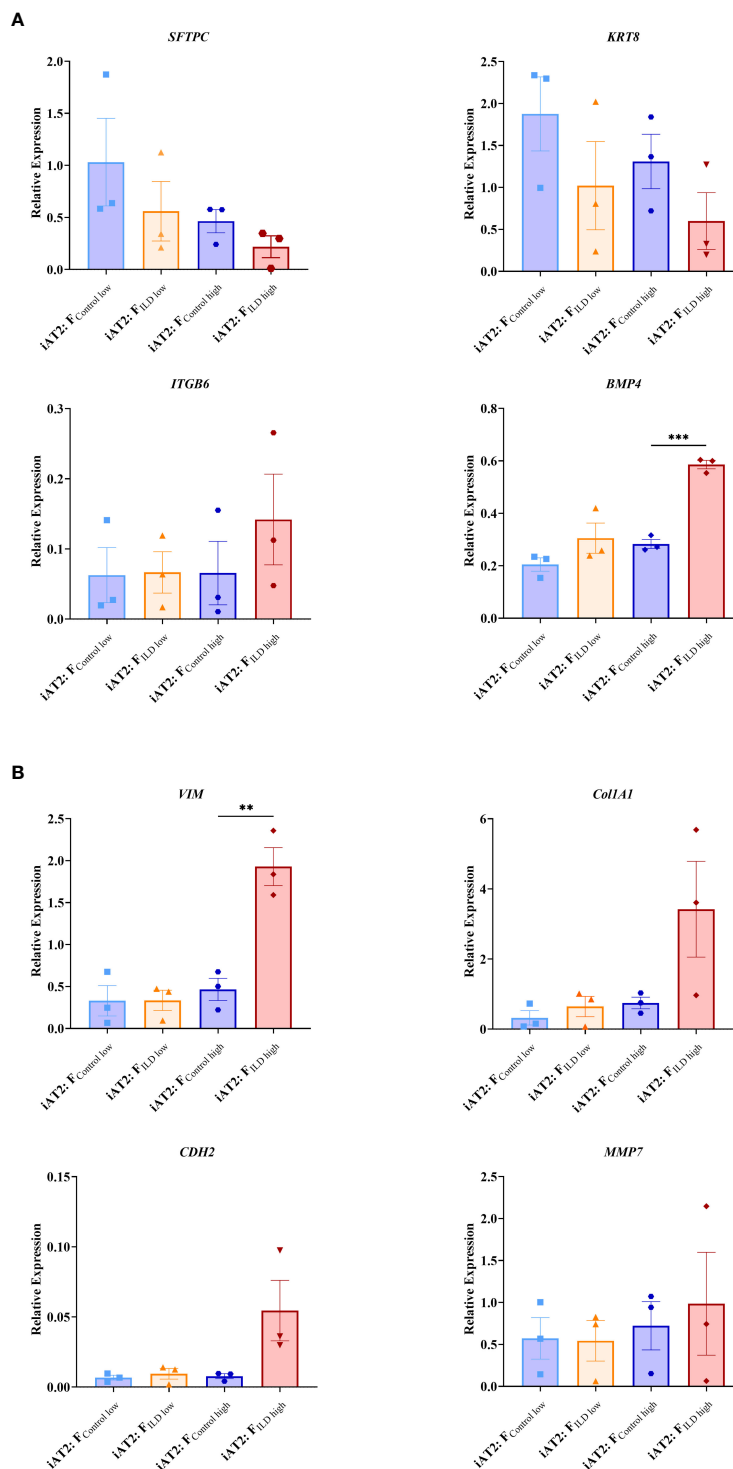
FIGURE 2
Relative gene expression at day 12 measured in AT2s co-cultures with ILD or IMR90 control fibroblasts in two seeding densities (high or low) compared to reference gene expression (HK; average of ß-Actin *(ACTB)* and hypoxanthine guanine phosphoribosyl transferase *(HRPT)*). **(A)** Epithelial and stem cell markers and **(B)** Genes associated with aberrant differentiation of epithelium. N = 3, unpaired t-Test, **p<0.005, ***p<0.0005.

from day 7 - 14 of culture) (Figure 4D). In addition, treatment of growing alveolar organoid monocultures with *IL11* (20 ng/mL) led to an increase in alveolar organoid size followed by apoptosis within 5 days of culture.

4 Discussion

In ILD, sustained inflammation and scarring of the gas exchange area ultimately result in destruction of the pulmonary
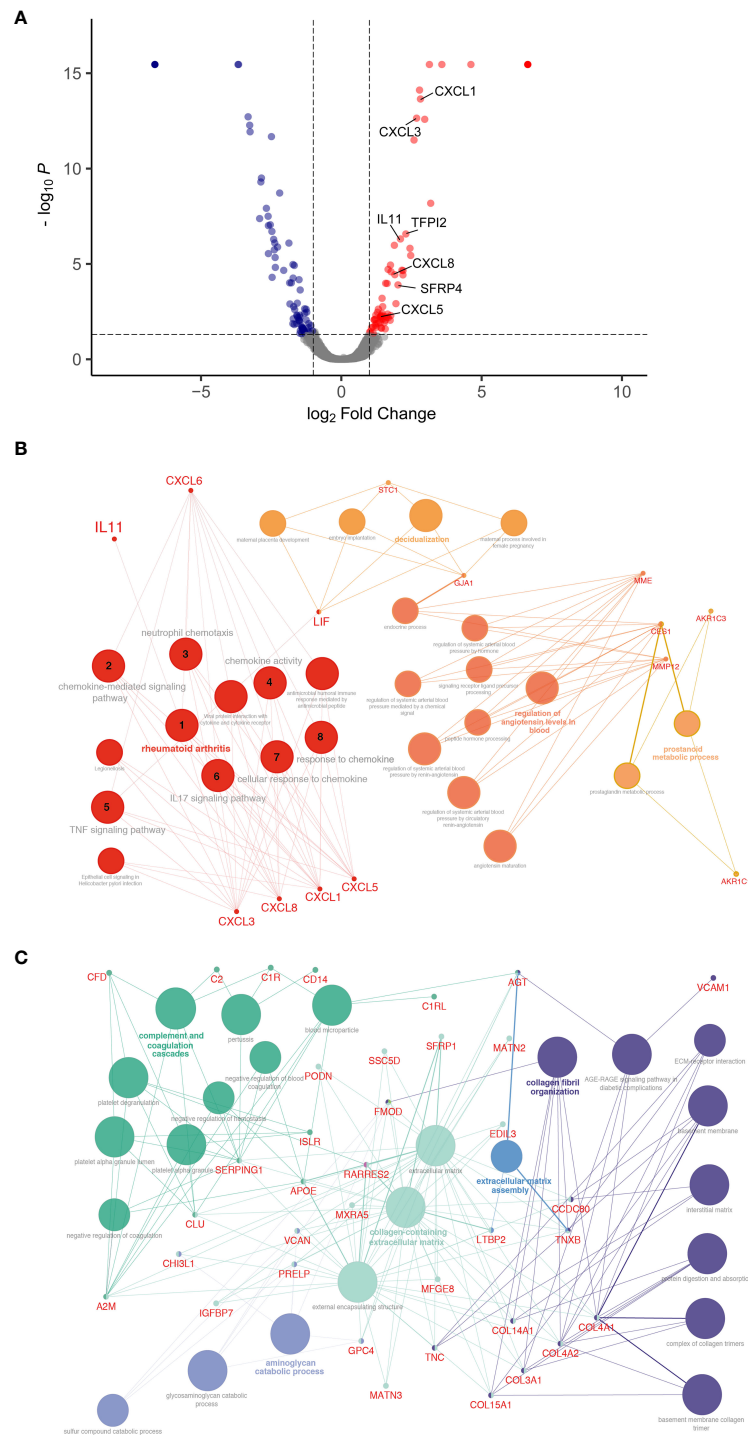
FIGURE 3

Differential protein expression comparing ILD fibroblasts (F_{ILD}) vs. non-chronic lung disease fibroblasts ($F_{control}$). **(A)** Volcano plot visualizing significantly regulated proteins (47 up, 55 down) detected by MS secretome analysis of ILD or non-CLD control fibroblasts. Data showing log_2 fold change against the adjusted P value [log10]. Significantly upregulated proteins are depicted in red and significantly downregulated proteins in blue. (Total: 102 significantly regulated proteins with 5% FDR < 0.05, adj. p_value < 0.05). Pathway enrichment and protein interaction network of proteins with **(B)** increased and **(C)** decreased abundance using the Cytoscape plugin ClueGo. The following ontologies were used: KEGG, molecular functions and biological processes. The connectivity of the pathways is described by functional nodes and edges that are shared between proteins with a kappa score of 0.4. Only enriched pathways are visualized and the node size indicates the p-value (p-value $\leq$ 0.05). Proteins from the same pathway share the same node color and the bold fonts indicate the most important functional pathways that define the names of each group. Enriched Pathways: 1. rheumatoid arthritis, 2. chemokine-mediated signaling pathway, 3. neutrophil chemotaxis, 4. chemokine activity, 5. *TNF* signaling pathway, 6. *IL17* signaling pathway, 7. cellular response to chemokine, 8. response to chemokine.
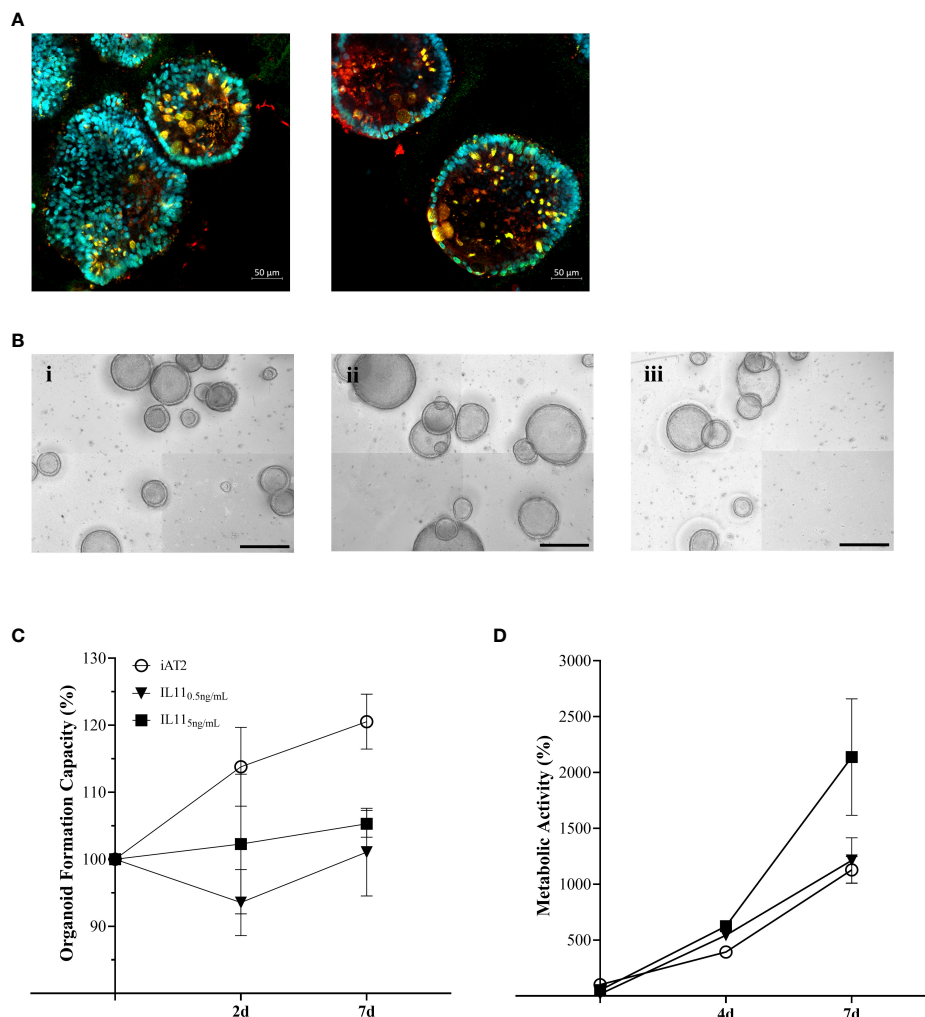
FIGURE 4

(A) Immunofluorescence of untreated alveolar organoids at day 14 of culture (*SFTPC*: red, *NKX2*.1: green, DAPI: cyan). **(B)** Representative maximum intensity projections from high-content images of (i) untreated alveolar organoids, (ii) 0.5 ng/mL or (iii) 5 ng/mL *IL11* treatment. Treatment started at day 7 of culture every 48h. Scale bar, 500 μm. **(C)** Organoid formation capacity of alveolar organoids treated with 0.5 or 5ng/mL *IL11*. **(D)** Metabolic activity of alveolar organoids treated with 0.5 or 5ng/mL *IL11*. **(C, D)** Each value is graphed as percentage of the respective starting culture at day 7 set to 100%.

scaffold and organ failure. Excessive deposition of ECM as well as epithelial damage and dedifferentiation is widely transmitted by the misguided interaction of fibroblasts and epithelial cells (27). Therefore, improved understanding of the mesenchymal-to-epithelial crosstalk remains a centerpiece in finding new avenues to monitor and treat ILD. However, signaling factors with functional relevance and their distinct role in ILD pathogenesis remain understudied.

This study aimed at deciphering disease-relevant candidates of mesenchymal-to-epithelial crosstalk that could serve as potential targets for future therapeutic strategies. By advancing a sensitive human iPSC-derived alveolar organoid culture into a human fibroblast co-culture model, we successfully demonstrated the importance of fibroblast-driven, cytokine-centered signaling in inducing the impairment of key epithelial cell functions, including differentiation and metabolism. In combination with an unbiased proteomic approach, we were able to identify important mediators

that translate these effects such as *IL11*, one of the top 15 proteins with increased abundance in ILD, in our study referring to cases of pulmonary fibrosis. The previously identified role of *IL11* in chronic inflammatory lung diseases in line with its potential to drive pro-fibrotic mesenchymal-epithelial crosstalk, supported the relevance of our approach on the one hand, while we were able to contribute the important functional consequences of its signaling in our human alveolar organoid model on the other (7, 8, 28).

In our *in vitro* co-culture approach, primary human pulmonary fibroblasts and iAT2s formed alveolar organoids that successfully recapitulated tissue characteristics of the distal lung in three dimensions, in contrast to 2D, plastic culture conditions (Figure 1). Primary human fibroblasts, both ILD-derived and IMR-90 control cells, demonstrated effects that correlated with seeding density leading to reduced organoid number and increased organoid size after 12 days of co-culture. The findings indicate that the co-culture with fibroblasts per se is able to change

the microenvironment of iAT2s, thereby impacting organoid formation. As studies indicated, that the activation of primary lung fibroblasts in a disease-comparable fashion is easily achieved (29), our findings likely explain the disease-independent fibroblast effects in alveolar organoids.

In contrast, the significant increase in metabolic activity was provoked by diseased human fibroblasts in high-seeding ratios, indicating their potential to impact on the metabolic program of the epithelial cell, potentially indicating epithelial dedifferentiation or EMT (30–32). These considerations are supported by the expression signature characterizing the co-cultures: The decrease in *SFTPC* expression (33–36) we observed in the ILD co-cultures points towards the loss of epithelial stem cell characteristics, as *SFTPC* expression is sensitive to epithelial inflammation and injury, lately supported by studies in Sars-CoV-2 infected alveolar organoids (10). Differentiation of AT2s is key for regeneration in injured alveoli marked by their expression of transient basaloid features such as *Keratin 5* (*KRT5*) and the amount of alveolar *KRT5*^{+} basaloid cells directly correlates with disease progression in pulmonary fibrosis (29, 37, 38), mirrored by the decreased expression observed in our study. Closely related, downregulation of *KRT8*, an important marker of AT2 to (pre)AT1 transdifferentiation during epithelial regeneration (38, 39) was associated with the increased expression of EMT markers in a murine bleomycin lung injury model including pro-fibrogenic proteins such as *ITGB6* (39). In line with these findings, we demonstrated increased *ITGB6* expression in ILD co-cultures. Its release from the plasma membrane potentially reflects the activation of EMT-like processes in lung organoids, accompanied by the decrease of expressed *KRT8*. Further supporting these findings, we showed the elevated expression of *BMP4* and *MMP7*, critical regulators of EMT in pulmonary fibrosis (40), in lung organoids co-cultured with ILD fibroblasts. *MMP7* has furthermore been highlighted for its function as a plasma biomarker in idiopathic pulmonary fibrosis (33, 41), in line with its detection in our study.

Co-culture of alveolar organoids with ILD fibroblasts also specifically changed the expression of genes involved in ECM biosynthesis including the increased transcription of *Col1A1*, *VIM* and *CDH2*, well-known players in fibrotic lung disease (33, 34) (38), as compared to organoid monocultures. Linking back to the indications of aberrant basal transdifferentiation in fibroblast co-culture discussed above (29), the basaloid cells show increased ECM protein expression, next to their increase in *BMP4* and *ITGB6* expression, again successfully detected in our model.

We next were able to provide deeper insight into the relevant mediators of mesenchymal-to-epithelial crosstalk related to the observed changes in organoid phenotype by screening the supernatant of ILD or control fibroblasts using mass spectrometry (42). Cytokines that belong to the C-X-C motif family dominated the protein signature in the secretome, demonstrating their increased abundance in ILD. These signaling molecules act on the *CXCR1* and *CXCR2* receptor, as well as regulate the expression of cytokines from the interleukin family, central to the pathogenesis of fibrotic and inflammatory lung diseases such as IPF and acute respiratory distress syndrome (3, 8, 36, 43). The majority of the differentially abundant proteins are proinflammatory cytokines that primarily act on neutrophil, monocyte or lymphocyte recruitment (*CXCL1, CXCL3, CXCL5, CXCL8*). The proinflammatory response is complemented by the regulation of proteins that play a role in cellular senescence and activation of *TGF-ß* such as the Pregnancy-Specific Glycoprotein (PSG) family, *PSG 4, 5, 6* or in the induction of a hypercoagulable tissue state (*TFPI2*). Other important proteins such as *SFRP4* directly inhibit WNT signaling, thereby modulating cell growth and differentiation, particularly of AT2s to AT1s (44). *WNT* serum levels are discussed as biomarkers for lung fibrosis and EMT. *WNT* modulation and *TGF-ß* solubilization in particular could account for the change in organoid number and size and support our observations in gene expression levels that indicate epithelial transdifferentiation into aberrant basaloid cells or EMT in the presence of ILD fibroblasts.

IL11, centrally orchestrating the ILD protein profile as observed by pathway enrichment, was identified among the top 15 candidates in the ILD fibroblast secretome. *IL11* is known to be expressed in pro-inflammatory fibroblasts extracted from IPF lungs. The cytokine belongs to the *IL6* family and is induced by *TGF-ß* and other proinflammatory mediators [*IL1ß, IL17, IL22*, reactive oxygen species (ROS)]. It can either activate fibroblasts to differentiate into myofibroblasts in an autocrine fashion through ERK/SMAD canonical signaling, which results in pro-fibrotic protein expression (*COL1A1, ACTA2*), or it stimulates epithelial cells (paracrine loop) through activating *ERK* signaling cascades, thereby inducing cellular senescence, EMT, cellular dysfunction and impaired regeneration (8). Results from our co-culture model indicate both autocrine and paracrine signaling of *IL11* as we demonstrated indication of EMT, stem cell dysfunction as well as ECM production, i.e., upregulation of collagen expression in line with 8 (8). Similar to the results obtained from ILD fibroblast co-culture in different seeding densities, *IL11* treatment of alveolar organoid monocultures resulted in a dose dependent increase in metabolic activity, elevated expression of mesenchymal markers and decreased AT2 stemness and identity. Dose-dependent, *IL11* even induced apoptotic cell death, in line with its role in senescence and stem cell function observed in alveolar organoids (36). Similarly, *IL11* alone induced fibrotic changes in healthy alveolar organoids whereas knock-out of *IL11* expression in diseased organoids reversed organoid fibrosis in a model of the Hermansky-Pudlak syndrome-associated interstitial pneumonia, a disease with high similarity to IPF (3). Supporting our co-culture findings in this regard, *IL11* exposure impacts on AT2 progenitor function, thereby likely suppressing the formation of mature AT2s as described by Kortekaas and colleagues (35, 36).

Taken together, our results strongly support the central role of *IL11* signaling as the cytokine holds the potential to strongly influence the intricate crosstalk between the (then activated (myo)) fibroblasts and the injured epithelium, central in the progression of fibrosis in ILD. We successfully demonstrated the potential of our lung organoid co-culture model derived from hiPSCs and primary fibroblasts to display critical consequences of the malfunctional crosstalk such as aberrant dedifferentiation and basaloid-prone signatures (33, 45). In this context, *IL11* likely holds an important role in misguided alveolar function, differentiation

and thereby regeneration, important functions as a potential therapeutic target to regain alveolar crosstalk homeostasis (46).

Data availability statement

The datasets presented in this study can be found in online repositories. The names of the repository/repositories and accession number(s) can be found in the article. The mass spectrometry proteomics data presented in the study have been deposited to the ProteomeXchange Consortium via the PRIDE partner repository with the dataset identifier PXD039554..

Ethics statement

The studies involving human participants were reviewed and approved by Ludwig-Maximilians University of Munich, Germany. (Ethic vote #333-10). The patients/participants provided their written informed consent to participate in this study.

Author contributions

MK, AH and CV conceived and planned the experiments. MK, EG-R, PC and EMG carried out the main experiments. FS and SA contributed to sample preparation. A-CK and SH performed the mass spectrometry analysis. LH performed additional data analysis and figure composition. CB, GB, MP and ML conceived, discussed and developed the AI based organoid counter. RAH headed patient sample retrieval and documentation and contributed clinical background to the study. MK, CV, TS, A-CK, SH, JB and AH contributed substantially to the interpretation of the results. MK and CV took the lead in writing the manuscript. All authors provided critical feedback and helped shape the research, analysis and drafting of the manuscript.

Funding

Acknowledgments

Conflict of interest

The authors declare that the research was conducted in the absence of any commercial or financial relationships that could be construed as a potential conflict of interest.

Publisher's note

All claims expressed in this article are solely those of the authors and do not necessarily represent those of their affiliated organizations, or those of the publisher, the editors and the reviewers. Any product that may be evaluated in this article, or claim that may be made by its manufacturer, is not guaranteed or endorsed by the publisher.

Supplementary material

The Supplementary Material for this article can be found online at: https://www.frontiersin.org/articles/10.3389/fimmu.2023.1128239/full#supplementary-material

References

1. Glasser SW, Hardie WD, Hagood JS. Pathogenesis of interstitial lung disease in children and adults. *Pediatr Allergy Immunol Pulmonol* (2010) 23(1):9–14. doi: 10.1089/ped.2010.0004

2. Lederer DJ, Martinez FJ. Idiopathic pulmonary fibrosis. *N Engl J Med* (2018) 378 (19):1811–23. doi: 10.1056/NEJMra1705751

3. Strikoudis A, Cieślak A, Loffredo L, Chen YW, Patel N, Saqi A, et al. Modeling of fibrotic lung disease using 3D organoids derived from human pluripotent stem cells. *Cell Rep* (2019) 27(12):3709–3723.e3705. doi: 10.1016/j.celrep.2019.05.077

4. Dwyer AR, Ellies LG, Holme AL, Pixley FJ. A three-dimensional co-culture system to investigate macrophage-dependent tumor cell invasion. *J Biol Methods* (2016) 3(3):e49. doi: 10.14440/jbm.2016.132

5. Kim KK, Sheppard D, Chapman HA. TGF-β1 signaling and tissue fibrosis. *Cold Spring Harb Perspect Biol* (2018) 10(4):a022293. doi: 10.1101/cshperspect.a022293

6. O'Dwyer DN, Ashley SL, Moore BB. Influences of innate immunity, autophagy, and fibroblast activation in the pathogenesis of lung fibrosis. *Am J Physiology-Lung Cell Mol Physiol* (2016) 311(3):L590–601. doi: 10.1152/ajplung.00221.2016

7. Ng B, Dong J, D'Agostino G, Viswanathan S, Widjaja AA, Lim WW, et al. Interleukin-11 is a therapeutic target in idiopathic pulmonary fibrosis. *Sci Transl Med* (2019) 11(511):eaaw1237. doi: 10.1126/scitranslmed.aaw1237

8. Ng B, Cook SA, Schafer S. Interleukin-11 signaling underlies fibrosis, parenchymal dysfunction, and chronic inflammation of the airway. *Exp Mol Med* (2020) 52(12):1871–8. doi: 10.1038/s12276-020-00531-5

9. Yao L, Zhou Y, Li J, Wickens L, Conforti F, Rattu A, et al. Bidirectional epithelial-mesenchymal crosstalk provides self-sustaining profibrotic signals in pulmonary fibrosis. *J Biol Chem* (2021) 297(3):101096. doi: 10.1016/j.jbc.2021.101096

10. Mou H. Induced pluripotent stem cell-derived alveolar type II heterogeneity: Revealed by SFTPC expression. *Am J Respir Cell Mol Biol* (2021) 65(4):345–6. doi: 10.1165/rcmb.2021-0242ED

11. Kong J, Wen S, Cao W, Yue P, Xu X, Zhang Y, et al. Lung organoids, useful tools for investigating epithelial repair after lung injury. *Stem Cell Res Ther* (2021) 12(1):95. doi: 10.1186/s13287-021-02172-5

12. Kastlmeier MT, Guenther EM, Stoeger T, Voss C. Lung organoids for hazard assessment of nanomaterials. *Int J Mol Sci* (2022) 23(24):15666. doi: 10.3390/ijms232415666

13. Nikolić MZ, Sun D, Rawlins EL. Human lung development: recent progress and new challenges. *Development* (2018) 145(16):dev163485. doi: 10.1242/dev.163485

14. Nikolić MZ, Hogan MZN. Lung stem cells in development, health and disease. In: *ERS monograph* (2021). doi: 10.1183/2312508X.erm9121

15. Hawkins F, Kramer P, Jacob A, Driver I, Thomas DC, McCauley KB, et al. Prospective isolation of NKX-2-1-expressing human lung progenitors derived from pluripotent stem cells. *J Clin Invest* (2017) 127(6):2277–94. doi: 10.1172/jci89950

16. Jacob A, Morley M, Hawkins F, McCauley KB, Jean JC, Heins H, et al. Differentiation of human pluripotent stem cells into functional lung alveolar epithelial cells. *Cell Stem Cell* (2017) 21(4):472–488.e410. doi: 10.1016/j.stem.2017.08.014

17. Jacob A, Vedaie M, Roberts DA, Thomas DC, Villacorta-Martin C, Alysandratos K-D, et al. Derivation of self-renewing lung alveolar epithelial type II cells from human pluripotent stem cells. *Nat Protoc* (2019) 14(12):3303–32. doi: 10.1038/s41596-019-0220-0

18. Heinzelmann K, Lehmann M, Gerckens M, Noskovičová N, Frankenberger M, Lindner M, et al. Cell-surface phenotyping identifies CD36 and CD97 as novel markers of fibroblast quiescence in lung fibrosis. *Am J Physiol Lung Cell Mol Physiol* (2018) 315 (5):L682–l696. doi: 10.1152/ajplung.00439.2017

19. Wiśniewski JR, Zougman A, Nagaraj N, Mann M. Universal sample preparation method for proteome analysis. *Nat Methods* (2009) 6(5):359–62. doi: 10.1038/nmeth.1322

20. Grosche A, Hauser A, Lepper MF, Mayo R, von Toerne C, Merl-Pham J, et al. The proteome of native adult müller glial cells from murine retina. *Mol Cell Proteomics* (2016) 15(2):462–80. doi: 10.1074/mcp.M115.052183

21. Deutsch EW, Bandeira N, Sharma V, Perez-Riverol Y, Carver JJ, Kundu DJ, et al. The ProteomeXchange consortium in 2020: enabling 'big data' approaches in proteomics. *Nucleic Acids Res* (2019) 48(D1):D1145–52. doi: 10.1093/nar/gkz984

22. Perez-Riverol Y, Bai J, Bandla C, García-Seisdedos D, Hewapathirana S, Kamatchinathan S, et al. The PRIDE database resources in 2022: a hub for mass spectrometry-based proteomics evidences. *Nucleic Acids Res* (2021) 50(D1):D543–52. doi: 10.1093/nar/gkab1038

23. Navarro P, Trevisan-Herraz M, Bonzon-Kulichenko E, Núñez E, Martínez-Acedo P, Pérez-Hernández D, et al. General statistical framework for quantitative proteomics by stable isotope labeling. *J Proteome Res* (2014) 13(3):1234–47. doi: 10.1021/pr4006958

24. Bindea G, Mlecnik B, Hackl H, Charoentong P, Tosolini M, Kirilovsky A, et al. ClueGO: a cytoscape plug-in to decipher functionally grouped gene ontology and pathway annotation networks. *Bioinformatics* (2009) 25(8):1091–3. doi: 10.1093/bioinformatics/btp101

25. Bukas C. *HelmholtzAI-Consultants-Munich/napari-organoid-counter: Latest versions of dependencies (v0.1.1)*. Zenodo (2022). doi: 10.5281/zenodo.7065206

26. Canny J. (1986). "A computational approach to edge detection," in: *IEEE Transactions on Pattern Analysis and Machine Intelligence*, Vol. PAMI-8. pp. 679–98. doi: 10.1109/TPAMI.1986.4767851

27. Lewis KJR, Hall JK, Kiyotake EA, Christensen T, Balasubramaniam V, Anseth KS. Epithelial-mesenchymal crosstalk influences cellular behavior in a 3D alveolus-fibroblast model system. *Biomaterials*. (2018) 115:124–34. doi: 10.1016/j.biomaterials.2017.11.008

28. Cook SA, Schafer S. Hiding in plain sight: Interleukin-11 emerges as a master regulator of fibrosis, tissue integrity, and stromal inflammation. *Annu Rev Med* (2020) 71:263–76. doi: 10.1146/annurev-med-041818-011649

29. Kathiriya JJ, Wang C, Zhou M, Brumwell A, Cassandras M, Le Saux CJ, et al. Human alveolar type 2 epithelium transdifferentiates into metaplastic KRT5+ basal cells. *Nat Cell Biol* (2022) 24(1):10–23. doi: 10.1038/s41556-021-00809-4

30. Kalluri R. EMT: When epithelial cells decide to become mesenchymal-like cells. *J Clin Invest* (2009) 119(6):1417–9. doi: 10.1172/JCI39675

31. Kalluri R, Weinberg RA. The basics of epithelial-mesenchymal transition. *J Clin Invest* (2009) 119(6):1420–8. doi: 10.1172/JCI39104

32. Wang Y, Dong C, Zhou BP. Metabolic reprogram associated with epithelial-mesenchymal transition in tumor progression and metastasis. *Genes Dis* (2020) 7 (2):172–84. doi: 10.1016/j.gendis.2019.09.012

33. Adams TS, Schupp JC, Poli S, Ayaub EA, Neumark N, Ahangari F, et al. Single-cell RNA-seq reveals ectopic and aberrant lung-resident cell populations in idiopathic pulmonary fibrosis. *Sci Adv* (2020) 6(28):eaba1983. doi: 10.1126/sciadv.aba1983

34. Katzen J, Beers MF. Contributions of alveolar epithelial cell quality control to pulmonary fibrosis. *J Clin Invest* (2020) 130(10):5088–99. doi: 10.1172/JCI139519

35. Kortekaas RK, Burgess JK, Webster M, Gosens R. IL11 negatively impacts adult lung alveolar organoid formation. *ERJ Open Res* (2021) 7(suppl 6):81. doi: 10.1183/23120541.Lsc-2021.81

36. Kortekaas R, Geillinger-Kästle K, Borghuis T, Belharch K, Webster M, Timens W, et al. IL-11 disrupts alveolar epithelial progenitor function. *bioRxiv* (2022). doi: 10.1101/2022.11.11.516088

37. Khan P, Roux J, Blumer S, Knudsen L, Jonigk D, Kuehnel MP, et al. Alveolar basal cells differentiate towards secretory epithelial- and aberrant basaloid-like cells *In vitro. Cells* (2022) 11(11):1820. doi: 10.3390/cells11111820

38. Ng B, Huang KY, Pua CJ, Lim W-W, Kuthubudeen F, Hii AA, et al. Interleukin-11 causes alveolar type 2 cell dysfunction and prevents alveolar regeneration. *bioRxiv* (2022). doi: 10.1101/2022.11.11.516109

39. Strunz M, Simon LM, Ansari M, Kathiriya JJ, Angelidis I, Mayr CH, et al. Alveolar regeneration through a Krt8+ transitional stem cell state that persists in human lung fibrosis. *Nat Commun* (2020) 11(1):3559. doi: 10.1038/s41467-020-17358-3

40. Molloy EL, Adams A, Moore JB, Masterson JC, Madrigal-Estebas L, Mahon BP, et al. BMP4 induces an epithelial-mesenchymal transition-like response in adult airway epithelial cells. *Growth Factors* (2008) 26(1):12–22. doi: 10.1080/08977190801987166

41. Bauer Y, White ES, de Bernard S, Cornelisse P, Leconte I, Morganti A, et al. MMP-7 is a predictive biomarker of disease progression in patients with idiopathic pulmonary fibrosis. *ERJ Open Res* (2017) 3(1):00074-2016. doi: 10.1183/23120541.00074-2016

42. Strieter RM, Gomperts BN, Keane MP. The role of CXC chemokines in pulmonary fibrosis. *J Clin Invest* (2007) 117(3):549–56. doi: 10.1172/jci30562

43. Mukaida N. Pathophysiological roles of interleukin-8/CXCL8 in pulmonary diseases. *Am J Physiology-Lung Cell Mol Physiol* (2003) 284(4):L566–77. doi: 10.1152/ajplung.00233.2002

44. Abdelwahab EMM, Rapp J, Feller D, Csongei V, Pal S, Bartis D, et al. Wnt signaling regulates trans-differentiation of stem cell like type 2 alveolar epithelial cells to type 1 epithelial cells. *Respir Res* (2019) 20(1):204. doi: 10.1186/s12931-019-1176-x

45. Habermann AC, Gutierrez AJ, Bui LT, Yahn SL, Winters NI, Calvi CL, et al. Single-cell RNA sequencing reveals profibrotic roles of distinct epithelial and mesenchymal lineages in pulmonary fibrosis. *Sci Adv* (2020) 6(28):eaba1972. doi: 10.1126/sciadv.aba1972

46. Lin CR, Bahmed K, Kosmider B. Impaired alveolar re-epithelialization in pulmonary emphysema. *Cells* (2022) 11(13):2055. doi: 10.3390/cells11132055

47. Kastlmeier MT, Rodriguez EG, Cabanis P, Guenther EM, König A-C, Han L, et al. Cytokine signaling converging on IL11 in ILD fibroblasts provokes aberrant epithelial differentiation signatures. *bioRxiv* (2022). doi: 10.1101/2022.12.20.521114

7.   References

Abo, K. M., Ma, L., Matte, T., Huang, J., Alysandratos, K. D., Werder, R. B., Mithal, A., Beermann, M. L., Lindstrom-Vautrin, J., Mostoslavsky, G., Ikonomou, L., Kotton, D. N., Hawkins, F., Wilson, A., & Villacorta-Martin, C. (2020). Human iPSC-derived alveolar and airway epithelial cells can be cultured at air-liquid interface and express SARS-CoV-2 host factors. *bioRxiv*, 2020.2006.2003.132639. https://doi.org/10.1101/2020.06.03.132639

Akella, A., & Deshpande, S. B. (2013). Pulmonary surfactants and their role in pathophysiology of lung disorders. *Indian J Exp Biol, 51*(1), 5-22.

Al-Shaikhly, T., & Ochs, H. D. (2019). Hyper IgE syndromes: clinical and molecular characteristics. *Immunol Cell Biol, 97*(4), 368-379. https://doi.org/10.1111/imcb.12209

Andreeva, A. V., Kutuzov, M. A., & Voyno-Yasenetskaya, T. A. (2007). Regulation of surfactant secretion in alveolar type II cells. *American Journal of Physiology-Lung Cellular and Molecular Physiology, 293*(2), L259-L271. https://doi.org/10.1152/ajplung.00112.2007

Bagnato, G., & Harari, S. (2015). Cellular interactions in the pathogenesis of interstitial lung diseases. *European Respiratory Review, 24*(135), 102-114. https://doi.org/10.1183/09059180.00003214

Barkauskas, C. E., Chung, M. I., Fioret, B., Gao, X., Katsura, H., & Hogan, B. L. (2017). Lung organoids: current uses and future promise. *Development, 144*(6), 986-997. https://doi.org/10.1242/dev.140103

Barkauskas, C. E., Cronce, M. J., Rackley, C. R., Bowie, E. J., Keene, D. R., Stripp, B. R., Randell, S. H., Noble, P. W., & Hogan, B. L. M. (2013). Type 2 alveolar cells are stem cells in adult lung. *The Journal of Clinical Investigation, 123*(7), 3025-3036. https://doi.org/10.1172/JCI68782

Basil, M. C., Katzen, J., Engler, A. E., Guo, M., Herriges, M. J., Kathiriya, J. J., Windmueller, R., Ysasi, A. B., Zacharias, W. J., Chapman, H. A., Kotton, D. N., Rock, J. R., Snoeck, H.-W., Vunjak-Novakovic, G., Whitsett, J. A., & Morrisey, E. E. (2020). The Cellular and Physiological Basis for Lung Repair and Regeneration: Past, Present, and Future. *Cell stem cell, 26*(4), 482-502. https://doi.org/10.1016/j.stem.2020.03.009

Beers, M. F., & Moodley, Y. (2017). When Is an Alveolar Type 2 Cell an Alveolar Type 2 Cell? A Conundrum for Lung Stem Cell Biology and Regenerative Medicine. *American journal of respiratory cell and molecular biology, 57*(1), 18-27. https://doi.org/10.1165/rcmb.2016-0426PS

Berggren-Nylund, R., Ryde, M., Löfdahl, A., Ibáñez-Fonseca, A., Kåredal, M., Westergren-Thorsson, G., Tufvesson, E., & Larsson-Callerfelt, A.-K. (2023). Effects of hypoxia on bronchial and alveolar epithelial cells linked to pathogenesis in chronic lung disorders [Original Research]. *Frontiers in Physiology, 14*. https://doi.org/10.3389/fphys.2023.1094245

A cellular reference atlas of the human lung. (2023). *Nature Medicine, 29*(6), 1338-1339. https://doi.org/10.1038/s41591-023-02329-0

Chan, M., & Liu, Y. (2022). Function of epithelial stem cell in the repair of alveolar injury. *Stem Cell Research & Therapy, 13*(1), 170. https://doi.org/10.1186/s13287-022-02847-7

Chandesris, M. O., Melki, I., Natividad, A., Puel, A., Fieschi, C., Yun, L., Thumerelle, C., Oksenhendler, E., Boutboul, D., Thomas, C., Hoarau, C., Lebranchu, Y., Stephan, J. L., Cazorla, C., Aladjidi, N., Micheau, M., Tron, F., Baruchel, A., Barlogis, V., . . . Picard, C. (2012). Autosomal dominant STAT3 deficiency and hyper-IgE syndrome: molecular, cellular, and clinical features from a French national survey. *Medicine (Baltimore), 91*(4), e1-e19. https://doi.org/10.1097/MD.0b013e31825f95b9

Choi, J., Park, J. E., Tsagkogeorga, G., Yanagita, M., Koo, B. K., Han, N., & Lee, J. H. (2020). Inflammatory Signals Induce AT2 Cell-Derived Damage-Associated Transient Progenitors that Mediate Alveolar Regeneration. *Cell stem cell, 27*(3), 366-382 e367. https://doi.org/10.1016/j.stem.2020.06.020

Chuquimia, O. D., Petursdottir, D. H., Periolo, N., & Fernández, C. (2013). Alveolar epithelial cells are critical in protection of the respiratory tract by secretion of factors able to

modulate the activity of pulmonary macrophages and directly control bacterial growth. *Infect Immun*, *81*(1), 381-389. https://doi.org/10.1128/iai.00950-12

Cidem, A., Bradbury, P., Traini, D., & Ong, H. X. (2020). Modifying and Integrating in vitro and ex vivo Respiratory Models for Inhalation Drug Screening. *Front Bioeng Biotechnol*, *8*, 581995. https://doi.org/10.3389/fbioe.2020.581995

Confalonieri, P., Volpe, M. C., Jacob, J., Maiocchi, S., Salton, F., Ruaro, B., Confalonieri, M., & Braga, L. (2022). Regeneration or Repair? The Role of Alveolar Epithelial Cells in the Pathogenesis of Idiopathic Pulmonary Fibrosis (IPF). *Cells*, *11*(13), 2095. https://www.mdpi.com/2073-4409/11/13/2095

D'Amico, S., Shi, J., Martin, B. L., Crawford, H. C., Petrenko, O., & Reich, N. C. (2018). STAT3 is a master regulator of epithelial identity and KRAS-driven tumorigenesis. *Genes Dev*, *32*(17-18), 1175-1187. https://doi.org/10.1101/gad.311852.118

Dayem, A. A., Choi, H. Y., Yang, G. M., Kim, K., Saha, S. K., Kim, J. H., & Cho, S. G. (2016). The potential of nanoparticles in stem cell differentiation and further therapeutic applications. *Biotechnol J*, *11*(12), 1550-1560. https://doi.org/10.1002/biot.201600453

Dockrell, D. H., Russell, C. D., McHugh, B., & Fraser, R. (2022). Does autonomous macrophage-driven inflammation promote alveolar damage in COVID-19? *European Respiratory Journal*, 2201521. https://doi.org/10.1183/13993003.01521-2022

Freeman, A. F., & Holland, S. M. (2008). The hyper-IgE syndromes. *Immunology and allergy clinics of North America*, *28*(2), 277-viii. https://doi.org/10.1016/j.iac.2008.01.005

Ghaedi, M., & Niklason, L. E. (2019). Human Pluripotent Stem Cells (iPSC) Generation, Culture, and Differentiation to Lung Progenitor Cells. *Methods Mol Biol*, *1576*, 55-92. https://doi.org/10.1007/7651_2016_11

Ghaedi, M., Niklason, L. E., & Williams, J. (2015). Development of Lung Epithelium from Induced Pluripotent Stem Cells. *Curr Transplant Rep*, *2*(1), 81-89. https://doi.org/10.1007/s40472-014-0039-0

Guillot, L., Nathan, N., Tabary, O., Thouvenin, G., Le Rouzic, P., Corvol, H., Amselem, S., & Clement, A. (2013). Alveolar epithelial cells: master regulators of lung homeostasis. *Int J Biochem Cell Biol*, *45*(11), 2568-2573. https://doi.org/10.1016/j.biocel.2013.08.009

Haddad, M., & Sharma, S. (2023). Physiology, Lung. In *StatPearls*. StatPearls Publishing
Copyright © 2023, StatPearls Publishing LLC.

Hite, R. D., Grier, B. L., Waite, B. M., Veldhuizen, R. A., Possmayer, F., Yao, L. J., & Seeds, M. C. (2012). Surfactant protein B inhibits secretory phospholipase A2 hydrolysis of surfactant phospholipids. *Am J Physiol Lung Cell Mol Physiol*, *302*(2), L257-265. https://doi.org/10.1152/ajplung.00054.2011

Holland, S. M., DeLeo, F. R., Elloumi, H. Z., Hsu, A. P., Uzel, G., Brodsky, N., Freeman, A. F., Demidowich, A., Davis, J., Turner, M. L., Anderson, V. L., Darnell, D. N., Welch, P. A., Kuhns, D. B., Frucht, D. M., Malech, H. L., Gallin, J. I., Kobayashi, S. D., Whitney, A. R., . . . Grimbacher, B. (2007). STAT3 Mutations in the Hyper-IgE Syndrome. *New England Journal of Medicine*, *357*(16), 1608-1619. https://doi.org/10.1056/NEJMoa073687

Jacob, A., Morley, M., Hawkins, F., McCauley, K. B., Jean, J. C., Heins, H., Na, C.-L., Weaver, T. E., Vedaie, M., Hurley, K., Hinds, A., Russo, S. J., Kook, S., Zacharias, W., Ochs, M., Traber, K., Quinton, L. J., Crane, A., Davis, B. R., . . . Kotton, D. N. (2017a). Differentiation of Human Pluripotent Stem Cells into Functional Lung Alveolar Epithelial Cells. *Cell stem cell*, *21*(4), 472-488.e410. https://doi.org/10.1016/j.stem.2017.08.014

Jacob, A., Morley, M., Hawkins, F., McCauley, K. B., Jean, J. C., Heins, H., Na, C.-L., Weaver, T. E., Vedaie, M., Hurley, K., Hinds, A., Russo, S. J., Kook, S., Zacharias, W., Ochs, M., Traber, K., Quinton, L. J., Crane, A., Davis, B. R., . . . Kotton, D. N. (2017b). Differentiation of Human Pluripotent Stem Cells into Functional Lung Alveolar Epithelial Cells. *Cell Stem Cell*. https://doi.org/https://doi.org/10.1016/j.stem.2017.08.014

Jacob, A., Morley, M., Hawkins, F., McCauley, K. B., Jean, J. C., Heins, H., Na, C. L., Weaver, T. E., Vedaie, M., Hurley, K., Hinds, A., Russo, S. J., Kook, S., Zacharias, W., Ochs, M., Traber, K., Quinton, L. J., Crane, A., Davis, B. R., . . . Kotton, D. N. (2017). Differentiation of Human Pluripotent Stem Cells into Functional Lung Alveolar Epithelial Cells. *Cell stem cell*, *21*(4), 472-488.e410. https://doi.org/10.1016/j.stem.2017.08.014

Jacob, A., Vedaie, M., Roberts, D. A., Thomas, D. C., Villacorta-Martin, C., Alysandratos, K.-D., Hawkins, F., & Kotton, D. N. (2019). Derivation of self-renewing lung alveolar epithelial type II cells from human pluripotent stem cells. *Nature protocols*, *14*(12), 3303-3332. https://doi.org/10.1038/s41596-019-0220-0

Jake Le Suer, R. S., Finn Hawkins, Amy L. Ryan. (2021). Induced pluripotent stem cells for generating lung airway stem cells and modelling respiratory disease. *Eur Respir Monogr 2021*, 190-204.

Kadzik, R. S., & Morrisey, E. E. (2012). Directing lung endoderm differentiation in pluripotent stem cells. *Cell stem cell*, *10*(4), 355-361. https://doi.org/10.1016/j.stem.2012.03.013

Kastlmeier, M. T., Guenther, E. M., Stoeger, T., & Voss, C. (2022). Lung Organoids for Hazard Assessment of Nanomaterials. *International Journal of Molecular Sciences*, *23*(24), 15666. https://www.mdpi.com/1422-0067/23/24/15666

Katzen, J., & Beers, M. F. (2020). Contributions of alveolar epithelial cell quality control to pulmonary fibrosis. *The Journal of Clinical Investigation*, *130*(10), 5088-5099. https://doi.org/10.1172/JCI139519

Khudadah, K., Ramadan, A., Othman, A., Refaey, N., Elrosasy, A., Rezkallah, A., Heseba, T., Moawad, M., Mektebi, A., Elejla, S. A., Abouzid, M., & Abdelazeem, B. (2023). Surfactant replacement therapy as promising treatment for COVID-19: an updated narrative review. *Biosci Rep*, *43*(8). https://doi.org/10.1042/bsr20230504

Kim, J., Koo, B.-K., & Knoblich, J. A. (2020). Human organoids: model systems for human biology and medicine. *Nature Reviews Molecular Cell Biology*, *21*(10), 571-584. https://doi.org/10.1038/s41580-020-0259-3

Knudsen, L., & Ochs, M. (2018). The micromechanics of lung alveoli: structure and function of surfactant and tissue components. *Histochemistry and Cell Biology*, *150*(6), 661-676. https://doi.org/10.1007/s00418-018-1747-9

Kong, J., Wen, S., Cao, W., Yue, P., Xu, X., Zhang, Y., Luo, L., Chen, T., Li, L., Wang, F., Tao, J., Zhou, G., Luo, S., Liu, A., & Bao, F. (2021). Lung organoids, useful tools for investigating epithelial repair after lung injury. *Stem Cell Research & Therapy*, *12*(1), 95. https://doi.org/10.1186/s13287-021-02172-5

Kortekaas, R., Geillinger-Kästle, K., Borghuis, T., Belharch, K., Webster, M., Timens, W., Burgess, J., & Gosens, R. (2022). IL-11 disrupts alveolar epithelial progenitor function. In: bioRxiv.

Kortekaas, R. K., Burgess, J. K., Webster, M., & Gosens, R. (2021). IL11 negatively impacts adult lung alveolar organoid formation. *ERJ Open Research*, *7*(suppl 6), 81. https://doi.org/10.1183/23120541.Lsc-2021.81

Kröner, C., Neumann, J., Ley-Zaporozhan, J., Hagl, B., Meixner, I., Spielberger, B. D., Dückers, G., Belohradsky, B. H., Niehues, T., Borte, M., Rosenecker, J., Kappler, M., Nährig, S., Reu, S., Griese, M., & Renner, E. D. (2019). Lung disease in STAT3 hyper-IgE syndrome requires intense therapy. *Allergy*, *74*(9), 1691-1702. https://doi.org/10.1111/all.13753

Land, S. C., Scott, C. L., & Walker, D. (2014). mTOR signalling, embryogenesis and the control of lung development. *Seminars in Cell & Developmental Biology*, *36*, 68-78. https://doi.org/https://doi.org/10.1016/j.semcdb.2014.09.023

Leibel, S. L., McVicar, R. N., Winquist, A. M., & Snyder, E. Y. (2021). Generation of 3D Whole Lung Organoids from Induced Pluripotent Stem Cells for Modeling Lung Developmental Biology and Disease. *J Vis Exp*(170). https://doi.org/10.3791/62456

Lowry, W. E., Richter, L., Yachechko, R., Pyle, A. D., Tchieu, J., Sridharan, R., Clark, A. T., & Plath, K. (2008). Generation of human induced pluripotent stem cells from dermal fibroblasts. *Proceedings of the National Academy of Sciences of the United States of America*, *105*(8), 2883-2888. https://doi.org/10.1073/pnas.0711983105

Matsuzaki, Y., Besnard, V., Clark, J. C., Xu, Y., Wert, S. E., Ikegami, M., & Whitsett, J. A. (2008). STAT3 regulates ABCA3 expression and influences lamellar body formation in alveolar type II cells. *American journal of respiratory cell and molecular biology*, *38*(5), 551-558. https://doi.org/10.1165/rcmb.2007-0311OC

Miller, A. J., Dye, B. R., Ferrer-Torres, D., Hill, D. R., Overeem, A. W., Shea, L. D., & Spence, J. R. (2019). Generation of lung organoids from human pluripotent stem cells in vitro. *Nature protocols*, *14*(2), 518-540. https://doi.org/10.1038/s41596-018-0104-8

Miller, A. J., & Spence, J. R. (2017). In Vitro Models to Study Human Lung Development, Disease and Homeostasis. *Physiology, 32*(3), 246-260. https://doi.org/10.1152/physiol.00041.2016

Minegishi, Y., Saito, M., Tsuchiya, S., Tsuge, I., Takada, H., Hara, T., Kawamura, N., Ariga, T., Pasic, S., Stojkovic, O., Metin, A., & Karasuyama, H. (2007). Dominant-negative mutations in the DNA-binding domain of STAT3 cause hyper-IgE syndrome. *Nature, 448*(7157), 1058-1062. https://doi.org/10.1038/nature06096

Morrisey, E. E., & Hogan, B. L. M. (2010). Preparing for the first breath: genetic and cellular mechanisms in lung development. *Developmental cell, 18*(1), 8-23. https://doi.org/10.1016/j.devcel.2009.12.010

Nikolić, M. Z., Sun, D., & Rawlins, E. L. (2018). Human lung development: recent progress and new challenges. *Development, 145*(16). https://doi.org/10.1242/dev.163485

Noble, P. W. (2008). Epithelial fibroblast triggering and interactions in pulmonary fibrosis. *European Respiratory Review, 17*(109), 123-129. https://doi.org/10.1183/09059180.00010904

Olajuyin, A. M., Zhang, X., & Ji, H.-L. (2019). Alveolar type 2 progenitor cells for lung injury repair. *Cell Death Discovery, 5*(1), 63. https://doi.org/10.1038/s41420-019-0147-9

Parimon, T., Yao, C., Stripp, B. R., Noble, P. W., & Chen, P. (2020). Alveolar Epithelial Type II Cells as Drivers of Lung Fibrosis in Idiopathic Pulmonary Fibrosis. *International Journal of Molecular Sciences, 21*(7), 2269. https://www.mdpi.com/1422-0067/21/7/2269

Paris, A. J., Hayer, K. E., Oved, J. H., Avgousti, D. C., Toulmin, S. A., Zepp, J. A., Zacharias, W. J., Katzen, J. B., Basil, M. C., Kremp, M. M., Slamowitz, A. R., Jayachandran, S., Sivakumar, A., Dai, N., Wang, P., Frank, D. B., Eisenlohr, L. C., Cantu, E., Beers, M. F., . . . Worthen, G. S. (2020). STAT3–BDNF–TrkB signalling promotes alveolar epithelial regeneration after lung injury. *Nature Cell Biology, 22*(10), 1197-1210. https://doi.org/10.1038/s41556-020-0569-x

Pavelka, M., & Roth, J. (2010). Alveoli: Gas Exchange and Host Defense. In M. Pavelka & J. Roth (Eds.), *Functional Ultrastructure: Atlas of Tissue Biology and Pathology* (pp. 248-249). Springer Vienna. https://doi.org/10.1007/978-3-211-99390-3_128

Pedroza, M., Le, T. T., Lewis, K., Karmouty-Quintana, H., To, S., George, A. T., Blackburn, M. R., Tweardy, D. J., & Agarwal, S. K. (2016). STAT-3 contributes to pulmonary fibrosis through epithelial injury and fibroblast-myofibroblast differentiation. *Faseb j, 30*(1), 129-140. https://doi.org/10.1096/fj.15-273953

Pérez-Gil, J. (2008). Structure of pulmonary surfactant membranes and films: The role of proteins and lipid–protein interactions. *Biochimica et Biophysica Acta (BBA) - Biomembranes, 1778*(7), 1676-1695. https://doi.org/https://doi.org/10.1016/j.bbamem.2008.05.003

Prange, H. D. (2003). LAPLACE'S LAW AND THE ALVEOLUS: A MISCONCEPTION OF ANATOMY AND A MISAPPLICATION OF PHYSICS. *Advances in Physiology Education, 27*(1), 34-40. https://doi.org/10.1152/advan.00024.2002

Rout-Pitt, N., Farrow, N., Parsons, D., & Donnelley, M. (2018). Epithelial mesenchymal transition (EMT): a universal process in lung diseases with implications for cystic fibrosis pathophysiology. *Respiratory Research, 19*(1), 136. https://doi.org/10.1186/s12931-018-0834-8

Sanches Santos Rizzo Zuttion, M., Moore, S. K. L., Chen, P., Beppu, A. K., & Hook, J. L. (2022). New Insights into the Alveolar Epithelium as a Driver of Acute Respiratory Distress Syndrome. *Biomolecules, 12*(9), 1273. https://www.mdpi.com/2218-273X/12/9/1273

Satora, L., Gawlikowski, T., Tański, A., & Formicki, K. (2022). Quest for breathing: proliferation of alveolar type 1 cells. *Histochemistry and Cell Biology, 157*(4), 393-401. https://doi.org/10.1007/s00418-022-02073-5

Sharma, A., Sances, S., Workman, M. J., & Svendsen, C. N. (2020). Multi-lineage Human iPSC-Derived Platforms for Disease Modeling and Drug Discovery. *Cell stem cell, 26*(3), 309-329. https://doi.org/https://doi.org/10.1016/j.stem.2020.02.011

Shi, Y., Inoue, H., Wu, J. C., & Yamanaka, S. (2017). Induced pluripotent stem cell technology: a decade of progress. *Nature Reviews Drug Discovery, 16*(2), 115-130. https://doi.org/10.1038/nrd.2016.245

Somers, A., Jean, J. C., Sommer, C. A., Omari, A., Ford, C. C., Mills, J. A., Ying, L., Sommer, A. G., Jean, J. M., Smith, B. W., Lafyatis, R., Demierre, M. F., Weiss, D. J., French, D. L., Gadue, P., Murphy, G. J., Mostoslavsky, G., & Kotton, D. N. (2010). Generation of transgene-free lung disease-specific human induced pluripotent stem cells using a single excisable lentiviral stem cell cassette. *Stem Cells*, *28*(10), 1728-1740. https://doi.org/10.1002/stem.495

Sommer, A. G., Rozelle, S. S., Sullivan, S., Mills, J. A., Park, S. M., Smith, B. W., Iyer, A. M., French, D. L., Kotton, D. N., Gadue, P., Murphy, G. J., & Mostoslavsky, G. (2012). Generation of human induced pluripotent stem cells from peripheral blood using the STEMCCA lentiviral vector. *J Vis Exp*(68). https://doi.org/10.3791/4327

Strunz, M., Simon, L. M., Ansari, M., Kathiriya, J. J., Angelidis, I., Mayr, C. H., Tsidiridis, G., Lange, M., Mattner, L. F., Yee, M., Ogar, P., Sengupta, A., Kukhtevich, I., Schneider, R., Zhao, Z., Voss, C., Stoeger, T., Neumann, J. H. L., Hilgendorff, A., . . . Schiller, H. B. (2020). Alveolar regeneration through a Krt8+ transitional stem cell state that persists in human lung fibrosis. *Nat Commun*, *11*(1), 3559. https://doi.org/10.1038/s41467-020-17358-3

Takahashi, K., Tanabe, K., Ohnuki, M., Narita, M., Ichisaka, T., Tomoda, K., & Yamanaka, S. (2007). Induction of pluripotent stem cells from adult human fibroblasts by defined factors. *Cell*, *131*(5), 861-872. https://doi.org/10.1016/j.cell.2007.11.019

Vadász, I., & Sznajder, J. I. (2017). Gas Exchange Disturbances Regulate Alveolar Fluid Clearance during Acute Lung Injury [Mini Review]. *Frontiers in Immunology*, *8*. https://doi.org/10.3389/fimmu.2017.00757

Wang, Y., Tang, Z., Huang, H., Li, J., Wang, Z., Yu, Y., Zhang, C., Li, J., Dai, H., Wang, F., Cai, T., & Tang, N. (2018). Pulmonary alveolar type I cell population consists of two distinct subtypes that differ in cell fate. *Proceedings of the National Academy of Sciences*, *115*(10), 2407-2412. https://doi.org/doi:10.1073/pnas.1719474115

Wu, H., & Tang, N. (2021). Stem cells in pulmonary alveolar regeneration. *Development*, *148*(2). https://doi.org/10.1242/dev.193458

Yang, J., Pan, X., Wang, L., & Yu, G. (2020). Alveolar cells under mechanical stressed niche: critical contributors to pulmonary fibrosis. *Molecular Medicine*, *26*(1), 95. https://doi.org/10.1186/s10020-020-00223-w

Appendix A: Publication III

Perspective

Lung organoids from hazard assessment of nanomaterials

by Miriam T. Kastlmeier [1,2,*], Eva M. Günter [1,2,*], Tobias Stoeger [1,2] and Carola Voss [1,2]

[1] Institute of Lung Health and Immunity (LHI), Comprehensive Pneumology Center Munich (CPC-M), Helmholtz Center Munich, Research Center for Environmental Health, 85764 München, Germany
[2] German Center of Lung Research (DZL), Comprehensive Pneumology Center Munich (CPC-M), 81377 München, Germany

*These authors contributed equally to this work.

Perspective

Lung Organoids for Hazard Assessment of Nanomaterials

Miriam T. Kastlmeier [1,2,†], Eva M. Guenther [1,2,†], Tobias Stoeger [1,2] and Carola Voss [1,2,*]

1 Institute of Lung Health and Immunity (LHI), Comprehensive Pneumology Center Munich (CPC-M), Helmholtz Center Munich, Research Center for Environmental Health, 85764 München, Germany
2 German Center of Lung Research (DZL), Comprehensive Pneumology Center Munich (CPC-M), 81377 München, Germany
* Correspondence: carola.voss@helmholtz-muenchen.de
† These authors contributed equally to this work.

Abstract: Lung epithelial organoids for the hazard assessment of inhaled nanomaterials offer a promising improvement to in vitro culture systems used so far. Organoids grow in three-dimensional (3D) spheres and can be derived from either induced pluripotent stem cells (iPSC) or primary lung tissue stem cells from either human or mouse. In this perspective we will highlight advantages and disadvantages of traditional culture systems frequently used for testing nanomaterials and compare them to lung epithelial organoids. We also discuss the differences between tissue and iPSC-derived organoids and give an outlook in which direction the whole field could possibly go with these versatile tools.

Keywords: nanomaterial; pulmonary particle exposure; organoids; 3D in vitro models; pluripotent stem cells; respiratory toxicity; hazard assessment

1. Background

Inhalation is by far the most important route of exposure for airborne pollutants and particles. Pulmonary particle exposure comprises airborne pathogens, including viruses and bacteria, but also ambient particulate matter, such as combustion-derived particles and even engineered nanomaterials (NM); the latter mainly at occupational settings during production, processing or decomposition. Depending on their aerodynamic diameter, airborne particles bigger than a few micrometers are deposited along the surface covered with mucus of the conducting airways by impaction, where they are rapidly removed via mucociliary clearance. Inhaled nanoparticles (NP) smaller than 100 nm in diameter deposit mainly by diffusion in the whole lung, but are especially efficient in the most distal and fragile parts of the lung, the alveoli [1]. While the alveolar region possesses over 90% of the lung's surface area, it also represents the most susceptible tissue interface to the environment with only a few 100 nm thickness of the alveolar walls, protected only by a thin liquid layer [2]. The primary interaction during inhalation of particles occurs, therefore, with either mucus covering the conducting airways or alveolar lining fluid of the respiratory tract. Pulmonary surfactant as the major component of the lining fluid, consists of a unique composition of 80–90% phospholipids, 5–10% neutral lipids and 10% surfactant-associated proteins (SP-A, B, C and D) [3]. The surfactant acts as a surface tension lowering film covering the alveolar surface, thereby protecting the alveoli from collapse during exhalation and reduces the effort of breathing [2]. In addition, any deposited material or particle is immersed into the lining fluid. The interaction between lining fluid and particles may also dramatically change the physical–chemical properties of alveolar deposited inhaled particles, causing immobilization or aggregation, and modifies their surface chemistry. Particle clearance is facilitated by either removal via the mucociliary escalator in conducting upper airways or phagocytosis by alveolar macrophages (AMs) roaming the alveolar surface. Ineffective clearance, repetitive inhalation as well as hotspots

of deposition formed at the bifurcations of terminal bronchioles and alveolar ducts, can lead to accumulation and high particle burden at specific areas of the respiratory tissue, and may thus increase the per cell delivered dose dramatically [4]. Furthermore, and in dependence of particle chemistry, its deposition may damage the surfactant function of the layer itself [5] and lead to a local inflammation [6].

Once reaching the alveolar surface, particles can lead to serious health consequences such as attenuated lung development for children exposed to combustion-derived traffic emissions [7,8], cardiovascular effects in susceptible adults as for diesel exhaust particles [9] and metal fume and polymer fume fever as for specific metal oxides and fluorinated polymers [10]. Depending on the pulmonary delivered dose, basically all materials can cause local inflammatory responses, in this context a variety of toxicological rodent studies support the respiratory toxicity of particles with particle surface area as the most valuable predictor for acute lung inflammation [11]. Detrimental long-term consequences including chronic inflammation, fibrosis and even tumor formation in lung tissue have been associated with inhalation of certain types of fiber shaped, high aspect ratio NPs [12]. Despite this knowledge, the ever-growing field of nanotechnology-associated nanomaterial toxicology requires smarter approaches for NM fabrication, grouping and testing, especially considering high throughput approaches, ethical commitment and at the same time replacing and reducing animal testing [13].

To achieve a smarter and more ethical approach to NM testing, the Adverse Outcome Pathway (AOP) framework has been established, which incorporates mechanistic knowledge generated from in vivo experiments to connect measured toxicological endpoints with a pathological consequence by a sequence of molecular initiating events (MIEs), consecutive key events (KEs) and the final adverse outcome ("disease"; AO). Several AOPs have been identified and shown to have strong correlation across published in vivo datasets [14]. To get robust information about the connection of KEs, AOPs need to particularly assess quantitative relationships, e.g., relevant NM doses. Furthermore, this AOP approach facilitates the design of superior in vitro testing strategies with the ultimate goal to reflect MIEs or KEs robustly in vitro, which would ultimately unburden safe-by-design strategies and reduce animal testing in the future. Recently, for the AOP 'chronic inflammation', an in vitro based test system has been demonstrated with highly specialized methods to reach superior predictive power for an ample set of NMs (metal oxide-based materials) [14]. AOPs are especially helpful for deciding which New Approach Methodology (NAM) could be used regarding NM toxicology studies [15]. With appropriate NAMs, toxicity testing is evidence-based, more predictive and reproducible. Hence, more and more predictive alternative and tissue specific in vitro models have to emerge based on AOPs. These will enable reliable and high throughput applicable cell-based studies, covering information from the molecular onset to the development of pathology, namely the identification of MIEs and KEs leading to AOPs in vivo.

In the following section, we will (1) portrait the difficulties of current in vitro models especially for specified AOP based testing, (2) introduce different lung organoid cultures as an alternative method and (3) give an outlook on these NAMs in the field of research.

2. Culture Methods for NM Hazard Assessment

Numerous studies display adverse effects of NM on the lung or lung cells, including cell proliferation, oxidative stress [16,17], DNA damage [18], pro-inflammatory [19,20] and pro-fibrotic response [21,22] using in vitro or in vivo systems to detect and compare molecular effects of different NMs, and to identify potential detrimental responses through nanoparticle-specific actions. For an in vitro set up, the standard and most simple technique in toxicological research is achieved by adding substances directly to the media of submerged cultures. However, for inhalation and particle toxicological studies this method is not decisive, since the process of particle–cell interaction as observed at the epithelial surface of the lung, is different to in medium submerged conditions [23,24]. The distribution pattern of NPs by inhalation is more critical than the stimulation itself [25]. Apart from

inappropriate biological conditions, obscure dosimetry, especially the dose interacting with and thus delivered to the cell at submerged conditions, is a major concern for poorly soluble particles that is challenging to determine and, moreover, is still rarely considered [24,26]. The unrealistic dose delivery for the lung surface is mainly due to factors driving the sedimentation route in submerged cultures. For example, the aggregation of NMs in serum protein containing media, or the possibility of dissolution of certain NMs in high volumes of media can result in an unrealistic distribution of particles across the exposed cells [27,28].

To overcome these disadvantages for inhaled particles, cells can be cultured on an Air–Liquid Interface (ALI). By placing the cells or tissue on a porous membrane and feeding them just from the basal side, the apical side is open for an inhalation like airborne exposure, thereby a comparable experimental set up to in vivo conditions arises. Hence, in vitro exposure at the ALI with airborne NMs is not only the more realistic approach, but also the one allowing defined cell delivered dose estimations compared to exposure under submerged conditions. ALI inhalation models have the potential for a more precise reproduction of the processes during exposure, as they can mimic the fragile respiratory epithelial region comparable to structural in vivo terms [29]. Especially for studying the effects of exposure to low solubility materials, a special Air–Liquid Interface cell exposure (ALICE) system was developed, which uses a nebulizer to generate a droplet cloud of dispersed particles. Then, in the exposure chamber, the created moisture cloud finally drives the applied NMs to gravimetrically deposit onto the culture [28]. Instead of the use of gravimetric force, which requires aqueous dispersion for nebulization, other methods use electrostatic force to improve the deposition efficiency on the ALI surface [30]. Alternatively, ALI cultured cells can be exposed by using continuous flow systems (CFSs), which offer more realistic dose rates. CFSs may be especially advantageous where the cell exposure shall get directly linked downstream of particle emission or production [31]. In this context it must be mentioned that the exposed cells are often immortalized cell lines, which may resemble the natural cell characteristics only partly. In recent years, primary cells have been increasingly used to recapitulate physiological features in a feasible manner. In addition, the porous membranes used as substrate for the cell medium interface usually exceed realistic dimensions. Notably, well-working approaches to overcome this problem with advanced biomimetic membranes already exist [32].

Even with the most desired advanced models, it is noted that the results generated by inhalation of nanoparticles in vivo cannot be fully and properly represented in vitro. Previous studies have shown that the use of immortalized cell lines does not represent the in vivo situation completely, so does not provide fully comparable results to those obtained in vivo. This relates to the fact that immortalized cell lines often lose polarity and lack key morphology features, which may biologically distinguish respective cells in the context of tissue. Furthermore, as the immortalized cells do not have a natural proliferation cycle due to mutation or manipulation, they have evaded normal cellular senescence and instead can keep undergoing division, which could lead to functional alterations and genetic drifts [33,34]. In general, any cell model will only model a certain biological aspect of the in vivo situation and this aspect and its limitations have to be well-known to the researcher to use the model appropriately. Several human alveolar epithelial cell lines, for example A549, NCI-H441, TT1 and hAELVi, are commercially available. The ones originating from alveolar type 2 cells (AT2s) mostly lost their stem cell character, referring to the possibility to differentiate into alveolar type 1 like-cells (AT1s), with protein expression of Aquaporin-5 (AQP5) or Podoplanin (PDPN) [35–37] as it occurs in the lung. TT1 and hAELVi represent cells with an AT1-like phenotype regarding morphology and caveolae presence, although they do not display other common AT1 markers like AQP5 or, in the case of TT1, only show discontinuous tight junctions [38–41]. To get a human epithelial cell line representing the bronchial epithelium, for example BEAS-2B, 16HBE14o or Calu-3 are well established [42]. Indeed, there are also murine lung epithelial cell lines, namely MLE-12 or LA-4, representing the alveolar compartment. Therefore, the lack of

reproducibility between in vivo and in vitro data is not due to the applied in vitro model, but rather to the cells chosen for the particular research aim.

A promising approach to overcome disadvantages of currently widely used immortalized cell lines and to compare results created in vivo with in vitro data is the use of three-dimensional (3D) cell cultures, the so-called lung organoids. Organoids are defined as three-dimensional, mostly spherical shaped constructs cultured in vitro in an extracellular matrix. They self-organize from single stem cells into multicellular structures and mimic the in vivo organ, in this case the bronchiolar or alveolar region of the lung [43]. An overview of different ways to generate lung organoids and their cells of origin is shown in Figure 1.
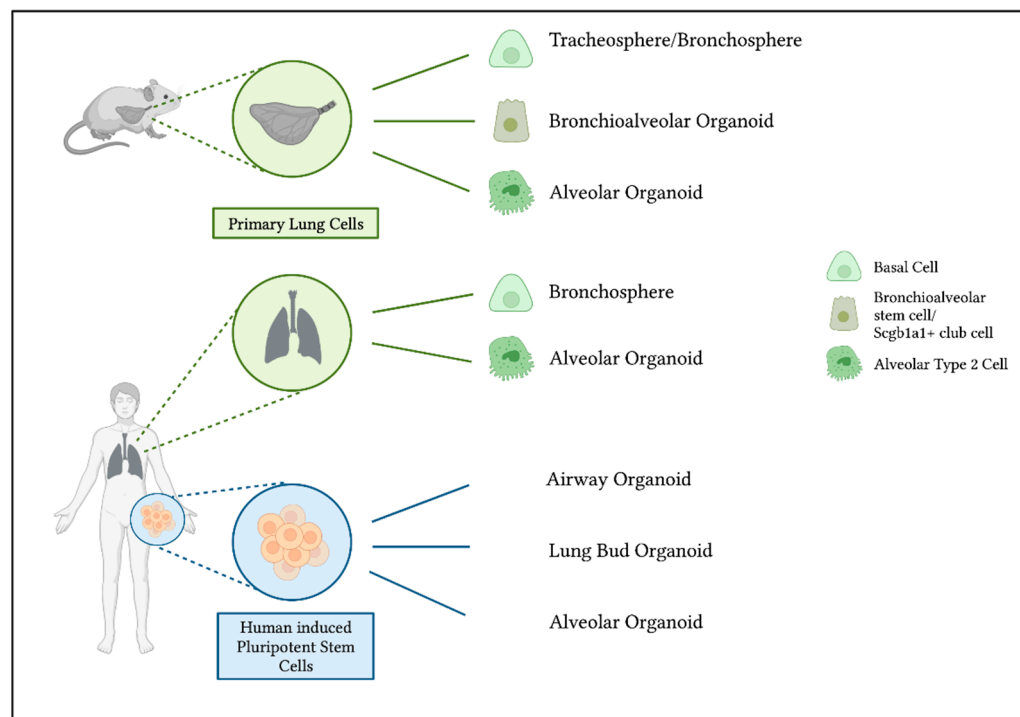

Figure 1. Generation of murine and human lung organoids and their cells of origin. Organoids can be derived from primary murine and human lung cells. Tracheospheres and bronchospheres originate from airway basal cells [44,45]. To generate bronchioalveolar organoids from murine lungs, bronchioalveolar stem cells or Scgb1a1+ club cells can act as progenitors to bronchiolar as well as alveolar cells [46,47]. Primary isolated alveolar type 2 cells are able to differentiate into alveolar organoids [48,49]. Another possibility to generate lung organoids is the use of human induced pluripotent stem cells. The use of different growth factors and conditions results in either airway [50] or alveolar organoids [51,52]. Organoids that include bronchial as well as alveolar cells can be derived as so-called lung bud organoids [53].

One method to grow lung organoids is to isolate primary epithelial cells out of lung tissue. This is possible with murine lungs as well as human tissue, although the availability of human lung tissue is limited. Basal cells act as progenitor cells in the tracheal and bronchial region of the lungs [54]. When isolated and cultured in a complex matrix, airway basal cells can form bronchospheres and contain multiple airway cell types, including ciliated, goblet and secretory cells, with expression of markers as Forkhead Box J1 (FoxJ1), acetylated a-tubulin, Mucin 5AC (MUC5AC), Cystic Fibrosis Transmembrane Conductance Regulator (CFTR) or secretoglobin family 1A member 1 (SCGB1A1). The human and murine bronchospheres still contain basal cells expressing for example p63, enabling them to self-renew [44,45]. In the alveolar region, AT2s have stem cell character and can proliferate and differentiate into AT1s [48]. To obtain organoids, mesenchymal support cells are often needed to help the organoids grow. Human mature alveolar organoids show AT2

markers such as surfactant protein-C (SFTPC) and HTII-280. Murine alveolar organoids also contain SFTPC expressing cells and, in addition, cells showing AT1 characteristics [48,49] (Figure 2a,b). Thus, stem cell properties are retained within a 3D culture, in contrast to traditional culture methods with cell lines. In addition to these two organoid types, the bronchospheres and the alveolar organoids, it is also possible to obtain bronchioalveolar organoids from distinct cell populations in mouse lungs. The so-called bronchioalveolar stem cells (BASCs) and Scgb1a1 positive club cells are able to give rise to organoids containing cells with an airway phenotype as well as alveolar characteristics. They combine both lung compartments in vitro, with bronchiolar cells in the center followed by an outer part of branching alveolar structures [46,47].
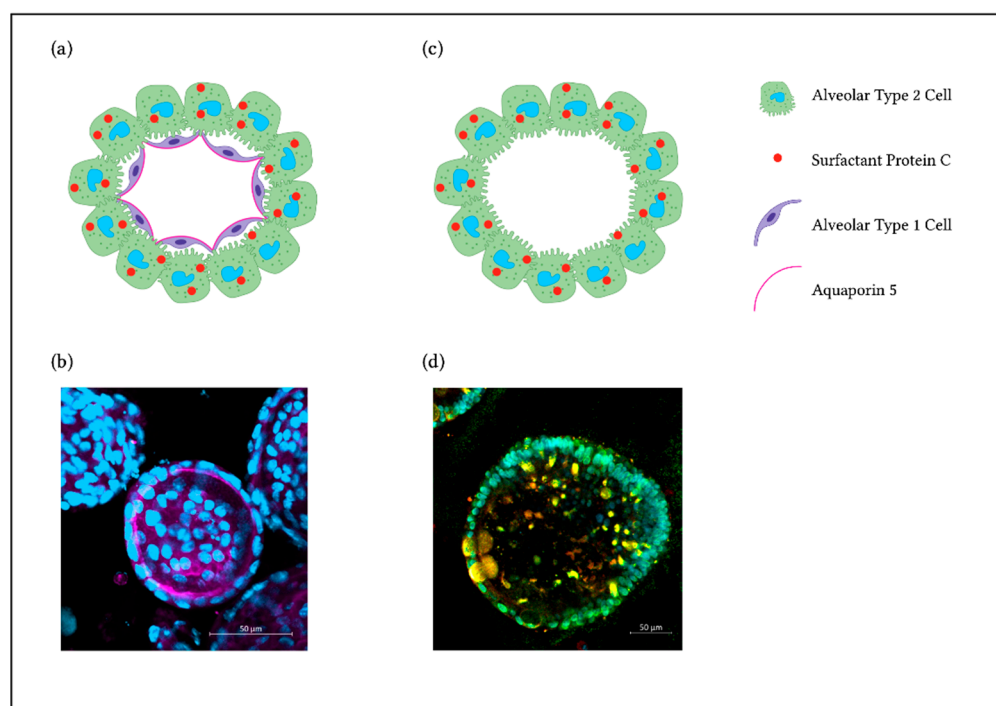

Figure 2. 3D Alveolar Organoids. (**a**) Illustration showing a primary murine alveolar organoid. (**b**) Representative immunofluorescence staining of a murine alveolar organoid showing AQP5 staining as a marker for AT1s (pink) and nuclei (DAPI, blue). (**c**) Illustration showing a hiPSC-derived alveolar organoid. (**d**) Representative immunofluorescence staining with AT2s expressing SP-C (red), NKX2.1 (green) and nuclei (DAPI, cyan).

An alternative to primary lung epithelial cells for generating lung organoids is the use of directed differentiation of induced pluripotent stem cells (iPSCs). Since the discovery of human iPSCs [55], they are considered a valuable alternative to the problematic use of embryonic stem cells (ESCs) and to provide comparable in vitro models in relation to the actual disease pattern in humans with the potential of long term and repetitive experiments.

The experimental set-ups of in vitro lung models are based on biochemical differentiation of hiPSCs into lung lineages. Organoids derived from stem cells (ESC or hiPSC) are able to differentiate and self-organize through lineage bonding comparable to processes taking place during development in vivo [56].

hiPSCs differentiated into lung progenitors can be used for deriving airway organoids. They contain SCGB1A1+ secretory cells, multiciliated cells expressing FOXJ1 and basal cells, amongst others [50]. In modified conditions, lung progenitors can grow into mature alveolar epithelium with specific cell expression markers of AT2s (and AT1s), e.g., SP-C [51,52]. As shown in Jacob et al. 2017 [51], NKX2.1 is highly expressed in tightly packed lung progenitor colonies. At a later stage of differentiation, lung progenitors resulted in self-renewal and high yield of SP-C expressing iAT2s (Figure 2c,d). An interesting approach

to obtain lung organoids that contain AT2s, AT1s as well as airway goblet cells, is to generate lung bud organoids by prolonged differentiation in a 3D matrix. With this method, mesenchymal cells expressing Vimentin (VIM) arise, surrounding the organoids [53].

Great advantages of 3D lung organoid cultures compared to conventional cell lines are the comparable cellular identity and functionality to the in vivo situation, and the potential to differentiate into several epithelial cell types. This enables us to perform disease modeling, developmental and regeneration studies, identify roles of the distinct cell types regarding cellular communication in defined settings and create a representative model of airway and/or alveolar lung compartments. When comparing architecture and functional readouts of lung tissue, a 3D cell culture system creates much better and even more realistic conditions than a cell monolayer culture system [57,58]. A feature of mature AT2s in a 3D cell culture system, is the ability to produce lamellar body-like inclusions, including mature SP-B and SP-C protein forms, and thus further supporting their self-renewing capacity, which is desperately needed for a constant repetition of experimental set-ups. Lipidomic analysis of the intracellular and extracellular material from alveolar organoids show amounts of dipalmitoylphosphatidylcholine (DPPC), the main phospholipid in surfactant, and thus the presence of functional lamellar bodies that synthesize and secrete surfactant from phenotypically mature AT2s [51]. At the moment, this prominent feature of AT2s is only found in stem cell derived 3D cultures. Another advantage of organoid cultures, either originating from primary lung cells or iPSCs, is the possibility to include multiple defined cell types into a co-culture system. The defined, but superior model can incorporate different cells representing lung epithelial cells interacting with fibroblasts, endothelial cells or immune cells [46,59–62], thus promoting interactions and displaying inflammation and cell-matrix alterations, for example. Especially, studying cell–cell interactions with regard to therapeutic efficacy and toxicity of delivered drugs is possible in 3D microtissue models. One thing to highlight as an advantage of human organoid cultures is they provide faster and more robust outcomes, as well as a more accurate representation of human tissue than animal models [63]. Notably, from hiPSCs, generated lung organoids can be passaged for up to 300 days and retain their typical alveolar characteristics [52,64]. In contrast to all of these advantages of using iPSC derived organoids, their generation is quite laborious. For human tissue derived lung organoids, the availability of lung samples to perform epithelial cell isolation is restricted, and obvious ethical issues arise in this context. An additional dilemma regarding human lung tissue samples is that it is not feasible to get completely healthy tissue, only, for example, peritumoral samples. Although murine lung organoids can be derived from various genetic backgrounds, this method is still dependent on animal experiments and is not the replacement that traditional culture models are. Nevertheless, murine as well as human organoid experiments could help to reduce the number of research animals used in accordance to the 3R principles [65] and additionally, using human cells would increase the translational aspect and allow patient-associated studies. Especially in the context of NM toxicity assessments, it is advisable to take advantage of the benefits 3D organoids offer. Lung organoids are already used for different research questions regarding NM toxicity. Readouts including reactive oxygen species (ROS) production, epithelial cell differentiation and regeneration, NP internalization or surfactant production can be assessed easily, and help to elucidate the mechanisms underlying disease progression in the lung after NP exposure [66–68]. Toxicity testing in organoids is not yet used often, but these examples already show the numerous opportunities with 3D lung cultures. However, one difficulty still is to imitate the inhalation of NMs. For example, in Yu et al. 2022 [68], the particles to be tested are mixed into the culture medium, which is without a doubt a convenient and high throughput suitable approach for NM exposure, but leads to similar problems regarding the cell delivered dose and the particle–cell interaction as a conventional 2D submerged cell culture does. Nevertheless, 3D organoids are able to respond to stimuli and can recapitulate epithelial cell responses more accurately than 2D culture [69]. In addition, usually grown alveolar organoids are polarized in such a way that the surfactant producing apical side is faced towards the lumen of the sphere. Thus,

exposure to NMs through the media or matrix does not reach the epithelial cells as it would in vivo, which are exposed from the basal side. One possible idea to overcome this issue is to microinject the desired harmful substance directly into the lumen of the organoid, which is not yet performed with NMs, but within several other contexts [59,70]. This brings the NMs or pathogens directly to the site of action and the exact dose delivered to the cells is known. Nevertheless, microinjection of NM into lung organoids is not done so far as it is challenging to generate high throughput. In order to get a relevant outcome, this method requires experience regarding the microinjector. On the other hand, there are already approaches to change the polarity of distal lung organoids towards an apical-out polarization [71] This method could be used to expose lung organoids to NMs easier from the apical cell side. Still, organoids are grown in matrix with feeding medium, this means a direct contact or defined cell delivered dose is difficult to achieve under these conditions.

Another approach to take advantage of the stem cell character that cells keep in organoid culture is to dissociate the cultured 3D organoids into single cells again. When cultured in Transwell inserts, organoid derived epithelial cells can form an intact epithelial barrier [72].

In this setting, exposure to NMs using the ALICE system, where particles are nebulized and a defined dose is distributed equally upon the cells, is feasible. The combination of using cells with functions and properties as in vivo, and the inhalation-like exposure to particles with the ALICE system makes this culture method interesting. In summary, the combination of organoid culture and subsequent ALI exposure to balance the limitations of each individual model will be a useful approach to assess NM hazards.

3. Future Direction

Lung organoid technology has developed quickly in the last years and became a useful tool for modeling perpetuating lung diseases and hazards affecting the lung [72]. With reference to previous research, it is evident that a holistic in vitro model of the lung cannot be generated. Therefore, it is absolutely essential for a comprehensive, accurate and above all realistic test result to relate the model to the specific research question. It must be clarified from the beginning whether a 2D submerged, ALI model or a 3D cell culture model would be the right choice for the problem posed. For investigations, particularly with regard to epithelial responses, epithelial cell differentiation and epithelial recovery, organoids are a suitable instrument [72].

Thus, the choice of cells used should be thoroughly considered, especially concerning their respective properties, such as forming lamellar bodies, producing surfactant or retaining stem cell character. It becomes clear that there is not one overall cell line for a general experimental setup, for instance with regard to NM inhalation, where particle–cell interactions in a realistic environment are of particular importance. Therefore, using advanced target cells that are able to create a liquid lining layer would improve the comparability of in vitro studies to in vivo findings and lead to extended outcomes (Table 1).

One important step in the future is to increase the use of stem cell derived murine or, even better, human cells that adequately reflect the disease pattern for monitoring and understanding the underlying cell–cell interactions after NM exposure. For instance, the use of immortalized cell lines within an in vitro experiment has shown to be not comparable to a clinical picture. Isolated human primary cells can only be passaged for a short period of time and are therefore also not sufficiently suitable for a complex experimental set-up with necessary replicates. At this point, an adapted experimental setup with hiPSCs would be a desirable and new promising approach. Due to their close resemblance to the primary cells, despite their durability and the possibility to be passaged over a long period, hiPSC derived organoids should be the prospective choice for human in vitro experiments.

Table 1. Comparison of cell lines and organoids and exposure recommendations.

		Accessibility	Feasibility	Physiological Characteristics	Represented Cell Types	Co-Culture	Exposure Methods for Hazard Assessment			
							Submerged	ALI	CFS	Microinjection
Cell Lines		Commercially available, many passages	Easy to maintain	Partially preserved	Single	2D layered structure, often with use of membranes possible	Easy to apply, cell-delivered dose challenging to determine, HTS	Mimics deposition of inhaled particles, defined cell-delivered dose, realistic nano-bio interphase (surfactant etc.)	Mimics deposition of inhaled particles with realistic dose rate, defined cell-delivered dose, realistic nano-bio interphase (surfactant etc.)	3D structure required
Primary Cells		Animal or human tissue required, limited passaging	Isolation expertise required	Partially preserved	Single	2D layered structure, often with use of membranes possible	Easy to apply, cell-delivered dose challenging to determine, improved IVIVC			
Organoids	**Primary Cell-Derived**	Animal or human tissue required, limited passaging	Isolation expertise required	Mostly preserved	Formation into organoids containing AT2s, AT1s and airway epithelial organoids in the same culture	Organotypic, 3D self-assembly, possible	Easy to apply, cell-delivered dose challenging to determine, improved IVIVC, HTS exposure from basal instead of apical side	2D structure and ALI culture required		Delivers NM directly to apical side within the organoid lumen, high IVIVC, technologically challenging
	hiPSC-derived	Long-time passaging of organoids	Complex differentiation procedure, high level of organoid maintenance	Comparable to in vivo	Differentiation into organoids containing AT2s, (AT1s) or airway organoids	Organotypic, 3D self-assembly, possible				

In addition, an adequate murine in vitro 3D culture system has several advantages. It is important to create setups reflecting and confirming the findings observed in previous in vivo studies. This enables us to elucidate cell–cell interactions and events happening on cellular, protein and gene levels, while reducing the number of animals used in similar in vivo testing according to the 3R principles. Based on the AOP framework regarding NM toxicity, lung organoid culture could be a helpful NAM to obtain results representing in vivo conditions more accurately. With the emergence of new analytical techniques, profiling cellular responses at the single cell level, we realize that a tissue such as the lung consists of over 50 different cell types [73]. Yet these new approaches, such as single cell transcriptomics, raise the awareness that very specific cellular niches might be required to sense injury. For example, an AOP initiating event caused by inhaled particles, and a distinct cell–cell communication network are then required to develop the pathological outcome. For the lungs, these cellular networks and outcomes are now increasingly described for SARS-CoV-2 infection and pulmonary fibrosis [74], but similar communications are likely required for nanoparticle triggered AOPs. Reproducing the underlying key events and cell interactions at the in vitro level will be of great impact for future safety testing and organoids because of the maintained cellular plasticity and more natural cellular communications hold great promise.

In summary, we illustrate that already established experimental setups with new and adapted cells will lead to potentially improved or even new results and findings. Lung organoids include these particular cells, enabling us to perform hazard assessments for NMs within suitable models.

Institutional Review Board Statement: Not applicable.

Informed Consent Statement: Not applicable.

Data Availability Statement: Data sharing not applicable.

Conflicts of Interest: The authors declare no conflict of interest.

References

1. Fröhlich, E.; Salar-Behzadi, S. Toxicological Assessment of Inhaled Nanoparticles: Role of in Vivo, ex Vivo, in Vitro, and in Silico Studies. *Int. J. Mol. Sci.* **2014**, *15*, 4795–4822. [CrossRef] [PubMed]
2. Knudsen, L.; Ochs, M. The micromechanics of lung alveoli: Structure and function of surfactant and tissue components. *Histochem. Cell Biol.* **2018**, *150*, 661–676. [CrossRef] [PubMed]
3. Hite, R.D.; Grier, B.L.; Waite, B.M.; Veldhuizen, R.A.; Possmayer, F.; Yao, L.J.; Seeds, M.C. Surfactant protein B inhibits secretory phospholipase A2 hydrolysis of surfactant phospholipids. *Am. J. Physiol. Lung Cell Mol. Physiol.* **2012**, *302*, L257–L265. [CrossRef] [PubMed]
4. Lippmann, M.; Yeates, D.B.; Albert, R.E. Deposition, retention, and clearance of inhaled particles. *Br. J. Ind. Med.* **1980**, *37*, 337–362. [CrossRef]
5. Da Silva, E.; Vogel, U.; Hougaard, K.S.; Pérez-Gil, J.; Zuo, Y.Y.; Sørli, J.B. An adverse outcome pathway for lung surfactant function inhibition leading to decreased lung function. *Curr. Res. Toxicol.* **2021**, *2*, 225–236. [CrossRef]
6. Chen, S.; Yin, R.; Mutze, K.; Yu, Y.; Takenaka, S.; Konigshoff, M.; Stoeger, T. No involvement of alveolar macrophages in the initiation of carbon nanoparticle induced acute lung inflammation in mice. *Part. Fibre Toxicol.* **2016**, *13*, 33. [CrossRef]
7. Barraza-Villarreal, A.; Escamilla-Nuñez, M.C.; Hernández-Cadena, L.; Texcalac-Sangrador, J.L.; Sienra-Monge, J.J.; Del Río-Navarro, B.E.; Cortez-Lugo, M.; Sly, P.D.; Romieu, I. Elemental carbon exposure and lung function in school children from Mexico City. *Eur. Respir. J.* **2011**, *38*, 548–552. [CrossRef]
8. Kulkarni, N.; Pierse, N.; Rushton, L.; Grigg, J. Carbon in Airway Macrophages and Lung Function in Children. *N. Engl. J. Med.* **2006**, *355*, 21–30. [CrossRef]
9. Weitekamp, C.A.; Kerr, L.B.; Dishaw, L.; Nichols, J.; Lein, M.; Stewart, M.J. A systematic review of the health effects associated with the inhalation of particle-filtered and whole diesel exhaust. *Inhal. Toxicol.* **2020**, *32*, 1–13. [CrossRef]
10. Greenberg, M.I.; Vearrier, D. Metal fume fever and polymer fume fever. *Clin. Toxicol.* **2015**, *53*, 195–203. [CrossRef]
11. Schmid, O.; Stoeger, T. Surface area is the biologically most effective dose metric for acute nanoparticle toxicity in the lung. *J. Aerosol Sci.* **2016**, *99*, 133–143. [CrossRef]
12. Ciabattini, M.; Rizzello, E.; Lucaroni, F.; Palombi, L.; Boffetta, P. Systematic review and meta-analysis of recent high-quality studies on exposure to particulate matter and risk of lung cancer. *Env. Res.* **2021**, *196*, 110440. [CrossRef] [PubMed]
13. Burden, N.; Aschberger, K.; Chaudhry, Q.; Clift, M.J.D.; Doak, S.H.; Fowler, P.; Johnston, H.; Landsiedel, R.; Rowland, J.; Stone, V. The 3Rs as a framework to support a 21st century approach for nanosafety assessment. *Nano Today* **2017**, *12*, 10–13. [CrossRef]
14. Halappanavar, S.; van den Brule, S.; Nymark, P.; Gaté, L.; Seidel, C.; Valentino, S.; Zhernovkov, V.; Høgh Danielsen, P.; De Vizcaya, A.; Wolff, H.; et al. Adverse outcome pathways as a tool for the design of testing strategies to support the safety assessment of emerging advanced materials at the nanoscale. *Part. Fibre Toxicol.* **2020**, *17*, 16. [CrossRef] [PubMed]
15. Hoffmann, S.; Aiassa, E.; Angrish, M.; Beausoleil, C.; Bois, F.Y.; Ciccolallo, L.; Craig, P.S.; De Vries, R.B.M.; Dorne, J.; Druwe, I.L.; et al. Application of evidence-based methods to construct mechanism-driven chemical assessment frameworks. *ALTEX* **2022**, *39*, 499–518. [CrossRef] [PubMed]
16. Limbach, L.K.; Wick, P.; Manser, P.; Grass, R.N.; Bruinink, A.; Stark, W.J. Exposure of Engineered Nanoparticles to Human Lung Epithelial Cells: Influence of Chemical Composition and Catalytic Activity on Oxidative Stress. *Environ. Sci. Technol.* **2007**, *41*, 4158–4163. [CrossRef] [PubMed]
17. Lin, Z.; Ma, L.; Zhang, H.; Lin, B. A comparative study of lung toxicity in rats induced by three types of nanomaterials. *Nanoscale Res. Lett.* **2013**, *8*, 521. [CrossRef]
18. Lindberg, H.K.; Falck, G.C.M.; Suhonen, S.; Vippola, M.; Vanhala, E.; Catalán, J.; Savolainen, K.; Norppa, H. Genotoxicity of nanomaterials: DNA damage and micronuclei induced by carbon nanotubes and graphite nanofibres in human bronchial epithelial cells in vitro. *Toxicol. Lett.* **2009**, *186*, 166–173. [CrossRef]
19. Braakhuis, H.M.; Park, M.V.D.Z.; Gosens, I.; De Jong, W.H.; Cassee, F.R. Physicochemical characteristics of nanomaterials that affect pulmonary inflammation. *Part. Fibre Toxicol.* **2014**, *11*, 18. [CrossRef] [PubMed]
20. Warheit, D.B.; Laurence, B.R.; Reed, K.L.; Roach, D.H.; Reynolds, G.A.M.; Webb, T.R. Comparative Pulmonary Toxicity Assessment of Single-wall Carbon Nanotubes in Rats. *Toxicol. Sci.* **2004**, *77*, 117–125. [CrossRef]

21. Poulsen, S.S.; Saber, A.T.; Williams, A.; Andersen, O.; Købler, C.; Atluri, R.; Pozzebon, M.E.; Mucelli, S.P.; Simion, M.; Rickerby, D.; et al. MWCNTs of different physicochemical properties cause similar inflammatory responses, but differences in transcriptional and histological markers of fibrosis in mouse lungs. *Toxicol. Appl. Pharmacol.* **2015**, *284*, 16–32. [CrossRef]

22. Manke, A.; Luanpitpong, S.; Dong, C.; Wang, L.; He, X.; Battelli, L.; Derk, R.; Stueckle, T.A.; Porter, D.W.; Sager, T.; et al. Effect of Fiber Length on Carbon Nanotube-Induced Fibrogenesis. *Int. J. Mol. Sci.* **2014**, *15*, 7444–7461. [CrossRef]

23. Maier, K.L.; Alessandrini, F.; Beck-Speier, I.; Josef Hofer, T.P.; Diabaté, S.; Bitterle, E.; Stöger, T.; Jakob, T.; Behrendt, H.; Horsch, M.; et al. Health Effects of Ambient Particulate Matter—Biological Mechanisms and Inflammatory Responses to In Vitro and In Vivo Particle Exposures. *Inhal. Toxicol.* **2008**, *20*, 319–337. [CrossRef]

24. Lenz, A.-G.; Karg, E.; Brendel, E.; Hinze-Heyn, H.; Maier, K.L.; Eickelberg, O.; Stoeger, T.; Schmid, O. Inflammatory and Oxidative Stress Responses of an Alveolar Epithelial Cell Line to Airborne Zinc Oxide Nanoparticles at the Air-Liquid Interface: A Comparison with Conventional, Submerged Cell-Culture Conditions. *BioMed Res. Int.* **2013**, *2013*, 652632. [CrossRef] [PubMed]

25. Air–Liquid Interface In Vitro Models for Respiratory Toxicology Research: Consensus Workshop and Recommendations. *Appl. Vitr. Toxicol.* **2018**, *4*, 91–106. [CrossRef] [PubMed]

26. Schmid, O.; Cassee, F.R. On the pivotal role of dose for particle toxicology and risk assessment: Exposure is a poor surrogate for delivered dose. *Part. Fibre Toxicol.* **2017**, *14*, 52. [CrossRef] [PubMed]

27. Moore, T.L.; Rodriguez-Lorenzo, L.; Hirsch, V.; Balog, S.; Urban, D.; Jud, C.; Rothen-Rutishauser, B.; Lattuada, M.; Petri-Fink, A. Nanoparticle colloidal stability in cell culture media and impact on cellular interactions. *Chem. Soc. Rev.* **2015**, *44*, 6287–6305. [CrossRef]

28. Lenz, A.G.; Karg, E.; Lentner, B.; Dittrich, V.; Brandenberger, C.; Rothen-Rutishauser, B.; Schulz, H.; Ferron, G.A.; Schmid, O. A dose-controlled system for air-liquid interface cell exposure and application to zinc oxide nanoparticles. *Part. Fibre Toxicol.* **2009**, *6*, 32. [CrossRef]

29. Upadhyay, S.; Palmberg, L. Air-Liquid Interface: Relevant In Vitro Models for Investigating Air Pollutant-Induced Pulmonary Toxicity. *Toxicol. Sci.* **2018**, *164*, 21–30. [CrossRef]

30. Diabaté, S.; Armand, L.; Murugadoss, S.; Dilger, M.; Fritsch-Decker, S.; Schlager, C.; Béal, D.; Arnal, M.E.; Biola-Clier, M.; Ambrose, S.; et al. Air-Liquid Interface Exposure of Lung Epithelial Cells to Low Doses of Nanoparticles to Assess Pulmonary Adverse Effects. *Nanomaterials* **2020**, *11*, 65. [CrossRef]

31. Braakhuis, H.M.; He, R.; Vandebriel, R.J.; Gremmer, E.R.; Zwart, E.; Vermeulen, J.P.; Fokkens, P.; Boere, J.; Gosens, I.; Cassee, F.R. An Air-liquid Interface Bronchial Epithelial Model for Realistic, Repeated Inhalation Exposure to Airborne Particles for Toxicity Testing. *J. Vis. Exp.* **2020**, *159*, e61210. [CrossRef] [PubMed]

32. Doryab, A.; Taskin, M.B.; Stahlhut, P.; Groll, J.; Schmid, O. Real-Time Measurement of Cell Mechanics as a Clinically Relevant Readout of an In Vitro Lung Fibrosis Model Established on a Bioinspired Basement Membrane. *Adv. Mater.* **2022**, *34*, e2205083. [CrossRef] [PubMed]

33. Audesirk, G.J. 13.24—In Vitro Systems in Neurotoxicological Studies. In *Comprehensive Toxicology*, 2nd ed.; McQueen, C.A., Ed.; Elsevier: Oxford, UK, 2010; pp. 415–432.

34. Human Primary Cells and Immortal Cell Lines: Differences and Advantages. Available online: https://promocell.com/in-the-lab/human-primary-cells-and-immortal-cell-lines/ (accessed on 28 October 2022).

35. Salomon, J.J.; Muchitsch, V.E.; Gausterer, J.C.; Schwagerus, E.; Huwer, H.; Daum, N.; Lehr, C.M.; Ehrhardt, C. The cell line NCl-H441 is a useful in vitro model for transport studies of human distal lung epithelial barrier. *Mol. Pharm.* **2014**, *11*, 995–1006. [CrossRef] [PubMed]

36. Ren, H.; Birch, N.P.; Suresh, V. An Optimised Human Cell Culture Model for Alveolar Epithelial Transport. *PLoS ONE* **2016**, *11*, e0165225. [CrossRef] [PubMed]

37. Winton, H.L.; Wan, H.; Cannell, M.B.; Gruenert, D.C.; Thompson, P.J.; Garrod, D.R.; Stewart, G.A.; Robinson, C. Cell lines of pulmonary and non-pulmonary origin as tools to study the effects of house dust mite proteinases on the regulation of epithelial permeability. *Clin. Exp. Allergy* **1998**, *28*, 1273–1285. [CrossRef]

38. Kemp, S.J.; Thorley, A.J.; Gorelik, J.; Seckl, M.J.; O'Hare, M.J.; Arcaro, A.; Korchev, Y.; Goldstraw, P.; Tetley, T.D. Immortalization of human alveolar epithelial cells to investigate nanoparticle uptake. *Am. J. Respir. Cell Mol. Biol.* **2008**, *39*, 591–597. [CrossRef]

39. van den Bogaard, E.H.; Dailey, L.A.; Thorley, A.J.; Tetley, T.D.; Forbes, B. Inflammatory response and barrier properties of a new alveolar type 1-like cell line (TT1). *Pharm. Res.* **2009**, *26*, 1172–1180. [CrossRef]

40. Kuehn, A.; Kletting, S.; de Souza Carvalho-Wodarz, C.; Repnik, U.; Griffiths, G.; Fischer, U.; Meese, E.; Huwer, H.; Wirth, D.; May, T.; et al. Human alveolar epithelial cells expressing tight junctions to model the air-blood barrier. *ALTEX* **2016**, *33*, 251–260. [CrossRef]

41. Mills-Goodlet, R.; Schenck, M.; Chary, A.; Geppert, M.; Serchi, T.; Hofer, S.; Hofstätter, N.; Feinle, A.; Hüsing, N.; Gutleb, A.C.; et al. Biological effects of allergen–nanoparticle conjugates: Uptake and immune effects determined on hAELVi cells under submerged vs. air–liquid interface conditions. *Environ. Sci. Nano* **2020**, *7*, 2073–2086. [CrossRef]

42. Hermanns, M.I.; Freese, C.; Anspach, L.; Grützner, V.; Pohl, C.; Unger, R.E.; Kirkpatrick, C.J. 3.15 Cell Culture Systems for Studying Biomaterial Interactions With Biological Barriers. In *Comprehensive Biomaterials II*; Ducheyne, P., Ed.; Elsevier: Oxford, UK, 2017; pp. 295–334.

43. de Souza, N. Organoids. *Nat. Methods* **2018**, *15*, 23. [CrossRef]

44. McQualter, J.L.; Yuen, K.; Williams, B.; Bertoncello, I. Evidence of an epithelial stem/progenitor cell hierarchy in the adult mouse lung. *Proc. Natl. Acad. Sci. USA* **2010**, *107*, 207107. [CrossRef] [PubMed]
45. Danahay, H.; Pessotti, A.D.; Coote, J.; Montgomery, B.E.; Xia, D.; Wilson, A.; Yang, H.; Wang, Z.; Bevan, L.; Thomas, C.; et al. Notch2 Is Required for Inflammatory Cytokine-Driven Goblet Cell Metaplasia in the Lung. *Cell Rep.* **2015**, *10*, 239–252. [CrossRef] [PubMed]
46. Lee, J.H.; Bhang, D.H.; Beede, A.; Huang, T.L.; Stripp, B.R.; Bloch, K.D.; Wagers, A.J.; Tseng, Y.H.; Ryeom, S.; Kim, C.F. Lung stem cell differentiation in mice directed by endothelial cells via a BMP4-NFATc1-thrombospondin-1 axis. *Cell* **2014**, *156*, 440–455. [CrossRef] [PubMed]
47. Lee, J.H.; Tammela, T.; Hofree, M.; Choi, J.; Marjanovic, N.D.; Han, S.; Canner, D.; Wu, K.; Paschini, M.; Bhang, D.H.; et al. Anatomically and Functionally Distinct Lung Mesenchymal Populations Marked by Lgr5 and Lgr6. *Cell* **2017**, *170*, 1149–1163.e1112. [CrossRef] [PubMed]
48. Barkauskas, C.E.; Cronce, M.J.; Rackley, C.R.; Bowie, E.J.; Keene, D.R.; Stripp, B.R.; Randell, S.H.; Noble, P.W.; Hogan, B.L.M. Type 2 alveolar cells are stem cells in adult lung. *J. Clin. Investig.* **2013**, *123*, 3025–3036. [CrossRef]
49. Youk, J.; Kim, T.; Evans, K.V.; Jeong, Y.-I.; Hur, Y.; Hong, S.P.; Kim, J.H.; Yi, K.; Kim, S.Y.; Na, K.J.; et al. Three-Dimensional Human Alveolar Stem Cell Culture Models Reveal Infection Response to SARS-CoV-2. *Cell Stem Cell* **2020**, *27*, 905–919.e910. [CrossRef] [PubMed]
50. McCauley, K.B.; Hawkins, F.; Serra, M.; Thomas, D.C.; Jacob, A.; Kotton, D.N. Efficient Derivation of Functional Human Airway Epithelium from Pluripotent Stem Cells via Temporal Regulation of Wnt Signaling. *Cell Stem Cell* **2017**, *20*, 844–857.e846. [CrossRef]
51. Jacob, A.; Morley, M.; Hawkins, F.; McCauley, K.B.; Jean, J.C.; Heins, H.; Na, C.L.; Weaver, T.E.; Vedaie, M.; Hurley, K.; et al. Differentiation of Human Pluripotent Stem Cells into Functional Lung Alveolar Epithelial Cells. *Cell Stem Cell* **2017**, *21*, 472–488.e410. [CrossRef]
52. Jacob, A.; Vedaie, M.; Roberts, D.A.; Thomas, D.C.; Villacorta-Martin, C.; Alysandratos, K.-D.; Hawkins, F.; Kotton, D.N. Derivation of self-renewing lung alveolar epithelial type II cells from human pluripotent stem cells. *Nat. Protoc.* **2019**, *14*, 3303–3332. [CrossRef]
53. Chen, Y.W.; Huang, S.X.; De Carvalho, A.; Ho, S.H.; Islam, M.N.; Volpi, S.; Notarangelo, L.D.; Ciancanelli, M.; Casanova, J.L.; Bhattacharya, J.; et al. A three-dimensional model of human lung development and disease from pluripotent stem cells. *Nat. Cell Biol.* **2017**, *19*, 542–549. [CrossRef]
54. Rock, J.R.; Onaitis, M.W.; Rawlins, E.L.; Lu, Y.; Clark, C.P.; Xue, Y.; Randell, S.H.; Hogan, B.L. Basal cells as stem cells of the mouse trachea and human airway epithelium. *Proc. Natl. Acad. Sci. USA* **2009**, *106*, 12771–12775. [CrossRef] [PubMed]
55. Takahashi, K.; Tanabe, K.; Ohnuki, M.; Narita, M.; Ichisaka, T.; Tomoda, K.; Yamanaka, S. Induction of pluripotent stem cells from adult human fibroblasts by defined factors. *Cell* **2007**, *131*, 861–872. [CrossRef] [PubMed]
56. Miller, A.J.; Spence, J.R. In Vitro Models to Study Human Lung Development, Disease and Homeostasis. *Physiology* **2017**, *32*, 246–260. [CrossRef] [PubMed]
57. Cidem, A.; Bradbury, P.; Traini, D.; Ong, H.X. Modifying and Integrating in vitro and ex vivo Respiratory Models for Inhalation Drug Screening. *Front. Bioeng. Biotechnol.* **2020**, *8*, 581995. [CrossRef] [PubMed]
58. Kabadi, P.K.; Rodd, A.L.; Simmons, A.E.; Messier, N.J.; Hurt, R.H.; Kane, A.B. A novel human 3D lung microtissue model for nanoparticle-induced cell-matrix alterations. *Part. Fibre Toxicol.* **2019**, *16*, 15. [CrossRef]
59. Vazquez-Armendariz, A.I.; Heiner, M.; El Agha, E.; Salwig, I.; Hoek, A.; Hessler, M.C.; Shalashova, I.; Shrestha, A.; Carraro, G.; Mengel, J.P.; et al. Multilineage murine stem cells generate complex organoids to model distal lung development and disease. *EMBO J.* **2020**, *39*, e103476. [CrossRef]
60. Lechner, A.J.; Driver, I.H.; Lee, J.; Conroy, C.M.; Nagle, A.; Locksley, R.M.; Rock, J.R. Recruited Monocytes and Type 2 Immunity Promote Lung Regeneration following Pneumonectomy. *Cell Stem Cell* **2017**, *21*, 120–134.e127. [CrossRef]
61. Leeman, K.T.; Pessina, P.; Lee, J.H.; Kim, C.F. Mesenchymal Stem Cells Increase Alveolar Differentiation in Lung Progenitor Organoid Cultures. *Sci. Rep.* **2019**, *9*, 6479. [CrossRef]
62. Barosova, H.; Maione, A.G.; Septiadi, D.; Sharma, M.; Haeni, L.; Balog, S.; O'Connell, O.; Jackson, G.R.; Brown, D.; Clippinger, A.J.; et al. Use of EpiAlveolar Lung Model to Predict Fibrotic Potential of Multiwalled Carbon Nanotubes. *ACS Nano* **2020**, *14*, 3941–3956. [CrossRef]
63. Kim, J.; Koo, B.-K.; Knoblich, J.A. Human organoids: Model systems for human biology and medicine. *Nat. Rev. Mol. Cell Biol.* **2020**, *21*, 571–584. [CrossRef]
64. Miller, A.J.; Dye, B.R.; Ferrer-Torres, D.; Hill, D.R.; Overeem, A.W.; Shea, L.D.; Spence, J.R. Generation of lung organoids from human pluripotent stem cells in vitro. *Nat. Protoc.* **2019**, *14*, 518–540. [CrossRef] [PubMed]
65. Rossi, G.; Manfrin, A.; Lutolf, M.P. Progress and potential in organoid research. *Nat. Rev. Genet.* **2018**, *19*, 671–687. [CrossRef] [PubMed]
66. Liu, S.; Yang, R.; Chen, Y.; Zhao, X.; Chen, S.; Yang, X.; Cheng, Z.; Hu, B.; Liang, X.; Yin, N.; et al. Development of Human Lung Induction Models for Air Pollutants' Toxicity Assessment. *Environ. Sci. Technol.* **2021**, *55*, 2440–2451. [CrossRef] [PubMed]
67. Wu, X.; Ciminieri, C.; Bos, I.S.T.; Woest, M.E.; D'Ambrosi, A.; Wardenaar, R.; Spierings, D.C.J.; Königshoff, M.; Schmidt, M.; Kistemaker, L.E.M.; et al. Diesel exhaust particles distort lung epithelial progenitors and their fibroblast niche. *Environ. Pollut.* **2022**, *305*, 119292. [CrossRef]

68. Yu, H.; Lin, Y.; Zhong, Y.; Guo, X.; Lin, Y.; Yang, S.; Liu, J.; Xie, X.; Sun, Y.; Wang, D.; et al. Impaired AT2 to AT1 cell transition in PM2.5-induced mouse model of chronic obstructive pulmonary disease. *Respir. Res.* **2022**, *23*, 70. [CrossRef]

69. Han, Y.; Yang, L.; Lacko, L.A.; Chen, S. Human organoid models to study SARS-CoV-2 infection. *Nat. Methods* **2022**, *19*, 418–428. [CrossRef] [PubMed]

70. Heo, I.; Dutta, D.; Schaefer, D.A.; Iakobachvili, N.; Artegiani, B.; Sachs, N.; Boonekamp, K.E.; Bowden, G.; Hendrickx, A.P.A.; Willems, R.J.L.; et al. Modelling Cryptosporidium infection in human small intestinal and lung organoids. *Nat. Microbiol.* **2018**, *3*, 814–823. [CrossRef] [PubMed]

71. Salahudeen, A.A.; Choi, S.S.; Rustagi, A.; Zhu, J.; Van Unen, V.; De la O Ryan, S.M.; Flynn, R.A.; Margalef-Català, M.; Santos, A.J.M.; Ju, J.; et al. Progenitor identification and SARS-CoV-2 infection in human distal lung organoids. *Nature* **2020**, *588*, 670–675. [CrossRef]

72. Zhou, J.; Li, C.; Sachs, N.; Chiu, M.C.; Wong, B.H.-Y.; Chu, H.; Poon, V.K.-M.; Wang, D.; Zhao, X.; Wen, L.; et al. Differentiated human airway organoids to assess infectivity of emerging influenza virus. *Proc. Natl. Acad. Sci. USA* **2018**, *115*, 308115. [CrossRef]

73. Travaglini, K.J.; Nabhan, A.N.; Penland, L.; Sinha, R.; Gillich, A.; Sit, R.V.; Chang, S.; Conley, S.D.; Mori, Y.; Seita, J.; et al. A molecular cell atlas of the human lung from single-cell RNA sequencing. *Nature* **2020**, *587*, 619–625. [CrossRef]

74. Strunz, M.; Simon, L.M.; Ansari, M.; Kathiriya, J.J.; Angelidis, I.; Mayr, C.H.; Tsidiridis, G.; Lange, M.; Mattner, L.F.; Yee, M.; et al. Alveolar regeneration through a Krt8+ transitional stem cell state that persists in human lung fibrosis. *Nat. Commun.* **2020**, *11*, 3559. [CrossRef] [PubMed]

Acknowledgement

"Sometimes I think you believe in me more than I do" said the boy. "You'll catch up" said the horse.
The Boy, the Mole, the Fox and the Horse. Charlie Mackesy

Thanks to all who believed that I could do it.